Physics – Uspekhi **68** (10) 1001 – 1028 (2025)

REVIEWS OF TOPICAL PROBLEMS

PACS numbers: 52.25.Dg, **72.15. – v,** 72.15.Gd, 72.25.Ba, 72.25.Dc, **75.30. – m,** 75.40.Gb, **75.76. + j, 85.75. – d,** 85.75.Bb, 85.75.Dd

Chiral spintronics of helimagnets

V.V. Ustinov, I.A. Yasyulevich

DOI: https://doi.org/10.3367/UFNe.2025.07.039974

Contents

Abstract. Chiral spintronics is a promising new branch of quantum electronics based on spin transport phenomena in materials with chiral symmetry. This review focuses on the development of chiral spintronics in helimagnets, materials characterized by a helical magnetic structure. The paper considers the general principles for describing electric and spin transport in conducting crystals in the presence of inhomogeneities in an external magnetic field and/or internal magnetic fields of exchange origin. It is demonstrated that the interaction of conduction electron spins with a spatially inhomogeneous exchange field in helimagnets provides a natural explanation for two experimentally observed spin-transport effects: the electrical magnetochiral effect and the kinetic magnetoelectric effect. An original technique for ascertaining the magnetic chirality of conductive helimagnets based on experimental studies of the aforementioned galvanomagnetic effects is presented. Constructing a theory of the spin-transfer torque effect in conductive chiral helimagnets is described, including an exploration of the influence of this effect on the magnetization and electrical resistance of helimagnets. The spin-transfer torque effect in helimagnets is demonstrated to cause rotation of the magnetization helix under the influence of an electric current. This can be used to create new devices of spin electronics in which conductive helimagnets will serve as the main functional components.

Keywords: chirality, helimagnet, spin current, spintronics, nonreciprocal transport, electrical magnetochiral effect, magnetochiral anisotropy, kinetic magnetoelectric effect, spin-transfer torque

V.V. Ustinov [(a)], **I.A. Yasyulevich** [(b)]
Mikheev Institute of Metal Physics,
Ural Branch of the Russian Academy of Sciences,
ul. S. Kovalevskoi 18, 620137 Ekaterinburg, Russian Federation
E-mail: [(a)] ustinov@imp.uran.ru, [(b)] yasyulevich@imp.uran.ru

Received 17 January 2025, revised 14 July 2025
Uspekhi Fizicheskikh Nauk **195** (10) 1062 – 1093 (2025)
Translated by V.L. Derbov

1. Introduction

1.1 Spintronics: etymology and chronology of terminology

Before discussing the subject of this review, the chiral spintronics of helimagnets, which is the newest branch of spintronics, we would like to remind the reader of the key milestones in the origin, formation, and development of spintronics in general, as well as the spin phenomena and effects that form its physical basis.

Spintronics is a branch of quantum electronics that studies the transport properties of conducting materials and nanostructures based on them, determined by the presence of electric charge and spin angular momentum in electrons [1–6].

The term 'spintronics' comes from the acronym 'SPINTRONICS,' introduced in 1996 by Wolf [7] as the name of a research program initiated by the Defense Advanced Research Projects Agency (DARPA) of the US Department of Defense. The acronym 'SPINTRONICS' is an abbreviation for 'SPIN TRansport electrONICS.' The program was aimed at studying magnetic nanostructures with the purpose of creating new magnetic field sensors and magnetic memory devices. To review advances in spintronics, the reader may refer to reviews published in *Physics–Uspekhi* [8–10], as well as the following books: *Spin Current*, edited by Maekawa, Valenzuela, Saitoh, and Kimura [11], *Spin Physics in Semiconductors*, edited by Dyakonov [12], and *Physics of Magnetic Materials and Nanostructures*, edited by Ustinov, Mushnikov, and Irkhin [13].

The first studies and discoveries in spintronics referred to nonmagnetic metals and semiconductors. Among them, the conduction-electron spin resonance (CESR) [14–21] and the spin Hall effect (SHE) [12, 22–31] should be particularly noted.

Conduction electron spin resonance is a phenomenon of resonant absorption of electromagnetic radiation energy by mobile charge and spin carriers in metals or semiconductors placed in a constant external magnetic field.

The term 'conduction electron spin resonance' was introduced in 1955 by Pines and Slichter [32]. The first registration of conduction electron spin resonance was made by Griswold, Kip, and Kittel [33]. Later, Feher and Kip experimentally discovered conduction electron spin resonance in Li, K, and Be [14]. Dyson [15] theoretically described the influence of the spin-diffusion nature of the motion of conduction electrons in a metal in the field of an electromagnetic wave attenuated in the skin layer of the metal on the resonant absorption of electromagnetic radiation energy. He showed that spin diffusion radically affects the shape of the conduction electron spin resonance line. The influence of surface and size effects on the nature of the resonant behavior of the spin system of conduction electrons under spin resonance conditions was theoretically studied by Ustinov [19, 20].

The spin Hall effect is a physical phenomenon in which the flow of electric current in a nonmagnetic conductor in the absence of an external magnetic field causes a transverse, pure spin current, unaccompanied by charge transfer. This phenomenon is caused by the spin-orbit coupling of conduction electrons with the crystal lattice and its defects.

The transverse, pure spin current induced by electric current in confined samples will cause the accumulation of nonequilibrium spin density on opposite faces of the sample. In the inverse spin Hall effect, the flow of spin current in a conductor causes the appearance of a transverse current of electric charge. The accumulation of nonequilibrium spin density on the faces of a conductor when an electric current flows through it was predicted in 1971 by Dyakonov and Perel [22, 23]. The name 'spin Hall effect' was given by Hirsch [25], who re-predicted this phenomenon in 1999. The spin Hall effect was experimentally discovered in 2004 by Kato et al. [27]; the inverse spin Hall effect was observed in 1984 by Bakun et al. [34].

Studies conducted in the late 1980s by Grünberg et al. [35, 36] and Fert et al. [37] initiated a rapid development in the study of spin and charge transport in nanostructures based on ferromagnetic metals. The branch of spintronics that studies spin and charge transport in nanostructures containing ferromagnetic layers is sometimes referred to as 'ferromagnetic spintronics' [38, 39]. In Refs [36, 37], it was shown that, in Fe/Cr superlattices and Fe/Cr/Fe nanostructures, a significant decrease in electrical resistance is observed under the influence of an external magnetic field. It was noted that the observed decrease in the electrical resistance of multilayer magnetic nanostructures is due to the dependence of the electron spin transport on the mutual orientation of the magnetizations of adjacent ferromagnetic layers, which changes under the influence of a magnetic field. This type of magnetoresistance has received a special name, 'giant magnetoresistance' (GMR), first used in 1988 by Fert et al. [37].

Later, giant magnetoresistance was discovered in planar nanoheterostructures of a special composition containing two layers of ferromagnetic metal separated by a layer of nonmagnetic conducting material and a layer of an antiferromagnet. In such nanoheterostructures, which were called 'spin valves' in a 1991 paper by Dieny et al. [40], the magnetization direction of one of the ferromagnetic layers is fixed in a certain way ('pinned'), for example, by an adjacent antiferromagnetic layer, while the magnetization of the other ferromagnetic layer can change its direction relatively freely under the influence of an external magnetic field. The magnetoresistance of such a spin valve depends significantly on the relative orientation of the magnetizations of the ferromagnetic layers. Giant magnetoresistance spin valves have found practical application in the creation of read heads in hard magnetic disks [41].

The discovery in 1996 by Slonczewski [42] and, independently, by Berger [43–45] of the spin-transfer torque (STT) effect led to the creation of fundamentally new spin devices for recording information on magnetic media, in which the magnetic state of individual ferromagnetic layers of a nanostructure is controlled not by an external magnetic field but directly by an electric current flowing through its layers [46]. The term 'spin-transfer torque' was introduced in 2002 in the papers by Stiles and Zangwill [47, 48]. In Refs [49–53], it was experimentally shown that, in spin devices consisting of a 'pinned' ferromagnetic layer, a nonmagnetic layer, and a 'free' ferromagnetic layer, the flow of spin-polarized conduction electrons formed in the pinned layer, due to the STT effect, can cause either a switch in the magnetization of the free layer from one static orientation to another, or a stationary precession of the magnetization of the free layer. The influence of the flowing electric current on the magnetization of the free ferromagnetic layer arises because the spin angular momentum of the conduction electrons, induced by the exchange interaction with electrons localized at the sites of the crystal lattice in the pinned layer, can be transferred by the current to the magnetic system of the free ferromagnetic layer due to the spin conservation law.

The ability to switch the magnetization in a free ferromagnetic layer of a spin valve between different static orientations by passing an electric current was used to create devices called 'magnetic tunnel junctions' (MTJs) [54, 55]. The term 'magnetic tunnel junction' was first introduced in 1996 by Lu et al. [56]. In its simplest form, such a device is a spin valve consisting of a pinned ferromagnetic layer, a nonconducting nonmagnetic layer, and a free ferromagnetic layer. Due to the STT effect, passing an electric current through a magnetic tunnel junction leads to a change in the mutual orientation of the ferromagnetic layers and, accordingly, to a giant change in the value of the tunnel magnetoresistance (TMR). The term 'tunnel magnetoresistance' was

first introduced in 1997 by Zhang [57] and, independently, by Bratkovsky [58]. Designs based on magnetic tunnel junctions have been used to create elements of magnetic random access memory (MRAM) [41, 59]. The term 'magnetic random access memory' has been used in the literature since 1996.

A device that exploits the possibility of an STT-induced precession of the free ferromagnetic layer magnetization in a spin valve when an electric current flows is called a spin-transfer nano-oscillator (STNO) [46, 60–69]. The abbreviation STNO is often used for the term 'spin-torque nano oscillator,' which is identical to spin-transfer nano-oscillator. This term was first introduced in 2005 [60]. In its simplest form, an STNO consists of a pinned ferromagnetic layer, a nonmagnetic layer, and a free ferromagnetic layer. The operating principle of an STNO is as follows: if the magnetization of the fixed ferromagnetic layer lies in the plane of the layer, then, to initiate oscillation, the magnetization of the free ferromagnetic layer should be deflected from the plane of the layer by a few degrees using a strong external magnetic field. A direct electric current that acquires spin polarization when flowing through a fixed ferromagnetic layer tends to return the magnetization of the free ferromagnetic layer to the plane of the layer due to the STT effect, which causes a precession of the magnetization of the free ferromagnetic layer. Such precession can be converted into high-frequency resistance/voltage oscillations through the effects of giant magnetoresistance or tunnel magnetoresistance. However, due to the small precession amplitude, the magnitude of the resulting microwave component in the electric current is small. To increase the microwave power, it was proposed to synchronize several STNOs [60, 70–72]. In Ref. [73], the synchronization of eight STNOs was reported, which, however, does not allow achieving the microwave power required for real electronic devices.

In connection with the need to create spin devices with broader functional capabilities and higher values of the corresponding magnetotransport characteristics, as well as to demonstrate ultrafast dynamics and resistance to external influences, it is proposed to use materials with a magnetic order different from ferromagnetic as functional components of spin devices. This has led to the emergence of new promising branches of spintronics, which have been named 'antiferromagnetic spintronics' [74–80] and 'ferrimagnetic spintronics' [81–83]. These terms were introduced into scientific use in 2005 [84] and 2017 [81], respectively.

1.2 Chiral spintronics: origins and recent history

In 2001, Rikken [85], using Onsager's general principles, demonstrated that nonreciprocal transport phenomena can arise in conducting chiral materials when time-reversal symmetry breaking by a magnetic field and parity breaking by chirality are simultaneously considered. This nonreciprocity manifests itself in the dependence of the electrical resistance of conductors on their chirality and on the relative orientation of the electric current and the external magnetic field. The latest promising branch of spintronics, which proposed utilizing the influence of chirality on spin and/or charge transport in the operation of spin devices, has been called 'chiral spintronics.'

The term 'chiral spintronics' was first introduced in 2016 in Paul's paper 'Stiffness in vortex-like structures due to chirality-domains within a coupled helical rare-earth superlattice' [86], published in *Scientific Reports*.

In a 2019 plenary talk, 'Rise of chiral spintronics' [87], presented at the American Physical Society March Meeting, Yang discussed the potential use of chiral domain walls and chiral molecules in spintronics.

In 2021, a review article by Yang, Naaman, Paltiel, and Parkin, 'Chiral spintronics' [88], published in *Nature Reviews Physics*, presented the current state of the art in chiral spintronics, which takes into account the features of spin and charge transport in chiral molecules [89, 90] and chiral domain walls [89, 91]. In the same year, Ustinov's plenary talk, 'Chiral spintronics of helimagnets' [92], presented at the International Conference 'Functional Materials,' discussed the potential of using helimagnets in future spin devices of chiral spintronics.

In his 2023 invited talk, 'Chiral Spintronics with Magnetic Insulators' [93], presented at the Materials for Sustainable Development conference, Velez investigated the role of chiral interactions in the generation of nonreciprocal phenomena in both magnon transport and magnetic texture dynamics in chiral magnetic insulators based on rare earth garnets.

Finally, at the 2023 Samarkand International Symposium on Magnetism, Parkin's plenary talk 'Chiral spintronics' [94] and Ustinov's 'Toward helimagnet-based spintronics' [95] presented the latest advances in chiral spintronics. Parkin's talk discussed the current state of the art in magnetic racetrack memory (MRM) developments [96]. In this type of memory, data is encoded in mobile chiral domain walls that move along magnetic nanowires under the influence of an electric current. Ustinov's report discussed the current state of a theoretical description of spin and charge transport in chiral helimagnets, as well as the influence of this transport on helimagnetism.

This review is devoted to achievements in the field of chiral spintronics of helimagnets. Emphasis is placed on those areas of chiral spintronics to which the authors of this review have made significant contributions through their own research [97–100].

1.3 Helimagnets and chirality: basic facts and classification

Helimagnets represent a special class of antiferromagnets. They can be thought of as magnetically layered magnets in which the magnetic moments of electrons localized on atoms in individual magnetic layers are co-directed, and this direction of magnetic moments changes by a constant angle when moving from one layer to another according to the screw rule (Fig. 1). Magnetic structures of this type are called magnetic helices.

Helical magnetism was discovered in heavy rare earth metals (Eu, Dy, Ho, Tb), in a large class of conducting cubic magnets without an inversion center (MnSi, $Fe_{1-x}Co_xSi$, $Mn_{1-x}Fe_xSi$, $Mn_{1-x}Co_xSi$, FeGe, MnGe, $Mn_{1-x}Fe_xGe$, $Fe_{1-x}Co_xGe$), and in a number of other compounds (see, e.g., the reviews by Izyumov [101], Kimura [102], Kishine in collaboration with Ovchinnikov [103] and in collaboration with Togawa, Kousaka, and Inoue [104], and Grigoriev et al. [105]). In Refs [106–122], it was demonstrated that magnetic helices can also be formed in various superlattices based on rare earth metals, in which the spin helix axis is perpendicular to the superlattice layers. Studies of multilayer magnetic 'spin valve' nanostructures based on rare earth metals Dy and Ho [123–130], conducted at the M.N. Mikheev Institute of Metal Physics, Ural Branch of the Russian Academy of Sciences, have shown that a helical magnetization structure can also

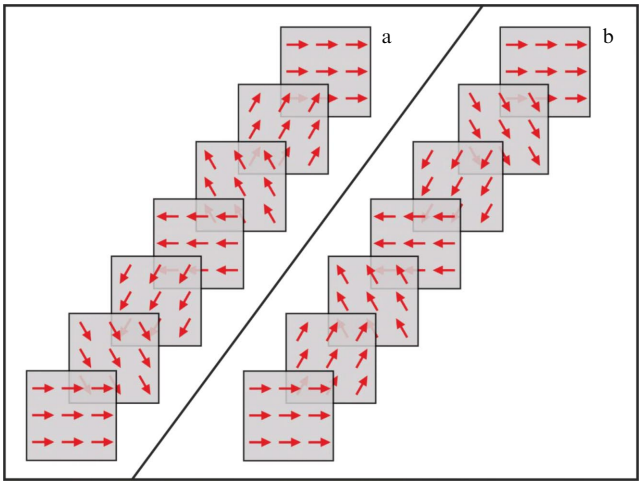

Figure 1. Schematic representation of helimagnets with right-handed (a) and left-handed (b) helices. Directions of arrows correspond to directions of magnetic moments of electrons of inner shells of atoms.

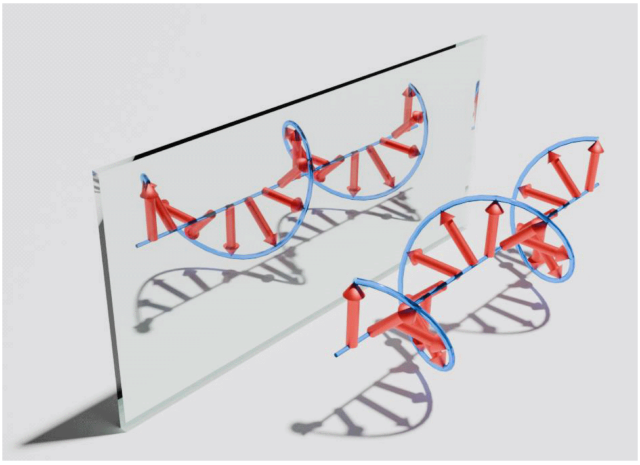

Figure 2. Demonstration of reflection of spin helix in a mirror. Directions of red arrows correspond to directions of magnetic moments of localized electrons of helimagnet. Shadows (gray) are shown for ease of perception. Mirror image of right-handed helix corresponds to left-handed one. Left-handed helix cannot be superimposed on right-handed one under any translations or rotations. This symmetry of helix is called chiral.

exist in individual nanolayers of dysprosium or holmium within a spin valve. Rotation of this helix under the influence of an external magnetic field leads to a change in the magnetotransport properties of such 'chiral spin valves.'

In crystals with a center of symmetry, helical ordering arises due to the presence of an indirect exchange interaction through conduction electrons — the Ruderman–Kittel–Kasuya–Yosida interaction. This interaction is long range and depends in a complex way on the distance between atoms. If the exchange interaction between the nearest atoms has a positive sign and the exchange interaction between the next behind the nearest neighbors is negative, helical spin structures can arise in crystals [131–135]. Helimagnets in which the spin helix is formed due to the presence of the Ruderman–Kittel–Kasuya–Yoshida interaction are called 'symmetric helimagnets' [103] or 'Yoshimori-type helimagnets' — after the author of Ref. [136].

In crystals without a center of symmetry, helical magnetic ordering arises as a result of the competition of three interactions [137, 138]. The strong symmetric isotropic Heisenberg exchange interaction tends to order neighboring spins parallel to each other. The isotropic antisymmetric Dzyaloshinskii–Moriya interaction [139–143] tends to return the interacting spins perpendicular to each other, but, due to its relative smallness, is only capable of rotating the spins by a small angle. An even weaker anisotropic exchange interaction fixes the direction of the helix axis. Helimagnets in which the spin helix is formed due to the presence of the Dzyaloshinskii–Moriya interaction are called 'chiral helimagnets' [103].

The magnetization helix can be either left-handed or right-handed (Fig. 2). To characterize the direction of helix twisting, the magnetic chirality of the helix K is introduced. A positive value of magnetic chirality $K = +1$ corresponds to a right-handed helix, while a negative magnetic chirality $K = -1$ characterizes a left-handed helix.

Detecting the helical ordering of magnetization in crystals is a rather complex problem, for the solution of which neutron diffraction methods [117, 144–153] or Lorentz transmission electron microscopy [154–161] are commonly used. However, an even more difficult task is the experimental determination of the type of magnetization helix realized in a helimagnet (either left-handed or right-handed). For this purpose, polarized neutron scattering [105, 162–181] and polarized synchrotron X-ray scattering [182–188] methods are currently used. It should be noted that the development of the polarized neutron scattering method, which has become the main one today for studying magnetic chirality, is largely associated with the fundamental work of Maleyev [162–167, 169, 170, 172–176] and Grigoriev [105, 162, 165, 169–178, 181].

Determining the magnetic chirality of crystals using polarized neutron scattering or polarized synchrotron X-rays requires the use of megascience facilities, which significantly complicates the creation of spin devices based on conducting helimagnets. Therefore, developing methods to determine the magnetic chirality of helimagnetic structures using standard laboratory techniques for studying the galvanomagnetic properties of crystals has become an important research field. The results of this work are presented in Section 5 of this review.

1.4 On inhomogeneous spin states of chiral helimagnets

In this review, we restrict ourselves to an analysis of the mutual influence of helical magnetism and transport in the simplest one-dimensional model of an unlimited ('infinite') conducting chiral magnet. We note that such a 'one-dimensional' approach to solving the above problem may become incorrect in a number of practically important cases, including the possible instability of the one-dimensional ground spin state of a chiral helimagnet. It should be noted that real helimagnet samples are always limited objects in which a 'multi-domain' state can be experimentally observed, where the directions of the magnetization helix axes differ in different parts of the sample and/or the helices have different magnetic chiralities.

The directions of the axes of the helices formed in the crystal of a chiral helimagnet are fixed by a weak anisotropic exchange interaction. For example, in hexagonal crystals, the anisotropic exchange interaction fixes the spin helix axis along the c-axis (see, e.g., [189]). Magnetic crystals in which the spin helix can align only along a single crystallographic

direction are called monoaxial helimagnets. Situations are also possible in which a weak anisotropic exchange interaction fixes several crystallographic directions in which helixes can align. Such a situation is observed in cubic magnets without an inversion center, in which a weak anisotropic exchange interaction tends to fix the directions of the helix axes along the principal directions of the cubic lattice [105, 162, 165, 169–178, 181].

It was experimentally shown in [170, 172, 177, 181] that, in cubic magnets without an inversion center, magnetization helices throughout the sample can be aligned in a single direction by applying an external magnetic field. In Refs [190, 191], numerical simulations were used to establish that an electric current in crystals without a center of symmetry can induce a transition from a multidomain state, in which the directions of the axes of the magnetization helices differ in different parts of the sample, to a single-domain state. There are also a number of studies in the literature [192–195] where it was shown both theoretically and experimentally that, in crystals with a center of symmetry, a multidomain state, characterized by a different magnetic chirality of the helices in different parts of the sample, can be transformed into a single-domain state by the simultaneous action of a high-density electric current and a magnetic field directed along the helix axis.

It should also be noted separately that, under certain conditions (for example, when applying an external magnetic field across the axis of a magnetization helix or in the case of limited samples), in addition to the helical magnetic ordering, the following may arise in crystals without a center of symmetry: a chiral soliton lattice (a sequence of ferromagnetic domains separated by 360° Bloch-type domain boundaries) [103, 156, 196]; a two-dimensional lattice of magnetic skyrmions or an A-phase (the magnetization in this phase can be approximated by a superposition of the magnetizations of three helical structures whose axes are perpendicular to the external magnetic field and rotated relative to each other by 120°) [197, 198]; 'chiral bobbers,' which are three-dimensionally localized solitons with finite energy, described by a smooth magnetization vector field with a 'hedgehog' topological feature [197, 198].

A consistent description of spin-transport effects in inhomogeneous helimagnets is an independent problem, beyond the scope of this paper.

1.5 Electron transport in helical magnets: known magneto-chiral effects and mechanical analogs of spin-transport phenomena

Studies of the influence of the magnetization helix of a helical magnet on electric current began in the mid-20th century. Elliott and Wedgwood [199] theoretically demonstrated that a helical magnetic structure can distort the Fermi surface, which, in turn, can lead to a change in electrical resistance. The influence of helical magnetism on electrical resistance was then observed experimentally (see, e.g., [200]). Experimental data showed that, when an electric current flows along the axis of a magnetic helix, the electrical resistance differs from that observed when the current flows perpendicular to the axis of the helix or in the absence of helical magnetic ordering. Subsequently, numerous studies were conducted to investigate the influence of the magnetic helix on the properties of charge transport in helimagnets (see, e.g., [131, 132, 134, 201–211]).

In 2008, Fraerman and Udalov [212] predicted the possibility of a diode effect in helimagnets with a conical helix manifesting itself in the appearance of a contribution to the electric current proportional to the square of the electric field. Chiral asymmetry of the electron energy spectrum and asymmetry of conduction electron scattering in internal helical exchange fields were considered as microscopic mechanisms causing the diode effect. In 2017, nonreciprocal transport was experimentally discovered in the metallic helimagnet MnSi [213]. It was shown that the electrical resistance along the helix axis depends on the magnetic chirality of the helimagnet and the relative orientation of the magnetic field and the electric current. This effect was called the 'electrical magnetochiral effect.' The authors of this review developed a theory [98] describing the occurrence of the electrical magnetochiral effect in helimagnets as a manifestation of the spin-transport properties of conduction electrons in the presence of an external magnetic field. It was shown that considering the quantum nature of the spin of conduction electrons moving in a nonuniform field of exchange origin created by the helically ordered magnetic moments of localized electrons gives rise to a quantum correction to the classical Lorentz force, which acts on conduction electrons and predetermines new quantum effects in charge transport in helimagnets. The electrical magnetochiral effect was also discovered in other metallic helimagnets, such as $CrNb_3S_6$ [214], MnP [192, 193], and $MnAu_2$ [195].

In 1985, manifestations of chirality effects in the formation of magnetotransport properties of conductors with mirror isomer symmetry were discovered [215]. The authors of [215], based on symmetry considerations, predicted the 'kinetic magnetoelectric effect' — the emergence of magnetization in charge carriers flowing through an isomer, which is proportional to the electric field acting in the conductor. For cubic crystals or isotropic stereoisometric materials, the proportionality coefficient between the magnetization vector and the electric field vector, according to [215], is a pseudoscalar having a different sign for the two isomeric modifications. Gor'kov and Sokol [216, 217] demonstrated that the kinetic magnetoelectric effect can arise in metallic antiferromagnets with a helical spin density wave. Numerical modeling conducted in [208] confirmed the presence of such an effect in helimagnets. In Ref. [218], the occurrence of the kinetic magnetoelectric effect when an electric current flows through a chiral domain wall was described. The authors of this review constructed a microscopic theory [97, 98] of the kinetic magnetoelectric effect caused by the exchange interaction of conduction electrons with localized electrons responsible for the formation of helimagnetism. It has been shown analytically that the kinetic magnetoelectric effect gives rise to magnetization in conduction electrons proportional to the electric current and directed along this current. Such magnetization has opposite directions for helices with different magnetic chiralities. In Ref. [219], the occurrence of the kinetic magnetoelectric effect was experimentally discovered when an electric current flows in the conducting helimagnet $CrNb_3S_6$.

In 2024, a paper [195] was published that successfully demonstrated the possibility of experimentally implementing a spin device that utilizes both the electrical magnetochiral and kinetic magnetoelectric effects occurring in a helimagnet.

It is known that, due to the spin-transfer torque effect, a flowing electric current can cause the motion of nonuniformly magnetized objects such as domain walls [220, 221], magnetic vortices [222], or skyrmions [223–227]. To facilitate understanding of how an electric current can influence the state of

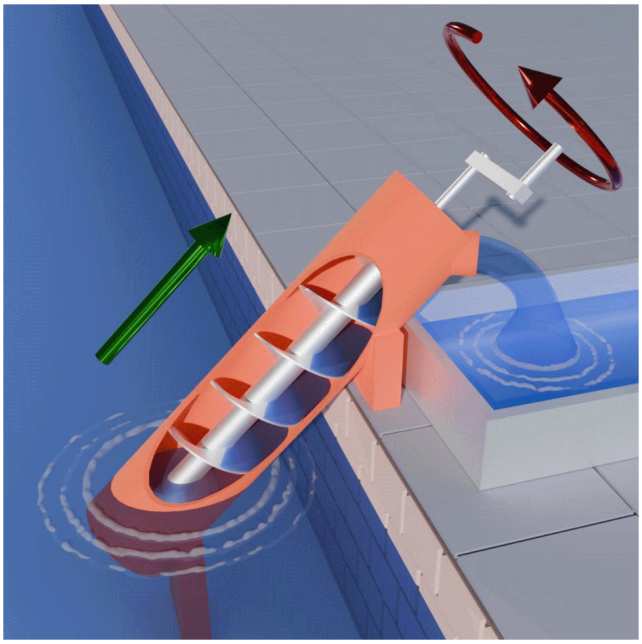

Figure 3. Schematic representation of Archimedes screw. Principle of operation of Archimedes screw is that rotation of helical-shaped screw causes water to move along axis of helicoid.

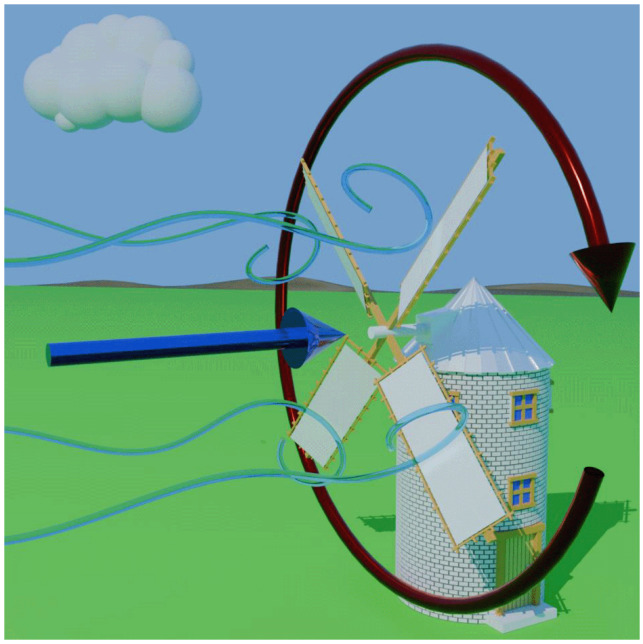

Figure 4. Schematic representation of windmill. Principle of operation of windmill is that wind flowing around helical-shaped screw causes screw to rotate.

the magnetization helix of helimagnets, we would like to refresh the reader's memory with some information about the known mechanical analogs of the magnets under consideration and the phenomena occurring in them.

The first of these is the Archimedes screw, invented by Archimedes in the 3rd century BCE, a mechanical device for moving water using a rotating helix screw (Fig. 3). A detailed technical description of this masterpiece of ancient Greek engineering was first given by Vitruvius. In the final, tenth volume of his seminal work, *Ten Books on Architecture* (Latin: *De architectura libri decern*), published in 13 BCE, he describes in detail the design of the Archimedes screw. To be fair, however, it should be noted that Vitruvius did not mention the inventor by name in his description (which, by today's standards, would be considered plagiarism). It is quite obvious that, if the rotation of an Archimedes screw causes water to move along its axis, then the flow of water through such a screw will also cause it to rotate.

A second analog is the wind turbine. This device converts the kinetic energy of the wind flow into the mechanical energy of a rotor with a special geometry. Windmills are the first historical realization of the idea of converting the linear motion of air into the rotational motion of the blades and rotor of a mill (Fig. 4). The first written references to a windmill as a technical device, by the Greek Heron, date back to the first century CE.

For both Archimedes's water screw and Heron's wind engine, the key factor is the interaction of the particle flow with a body of a special helicoidal shape possessing chiral symmetry.

Returning to the problem of the spin transport of conduction electrons in a conducting helimagnet, we can draw an analogy between ordinary atmospheric wind blowing over the blades of a windmill and the flow of spin moment of conduction electrons, which transfer their rotational angular momentum to the system of magnetic moments of the helimagnet's electrons localized at the crystal lattice sites. With this analogy in mind, in this section, we will use the term 'spin wind' as a poetic image of the well-known, more prosaic term 'spin current.'

Based on the mechanical analogies described above, we can expect that the spin wind 'blowing' in a chiral helimagnet will, under certain conditions, cause the helimagnet's entire magnetic system to rotate, just as ordinary wind rotates the blades of an air propeller.

In 2006, the dynamics of a helical spin density wave were studied in Ref. [228] for a current flowing in a helimagnet with easy-plane anisotropy using a combination of *ab initio* calculations and semiclassical linear response theory. It was shown that the current-induced torque causes rotation of the entire spin helix. In Refs [190, 229–232], the influence of current on the magnetization motion in a helimagnet was studied using numerical modeling of the solution of the Landau–Lifshitz–Gilbert equation supplemented by phenomenological 'adiabatic' and 'nonadiabatic' terms describing the STT effect. It was found that, when an electric current flows through a helimagnet, the entire spin helix shifts, which is equivalent to a harmonic rotation of the helix around its axis. It is shown that the helicoid displacement velocity depends linearly on the magnitude of the electric current flowing. It was also found that, when a current is passed through a helimagnet, a transition occurs from a 'simple helix' spin ordering to a 'conical helix' ordering, and the angle of deviation from the simple helix increases with increasing current. The authors of this review in Ref. [99] considered the occurrence of the spin-transfer torque effect in helimagnets due to the exchange interaction between the spins of conduction electrons and localized electrons. The analysis [99] showed that the electric current in a helimagnet can cause rotation of the magnetization helix, as well as a change in its shape, namely, the transformation of a simple helix into a conical one. It was shown that the rotation of the magnetization helix in helimagnets under the action of a flowing electric current leads to the generation of electromagnetic radiation.

The fact that a current pulse can change the arrangement of spin helices was experimentally discovered in the long-period metallic chiral helimagnet FeGe in [190]. Rotation of the chiral-spin structure by a pure spin current was observed experimentally in the noncollinear antiferromagnet Mn_3Sn [233]. We also note that the possibility of the emergence of coherent rotation of a magnetic helix formed in a system of interacting ferromagnetic nanodisks constituting a multilayer nanoparticle was theoretically demonstrated [234].

The authors of Ref. [235], using quantum kinetic methods, showed that a moving helical wave of spin density can cause the generation of an electric current. In [236], it was theoretically proven that a spatially uniform but harmonically changing magnetic field can cause rotation of the magnetization helix of helimagnets, which will ultimately lead to the generation of an electric current along the axis of the helix. The generation of an electric current due to the occurrence of helical rotation in a confined helimagnet was studied numerically in [237].

The purpose of this review is to introduce the reader to some of the achievements in the field of chiral spintronics of helimagnets. The review will demonstrate how the chirality of helimagnets affects the spin and charge currents in such materials, as well as how this fact can be used to determine the magnetic chirality of helimagnets using galvanomagnetic experiments. We will demonstrate how electric and spin currents influence the magnetization helix of a helical magnet and how this can be applied to the development of new spin devices.

The review is structured as follows. In Section 2, we will remind the reader how competition among the Heisenberg exchange interaction, the Dzyaloshinskii–Moriya interaction, and magnetocrystalline anisotropy leads to the emergence of helical ordering of magnetization in crystals. We will explicitly present the relationship between the effective magnetic field acting on the magnetization of conduction electrons and the effective magnetic field acting on the magnetization of localized electrons in chiral helical magnets, with the parameters of the quantum exchange Hamiltonian defining the helical magnetic ordering in a conducting crystal.

Section 3 briefly examines the characteristics of magnetization oscillations around the equilibrium helical state (spin waves), as well as the excitation of spin waves by an electric current flowing through a helimagnet.

Section 4 briefly outlines the construction of a theory suitable for describing spin-transport effects in conductors in the presence of inhomogeneities in an external magnetic field and/or internal fields of exchange origin.

Section 5, based on the theory presented in Section 4, describes the influence of helical magnetism on charge and spin transport and demonstrates the possibility of determining the magnetic chirality of a helimagnet using electrical magnetochiral or kinetic magnetoelectric effects.

Section 6 briefly discusses the effect of electric current on magnetization due to the transfer of spin moment using a joint solution to a system of equations for the magnetization of localized electrons and for the magnetization of conduction electrons. Using the developed theory, we describe the influence of the spin-transfer torque effect on the magnetization and electrical resistance of helimagnets. We also present schematics of possible new spin devices that utilize the rotation of the magnetization helix of a helimagnet under the action of an electric current.

2. Helical magnetism and exchange spin currents in chiral helimagnets

The magnetic order in a system of localized electrons in chiral helimagnets can be described by considering the direct Heisenberg exchange interaction and the Dzyaloshinskii–Moriya interaction between localized electrons, as well as magnetocrystalline anisotropy. The interaction of conduction electrons and localized electrons will be described within the framework of the $s-d\,(f\,)$ exchange model [131]. A highly efficient model method for describing interelectronic spin interactions is based on the idea that the quantum state of electrons localized at crystal lattice sites with numbers n can be described in terms of spin operators $\hat{\mathbf{S}}_n$. The spin operator of a conduction electron will be denoted by a lowercase letter $\hat{\mathbf{s}}$. The spin Hamiltonian of a system placed in a magnetic field $\mathbf{B}$ will be written as

$$\hat{\mathcal{H}} = -\frac{1}{2}\Big\{\sum_{n,m} I_{nm}\,\hat{\mathbf{S}}_n\cdot\hat{\mathbf{S}}_m + \sum_{n,m}\boldsymbol{\mathcal{D}}_{nm}\cdot\big[\hat{\mathbf{S}}_n\times\hat{\mathbf{S}}_m\big] - \mathcal{K}\sum_n\big(\hat{\mathbf{S}}_n\cdot\mathbf{e}_z\big)^2\Big\} + g\mu_{\mathrm{B}}\Big(\sum_n\hat{\mathbf{S}}_n + \sum_i\hat{\mathbf{s}}_i\Big)\cdot\mathbf{B} - \sum_{i,n} I\,(\mathbf{r}_i-\mathbf{r}_n)\,\hat{\mathbf{s}}_i\cdot\hat{\mathbf{S}}_n\,. \tag{1}$$

Here, I_{nm} are the values of the Heisenberg exchange interaction of spins localized at lattice sites with numbers n and m, the vector quantities $\boldsymbol{\mathcal{D}}_{nm}$ characterize the anisotropic Dzyaloshinskii–Moriya interaction between spins $\hat{\mathbf{S}}_n$ and $\hat{\mathbf{S}}_m$, $I\,(\mathbf{r}_i-\mathbf{r}_n)$ is the integral of $s-d\,(f\,)$ exchange interaction of a conduction electron with coordinate $\mathbf{r}_i$ and electrons localized at site $\mathbf{r}_n$, $\mathcal{K}$ is the single-ion anisotropy constant, g is the electron g-factor, μ_{B} is the Bohr magneton, and $\mathbf{e}_z$ is the unit vector oriented along the preferred direction in a magnetically uniaxial crystal, which in this paper is assumed to be coincident with the OZ axis.

We move from the quantum-mechanical description of the system in terms of spin operators $\hat{\mathbf{S}}_n$ and $\hat{\mathbf{s}}$ to the classical one by formally replacing the spin operators in the spin Hamiltonian $\hat{\mathcal{H}}$ with the classical vectors $\mathbf{S}_n = -(V/g\mu_{\mathrm{B}})\,\mathbf{M}\,(\mathbf{r}_n)$ and $\mathbf{s}_i = -(V/g\mu_{\mathrm{B}})\,\mathbf{m}\,(\mathbf{r}_i)$, where $\mathbf{M}(\mathbf{r}_n)$ is the magnetization of localized electrons at lattice sites $\mathbf{r}_n$, $\mathbf{m}\,(\mathbf{r}_i)$ is the magnetization of conduction electrons at a point with coordinate $\mathbf{r}_i$, and V is the volume of the Wigner–Seitz cell of the crystal. Exchange integrals I_{nm} and $\boldsymbol{\mathcal{D}}_{nm}$ in Eqn (1) rapidly decrease with increasing length of the vector $\delta\mathbf{r}_{mn} = \mathbf{r}_m - \mathbf{r}_n$. Consequently, assuming in the expression for the classical analogue of Hamiltonian (1) that the magnetization $\mathbf{M}(\mathbf{r})$ is a quantity continuously varying in coordinate space, we can represent the vector $\mathbf{M}(\mathbf{r}_m)\equiv\mathbf{M}(\mathbf{r}_n+\delta\mathbf{r}_{mn})$ as a power series, expanding $\mathbf{M}(\mathbf{r}_n+\delta\mathbf{r}_{mn})$ at the point $\mathbf{r}_n$ in powers of $\delta\mathbf{r}_{mn}$. Restricting this expansion to second-order terms, we obtain from Eqn (1) the following representation for the magnetic energy density $\mathcal{F}$ of the crystal in terms of the magnetizations of localized electrons $\mathbf{M}(\mathbf{r})$ and conduction electrons $\mathbf{m}(\mathbf{r})$:

$$\mathcal{F} = -\frac{1}{2}\big\{\mathbf{M}\cdot\nabla\cdot\boldsymbol{\mathcal{A}}\cdot\nabla\mathbf{M} - 2\mathbf{M}\cdot[\boldsymbol{\mathcal{D}}\cdot\nabla\times\mathbf{M}] - \mathcal{B}(\mathbf{M}\cdot\mathbf{e}_z)^2 + \mathcal{C}\mathbf{M}^2\big\} - (\mathbf{M}+\mathbf{m})\cdot\mathbf{B} - \Lambda\mathbf{M}\cdot\mathbf{m}\,. \tag{2}$$

In expression (2) for the energy density $\mathcal{F}$, the Heisenberg exchange interaction is characterized by tensor $\boldsymbol{\mathcal{A}} = (V/2g^2\mu_B^2)\sum_m I_{0m}\delta\mathbf{r}_{m0}\otimes\delta\mathbf{r}_{m0}$ and the scalar quantity $\mathcal{C} = (V/g^2\mu_B^2)\sum_m I_{0m}$, the Dzyaloshinskii–Moriya interaction by tensor $\boldsymbol{\mathcal{D}} = (V/2g^2\mu_B^2)\sum_m \boldsymbol{\mathcal{D}}_{0m}\otimes\delta\mathbf{r}_{m0}$, the single-axis magnetocrystalline anisotropy by constant $\mathcal{B} = (V/g^2\mu_B^2)\mathcal{K}$, and the $s-d(f)$ exchange interaction by parameter $\Lambda = (1/g^2\mu_B^2)\int I(\mathbf{r})\,\mathrm{d}^3\mathbf{r}$.The symbol '$\otimes$' is used to denote the tensor product of vectors.

Restricting ourselves to considering crystals with cubic symmetry, we present the tensors $\boldsymbol{\mathcal{A}}$ and $\boldsymbol{\mathcal{D}}$ in the form $\boldsymbol{\mathcal{A}} = \mathcal{A}\boldsymbol{\mathcal{E}}$ and $\boldsymbol{\mathcal{D}} = \mathcal{D}\boldsymbol{\mathcal{E}}$, where $\mathcal{A}$ and $\mathcal{D}$ are constants and $\boldsymbol{\mathcal{E}}$ is the unit tensor of the second rank. The quantity $\mathcal{A}$ characterizing direct exchange is called 'exchange stiffness.' For the descriptive identification of the quantity $\mathcal{D}$, arising from the Dzyaloshinskii–Moriya interaction, often employs the special term 'spiralization' [238–242].

Magnetic subsystems of localized electrons and conduction electrons with magnetizations **M** and **m** are coupled via an exchange interaction. This interaction results in the effective magnetic field acting on the magnetization of conduction electrons **m** from the localized electrons, and the effective magnetic field $\mathbf{B}_{\mathbf{m}}^{(\mathrm{eff})}$ acts on the magnetization of localized electrons **M** from the conduction electrons $\mathbf{B}_{\mathbf{M}}^{(\mathrm{eff})}$. By setting the magnetic energy of the crystal $F = \int \mathrm{d}^3\mathbf{r}\mathcal{F}$ and then calculating the variational derivatives of F with respect to the variables **m** and **M**, we find the effective magnetic fields $\mathbf{B}_{\mathbf{m}}^{(\mathrm{eff})} = -\delta F/\delta\mathbf{m}$ and $\mathbf{B}_{\mathbf{M}}^{(\mathrm{eff})} = -\delta F/\delta\mathbf{M}$ acting on the magnetizations **m** and **M** in the helimagnet:

$$\mathbf{B}_{\mathbf{m}}^{(\mathrm{eff})} = \mathbf{B} + \Lambda\mathbf{M}\,, \tag{3}$$

$$\mathbf{B}_{\mathbf{M}}^{(\mathrm{eff})} = \mathbf{B} + \Lambda\mathbf{m} + \mathcal{A}\Delta\mathbf{M} - \mathcal{B}(\mathbf{M}\cdot\mathbf{e}_z)\mathbf{e}_z + \mathcal{C}\mathbf{M} - 2\mathcal{D}\,[\nabla\times\mathbf{M}]\,. \tag{4}$$

It is important to emphasize that the effective magnetic field $\mathbf{B}_{\mathbf{M}}^{(\mathrm{eff})}$ acting on the magnetization **M** of localized electrons, according to Eqn (4), is determined not only by the external magnetic field **B** and the exchange field $\Lambda\mathbf{m}$ acting from the conduction electrons, but also by the magnetization **M** itself, i.e., $\mathbf{B}_{\mathbf{M}}^{(\mathrm{eff})}$ is a functional of magnetization **M**: $\mathbf{B}_{\mathbf{M}}^{(\mathrm{eff})} \equiv \mathbf{B}_{\mathbf{M}}^{(\mathrm{eff})}[\mathbf{M}(\mathbf{r},t)]$.

To describe the magnetization dynamics in the conducting helimagnets considered, it is first necessary to formulate equations describing the magnetization dynamics of localized electrons $\mathbf{M}(\mathbf{r},t)$. For this purpose, the well-known Landau–Lifshitz–Gilbert equation can be used,

$$\frac{\partial\mathbf{M}}{\partial t} + \gamma\left[\mathbf{M}\times\mathbf{B}_{\mathbf{M}}^{(\mathrm{eff})}\right] + \frac{\alpha}{M}\left[\frac{\partial\mathbf{M}}{\partial t}\times\mathbf{M}\right] = 0\,, \tag{5}$$

in which γ is the gyromagnetic ratio, and α is the Gilbert damping constant that specifies the decay rate of the oscillations of the magnetization **M**.

In a given constant magnetic field **B**, the magnetization $\mathbf{M}(\mathbf{r},t)$, satisfying equation (5), relaxes to its equilibrium value $\mathbf{M}_0 \equiv \mathbf{M}_0(\mathbf{r})$. The equilibrium distribution of magnetization $\mathbf{M}_0(\mathbf{r})$ is defined as the extremal of the functional $F[\mathbf{M}(\mathbf{r},t)]$, ensuring its minimum value $F[\mathbf{M}_0(\mathbf{r})]$. Below, we restrict ourselves to considering the case when the magnitude of the helimagnet magnetization remains a given constant: $|\mathbf{M}(\mathbf{r},t)| = M$. To find an extremal of the functional $F[\mathbf{M}(\mathbf{r},t)]$ with the additional condition $\mathbf{M}^2 - M^2 = 0$, it is necessary to solve the system of Euler–Poisson equations, which take the form $\mathbf{B}_{\mathbf{M}}^{(\mathrm{eff})}[\mathbf{M}] = l\mathbf{M}$, where l is the Lagrange multiplier to be found from these equations. Obviously, the solution $\mathbf{M}_0(\mathbf{r})$ of Euler–Poisson equations satisfies the condition

$$\left[\mathbf{M}_0\times\mathbf{B}_{\mathbf{M}}^{(\mathrm{eff})}[\mathbf{M}_0]\right] = 0\,. \tag{6}$$

Substituting expression (4) for the effective field $\mathbf{B}_{\mathbf{M}}^{(\mathrm{eff})}$ into Eqn (5) and making use of easily provable relations $[\mathbf{M}\times\Delta\mathbf{M}] = -\nabla\cdot[(\nabla\otimes\mathbf{M})\times\mathbf{M}]$ and $[\mathbf{M}\times[\nabla\times\mathbf{M}]] = -\nabla\cdot\mathbf{M}\otimes\mathbf{M}$ in the tensor algebra, we can write the Landau–Lifshitz–Gilbert equation (5) in the following form:

$$\frac{\partial\mathbf{M}}{\partial t} + \gamma\left[\mathbf{M}\times(\mathbf{B}+\mathbf{B}_a)\right] + \nabla\cdot\boldsymbol{J}_{\mathbf{M}} + \frac{\alpha}{M}\left[\frac{\partial\mathbf{M}}{\partial t}\times\mathbf{M}\right] + \gamma\Lambda[\mathbf{M}\times\mathbf{m}] = 0\,, \tag{7}$$

where $\mathbf{B}_a \equiv \mathcal{B}(\mathbf{M}\cdot\mathbf{e}_z)\,\mathbf{e}_z$ is the single-axis magnetic anisotropy field.

When writing the third term on the left-hand side of Eqn (7), we introduced a second-rank tensor

$$\boldsymbol{J}_{\mathbf{M}} = -\gamma\mathcal{A}\left[(\nabla\otimes\mathbf{M})\times\mathbf{M}\right] + 2\gamma\mathcal{D}\mathbf{M}\otimes\mathbf{M}\,. \tag{8}$$

The tensor $\boldsymbol{J}_{\mathbf{M}}$, which characterizes the influence of exchange interactions within the subsystem of localized moments on the motion of magnetization **M**, can be called the tensor of the flux density of magnetization **M**. For brevity, we will call $\boldsymbol{J}_{\mathbf{M}}$ the 'exchange spin current.' The exchange spin current $\boldsymbol{J}_{\mathbf{M}}$, determined by Eqn (8), contains two components. The first of them (the first term on the right-hand side of Eqn (8)) is due to the Heisenberg exchange of localized electrons, its magnitude being determined by the exchange stiffness $\mathcal{A}$. The second one is determined by the Dzyaloshinskii–Moriya exchange interaction; its magnitude is determined by the spiralization $\mathcal{D}$.

Initially, the term 'exchange spin current' was used to describe the dynamics of ferromagnets, in which only the symmetric exchange interaction was considered. This exchange spin current, determined by the first term on the right-hand side of definition (8), is described in detail in book [11], where a separate chapter is devoted to it. In Ref. [99], we expanded the scope of the 'exchange spin current' concept by describing the contribution to $\boldsymbol{J}_{\mathbf{M}}$ from the Dzyaloshinskii–Moriya exchange interaction, represented by the second term on the right-hand side of Eqn (8).

The introduction of the term 'exchange spin current' requires special clarification. The tensor operation $\nabla\cdot\boldsymbol{J}_{\mathbf{M}}$, in which the vector operator $\nabla \equiv \partial/\partial\boldsymbol{r}$ forms a scalar product with the tensor $\boldsymbol{J}_{\mathbf{M}}$, can be considered a tensor analogue of the well-known operation of calculating the divergence of a vector **j**, denoted as $\mathrm{div}\,\mathbf{j} \equiv \nabla\cdot\mathbf{j}$, in which the vector operator ∇ forms a scalar product with the vector **j**. If by vector **j** we understand the vector of the electric current density whose carriers are conduction electrons, then the scalar quantity $\nabla\cdot\mathbf{j}$, by virtue of the law of conservation of the number of particles, will characterize the rate of change over time of the electric charge density at a given point in space, caused by a change in the density of the electric current **j** at this point. Drawing an analogy between the operations $\nabla\cdot\mathbf{j}$ and $\nabla\cdot\boldsymbol{J}_{\mathbf{M}}$, we can assert that the quantity $\nabla\cdot\boldsymbol{J}_{\mathbf{M}}$ will characterize the rate of change over time of the magnetization density **M** of localized electrons at a given point in space, which is caused

by the behavior of the quantity $\boldsymbol{J}_{\mathbf{M}}$ we introduced at this point. This is precisely why the tensor $\boldsymbol{J}_{\mathbf{M}}$ itself has the meaning of the density of a certain current, and we call it the 'exchange spin current' tensor.

Without a doubt, the analogy drawn above between the electric current density $\mathbf{j}$ and the exchange spin current density $\boldsymbol{J}_{\mathbf{M}}$ is far from complete. Unlike an electric current, the flow of which is accompanied by the physical movement of conduction electrons in space and the corresponding transfer of electric charge, the exchange spin current $\boldsymbol{J}_{\mathbf{M}}$, which characterizes a system of localized electrons, is in no way connected with the macroscopic movement of electrons in coordinate space. The exchange spin current characterizes the specific property of a system of localized electrons, interconnected by exchange interactions of various types, to change the local magnetization of the system $\mathbf{M}$ at a given point of the crystal $\mathbf{r}$ if the magnetization at neighboring points of the system differs from $\mathbf{M}$.

We will further consider the case when a constant uniform magnetic field $\mathbf{B}$ acting in a helimagnet is directed along the OZ axis.

The equilibrium distribution of the magnetization of localized electrons $\mathbf{M}_0(z)$, which in the case considered will be a function of only one coordinate z, is defined as the extremal of the functional of the crystal magnetic energy F, satisfying the condition $|\mathbf{M}_0(z)| = M$. To find the extremal of the functional F, it is necessary to solve the system of Euler–Poisson equations. It can be shown that the solution to the system of Euler–Poisson equations with energy density (2), satisfying condition (6) under the additional requirement $\mathbf{M}_0^2 - M^2 = 0$, is a magnetic helicoid. The vector $\mathbf{M}_0$ of this helicoid can be represented as the sum of two components: the transverse (relative to the helical axis) component $\mathbf{M}_{0,t}$ and the longitudinal component $\mathbf{M}_{0,\ell}$: $\mathbf{M}_{0,t} + \mathbf{M}_{0,\ell}$.

The transverse component $\mathbf{M}_{0,t}$ periodically changes its direction in space with increasing coordinate z, remaining constant in magnitude: $\mathbf{M}_{0,t} = M_{0,t}(\mathbf{e}_x \cos Kq_0 z + \mathbf{e}_y \sin Kq_0 z)$, where $M_{0,t} = |\mathbf{M}_{0,t}|$, q_0 is the equilibrium wavenumber of the helicoid, $\mathbf{e}_x$ and $\mathbf{e}_y$ are unit vectors along the OX and OY axes, respectively, and $K = \pm 1$ is the magnetic chirality of the magnetization helix. A positive magnetic chirality $K = +1$ corresponds to a right-handed magnetization helix, while a negative magnetic chirality $K = -1$ characterizes a left-handed helix. To characterize a helicoid, in addition to the scalar quantity K, we will use the unit vector of magnetic chirality $\mathbf{k} = K\mathbf{e}_z$. We will also introduce the wave vector of the magnetic helix $\mathbf{q} = [\mathbf{M}_t \times \partial \mathbf{M}_t / \partial z] / M_t^2$. It is clear that $\mathbf{q} = q\mathbf{k} = Kq\,\mathbf{e}_z$, $q_z \equiv \mathbf{q} \cdot \mathbf{e}_z = Kq$, where $q = |\mathbf{q}|$.

In an equilibrium helimagnet with a helical wavenumber q_0, the direction of magnetization changes in space with a period $L_{\mathrm{H}} = 2\pi/q_0$. The minimum energy of the magnetic helix at equilibrium is achieved for the wavenumber $q_0 = |\mathcal{D}|/\mathcal{A}$ and the chirality $K = \operatorname{sgn} \mathcal{D}$. In this case, the relationship between the longitudinal component of magnetization $\mathbf{M}_{0,\ell}$ and the field $\mathbf{B}$ has the form

$$\mathbf{M}_{0,\ell} = \frac{1 + \chi\mathcal{A}}{\mathcal{B} + \mathcal{D}^2/\mathcal{A}}\,\mathbf{B}\,, \tag{9}$$

where χ is the Pauli electron gas magnetic susceptibility.

The ordering of the magnetic moments of localized electrons, in which $\mathbf{M}_{0,\ell} \equiv 0$ and the magnetization $\mathbf{M}_0$ lies in the XY plane, is called a 'simple helix.' This type of magnetic ordering is characteristic of most metallic helimagnets when an external magnetic field is absent. A schematic representation of a magnetic structure of the 'simple helix' type is shown in Fig. 5.

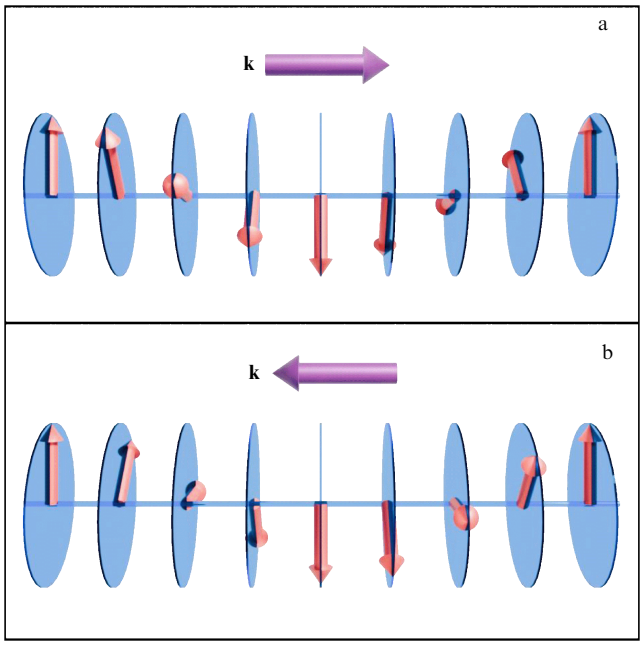

Figure 5. Schematic representation of 'simple helix' magnetic structure in a helimagnet with chirality vector $\mathbf{k}$ in the absence of magnetic field: (a) right-handed helix, chirality $K = +1$; (b) left-handed helix, chirality $K = -1$. Directions of red arrows correspond to directions of magnetic moments of localized electrons.

According to (9), a simple helix can be transformed into a conical helix under the action of a magnetic field $\mathbf{B}$ directed along the helicoid axis. When the field $\mathbf{B}$ is applied, the magnetization $\mathbf{M}_0$ deviates from the XY plane by a finite angle $\theta_0 = \theta_0(B)$, the magnitude of which depends on the magnitude of the magnetic field $B = |\mathbf{B}|$. We will assume that θ_0 is always positive; this means that it determines only the absolute value of the deviation angle but does not contain information about the direction in which the magnetization deviates from the plane perpendicular to the helix axis. The direction of the longitudinal magnetization vector of the helicoid $\mathbf{M}_{0,\ell}$ coincides with the direction of the field $\mathbf{B}$, specified by the unit vector $\mathbf{b} = \mathbf{B}/B$, where $B = |\mathbf{B}|$. Then, the components $\mathbf{M}_{0,\ell}$ and $\mathbf{M}_{0,t}$ of the vector $\mathbf{M}_0$ can be represented in the following form:

$$\mathbf{M}_{0,\ell} = \mathbf{b} M \sin\,\theta_0\,;$$

$$\mathbf{M}_{0,t} = M \cos\,\theta_0\,(\mathbf{e}_x \cos\,Kq_0 z + \mathbf{e}_y \sin\,Kq_0 z)\,. \tag{10}$$

A magnetic helix with a nonzero value of $\mathbf{M}_{0,\ell}$ is called a conical magnetic helix. A schematic representation of a conical helix magnetic structure formed from a simple helix under the action of a magnetic field directed along the axis of a magnetic helicoid is shown in Fig. 6.

When the magnetic field B reaches the value $B_{\mathrm{F}} = M(\mathcal{B} + \mathcal{D}^2/\mathcal{A})/(1 + \chi\mathcal{A})$, the conical helix undergoes a phase transition to an induced 'ferromagnetic' state, in which $|\mathbf{M}_{0,\ell}| = M$ and $\mathbf{M}_{0,t}(z) \equiv 0$.

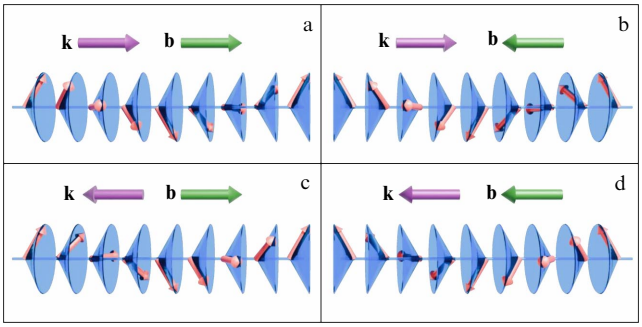

Figure 6. Diagram of configurations of conical magnetic helix of helimagnet at rest in magnetic field whose direction is given by unit vector $\mathbf{b} = \mathbf{B}/B$: (a) right-handed, $\mathbf{b} \uparrow\uparrow \mathbf{k}$; (b) right-handed, $\mathbf{b} \uparrow\downarrow \mathbf{k}$; (c) left-handed, $\mathbf{b} \uparrow\downarrow \mathbf{k}$; (d) left-handed, $\mathbf{b} \uparrow\uparrow \mathbf{k}$. Directions of red arrows correspond to directions of magnetic moments of localized electrons.

3. Spin waves in chiral helimagnets

In Section 2, it was shown that competition among the Heisenberg exchange interaction, the Dzyaloshinskii–Moriya interaction, and magnetocrystalline anisotropy leads to the formation of a magnetization helix of localized electrons in chiral helical magnets. In this section, we will briefly consider magnetization oscillations around the equilibrium helical state, i.e., spin waves in helimagnets, as well as the excitation of spin waves by an electric current flowing through a helimagnet.

3.1 Spin wave spectrum in chiral helimagnets

The spin wave spectrum in chiral helimagnets was described in Refs [137, 167, 243–248], and in symmetric helimagnets, in Refs [249–251]. Theoretical studies of the spectrum of coupled spin and elastic waves in helical magnets were reported in Refs [252–254]. Coupled electromagnetic and spin waves, as well as coupled electromagnetic, spin, and magnetoelastic waves in crystals with a helical magnetic structure, were studied in [255–260].

In Ref. [137], Bar'yakhtar and Stefanovskii proposed using the Holstein–Primakoff transformation to obtain the magnon spectrum in chiral helimagnets. In Ref. [244], Izyumov used the linearized Landau–Lifshitz equation to describe the dynamics of the magnetization helix. In the papers mentioned above, it was shown that the wave properties of magnons in helimagnets are in some respects analogous to the wave properties of electrons in the periodic potential of a crystal lattice, with the original helical magnetic structure playing the role of the source of the effective periodic field in which the magnons move. This leads to 'Bragg' reflections of the magnon from periodically repeating fragments of the helix if the magnon wave vector is equal to half the wave vector of the helix and to the formation of bands in the magnon energy spectrum. Quantum spin waves in helimagnets are called 'helimagnons'; this term was proposed by Belitz et al. in 2006 [261, 262].

Let us present an expression for the spectrum of helimagnons with wave vector $\mathbf{Q}$ for a chiral helimagnet in the absence of an external magnetic field, ignoring the contribution of conduction electrons. We assume that magnons propagate strictly along the axis of the magnetization helix, defined by the wave vector $\mathbf{q}_0 = Kq_0\mathbf{e}_z$. For the magnons under consideration, $\mathbf{Q} = Q\mathbf{e}_z$, where Q is the helimagnon wavenumber. The helix period L_H is equal to $2\pi/q_0$. Accordingly, the reduced

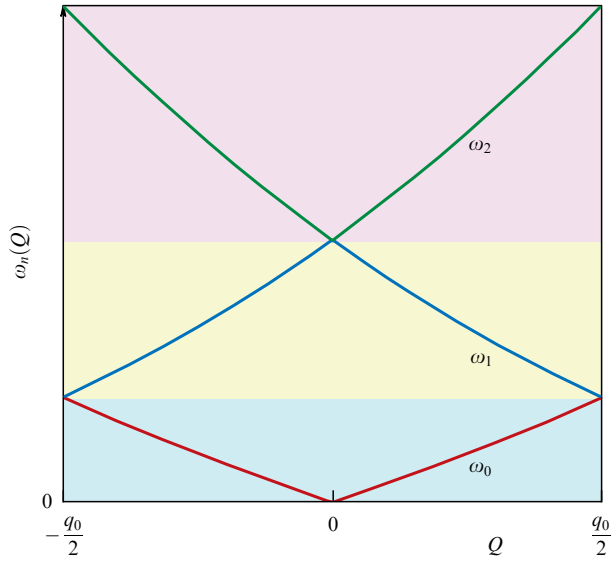

Figure 7. Band spectrum helimagnons $\omega_n(Q)$ in reduced zone diagram for $-q_0/2 \leqslant Q \leqslant q_0/2$. Three lower energy bands are shown: $\omega_0(Q)$, $\omega_1(Q)$, and $\omega_2(Q)$. For ease of perception, each band is highlighted in its own color.

zone of the space of wave vectors $\mathbf{Q}$ is specified by the inequality $|Q| \leqslant \pi/L_\mathrm{H} \equiv q_0/2$. According to Ref. [137], in the case under consideration, the helimagnon spectrum has a band character but does not contain any gaps. In the scheme of extended zones, the helimagnon spectrum for arbitrary values of Q is given by the function

$$\hbar\omega\,(Q) = \mu_\mathrm{B} M_0 \mathcal{A} |Q| \sqrt{Q^2 + q_0^2 + \frac{|\mathcal{B}|}{\mathcal{A}}}\,. \tag{11}$$

The gapless nature of the helimagnon spectrum propagating strictly along the helix axis is expressed in the fact that the function $\omega(Q)$ has no discontinuities at the boundaries of the reduced zone $Q = \pm q_0/2$ and all subsequent zones in reciprocal space.

In the reduced zone of the space of wave vectors, specified by the inequality $|Q| \leqslant q_0/2$, the band spectrum of helimagnons is determined by the multivalued function $\omega_n(Q)$, where the subscript n denotes the band number of the helimagnon energy spectrum, taking the series of values $n = 0, 1, 2, \ldots$. The band spectrum of helimagnons $\omega_n(Q)$ in the reduced zone $|Q| \leqslant q_0/2$ can be represented as

$$\omega_n(Q) = \begin{cases} \omega\left(|Q| + \dfrac{n}{2}\,q_0\right), & n = 0, 2, 4, \ldots, \\ \omega\left(|Q| - \dfrac{n+1}{2}\,q_0\right), & n = 1, 3, 5, \ldots. \end{cases} \tag{12}$$

A schematic representation of the helimagnon spectrum $\omega_n(Q)$, obtained using Eqns (11), (12), is shown in Fig. 7.

Among the branches of the multivalued function $\omega_n(Q)$ describing the various oscillation modes of the magnetic helix, the oscillation mode $\omega_n(Q)$ with $n = 0$ is of particular interest:

$$\hbar\omega_0(Q) = \mu_\mathrm{B} M_0 \mathcal{A} |Q| \sqrt{Q^2 + q_0^2 + \frac{|\mathcal{B}|}{\mathcal{A}}}\,, \quad -\frac{q_0}{2} \leqslant Q \leqslant \frac{q_0}{2}\,. \tag{13}$$

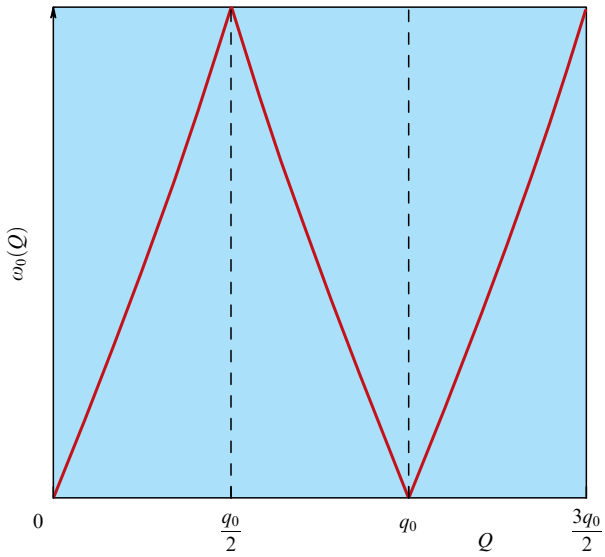

Figure 8. Spectrum of Goldstone mode of helix oscillations of chiral helimagnet $\omega_0(Q)$ in region $0 \leqslant Q \leqslant 3q_0/2$.

The frequency $\omega_0(Q)$ of this oscillation mode vanishes as the wave number Q tends to zero: $\omega_0(Q=0)=0$. The dispersion law $\omega_0(Q)$ of this mode at small Q is linear:

$$\hbar\omega_0(Q) \simeq \mu_B M_0 \mathcal{A} \sqrt{q_0^2 + \frac{|\mathcal{B}|}{\mathcal{A}}}\,|Q|\,, \quad |Q| \ll q_0\,. \tag{14}$$

It is easy to see that the branch $\omega_0(Q)$ with the properties described above represents the Goldstone mode of natural oscillations of the magnetic helix under consideration. In the extended-zone scheme, the Goldstone mode $\omega_0(Q)$, like all branches of the spectrum $\omega_n(Q)$, is periodic with a period q_0:

$$\omega_0(Q + q_0) = \omega_0(Q)\,. \tag{15}$$

The behavior of the mode $\omega_0(Q)$ in the extended-zone scheme for the region $0 \leqslant Q \leqslant 3q_0/2$ is shown in Fig. 8.

From definition (13) and property (15), it follows that the frequency $\omega_0(Q)$ of the Goldstone mode vanishes not only at $Q = 0$, but also at values of Q that are multiples of q_0, in particular, $\omega_0(q_0) = 0$. The dispersion law $\omega_0(Q)$ at small deviations of Q from q_0 is linear:

$$\hbar\omega_0(Q) \simeq \mu_B M_0 \mathcal{A} \sqrt{q_0^2 + \frac{|\mathcal{B}|}{\mathcal{A}}}\,|Q - q_0|\,, \quad |Q - q_0| \ll q_0\,. \tag{16}$$

The behavior described by Eqn (16) means that the Goldstone mode $\omega_0(Q)$, under the condition $Q \to q_0$, which is equivalent to the condition $Q \to 0$, describes the rotation of the entire magnetic helix. It is precisely the oscillations of a helix of this type that will be the subject of consideration in the subsequent sections of this paper.

It should be especially noted that the features of the helimagnon spectrum depend significantly on the direction of magnon propagation, as well as on the direction and magnitude of the applied magnetic field. The authors of [137] showed that, when the direction of the vector **Q** deviates from the helix axis, gaps appear in the band spectrum of helimagnons. The spectrum of spin waves in helimagnets in the presence of an external magnetic field is considered in Refs [243, 246–248]. In Ref. [247], it was shown that, when an external magnetic field is applied along the helix axis, the spectrum of helimagnons near the point $\mathbf{Q} = 0$ acquires a quadratic dependence on **Q**. In Ref. [243, 246], it was established that, in the presence of an external magnetic field directed perpendicular to the helix axis, a soliton lattice arises, in which the spectrum of spin waves has a two-band character (the spectrum of elementary excitations consists of acoustic and optical bands separated by an energy gap).

The nonlinear dynamics of spin waves in chiral helimagnets was studied in Ref. [196]. In Refs [263–266], it was shown that magnons with opposite wave vectors in chiral magnets have different group velocities, which leads to their nonreciprocal propagation.

3.2 Excitation of helimagnons by electric current

In this section, we briefly consider the basic principles of two different mechanisms for the excitation of spin waves in chiral helimagnets by electric current.

The first is the 'Cherenkov' emission of spin waves by a beam of charged particles. In Ref. [267] and monograph [268], Akhiezer, Bar'yakhtar, and Peletminskii theoretically demonstrated that a beam of electrons moving at a sufficiently high velocity through a ferromagnet will excite both electromagnetic and spin waves in it. This phenomenon is due to the fact that, under the influence of alternating fields arising from the combined action of beam particles and ferromagnet atoms, the density and velocity of beam particles will change in time and space. Additional information on the Cherenkov excitation of spin waves in antiferromagnets can be found in review [269].

The condition for Cherenkov excitation of helimagnons with spectrum $\omega(Q)$, given by equation (11), when an electric current created by electrons moving with drift velocity **w** flows through a helimagnet, according to [267, 268], can be written in the form

$$\omega(\mathbf{Q}) = \mathbf{Q} \cdot \mathbf{w}\,. \tag{17}$$

For $\mathbf{Q} = Q\mathbf{e}_z$ and $\mathbf{w} = w_z\mathbf{e}_z$, taking into account Eqn (11), condition (17) for finite values of Q can be written in the form of an equation

$$\frac{\mu_B}{\hbar}\, M_0 \mathcal{A} \sqrt{Q^2 + q_0^2 + \frac{|\mathcal{B}|}{\mathcal{A}}} = w\,, \tag{18}$$

where $w = |w_z|$. Considered as an equation for the wavenumber q at a given velocity w, Eqn (18) has a solution only if the electron velocity w exceeds a threshold value:

$$w_0 = \frac{\mu_B}{\hbar}\, M_0 \mathcal{A} \sqrt{q_0^2 + \frac{|\mathcal{B}|}{\mathcal{A}}}\,. \tag{19}$$

If $w \geqslant w_0$, then the wavenumber Q_w of magnons generated by an electron flow moving with velocity w is determined by the formula

$$Q_w = \frac{\hbar}{\mu_B M_0 \mathcal{A}} \sqrt{w^2 - w_0^2}\,, \quad w \geqslant w_0\,. \tag{20}$$

Accordingly, the frequency of the magnons generated is

$$\omega_w = \frac{\hbar}{\mu_B M_0 \mathcal{A}}\, w \sqrt{w^2 - w_0^2}\,, \quad w \geqslant w_0\,. \tag{21}$$

The obtained result demonstrates that the mechanism of Cherenkov excitation of helimagnons by an electron flow has a threshold nature. Estimates of the threshold drift velocity w_0 for metallic chiral helimagnets give, in order of magnitude, $w_0 \sim 10^4$ cm s^{-1}. The need to achieve such velocities is a significant limitation for the implementation of Cherenkov excitation of spin waves in conducting magnets. We also note that the presence of the skin effect in metallic conductors significantly complicates the excitation of magnons by a flow of charged particles via the Cherenkov mechanism.

The second mechanism for excitation of spin waves in chiral helimagnets that we consider is the transfer of spin angular momentum from an inhomogeneous spin system of conduction electrons with magnetization $\mathbf{m}(\mathbf{r}, t)$, moving with a given drift velocity $\mathbf{w}$, to a spin system of localized magnetic moments ordered into a helix $\mathbf{M}(\mathbf{r}, t)$. The motion of conduction electrons with a drift velocity $\mathbf{w}$ will cause the helix $\mathbf{m}(\mathbf{r}, t)$ to move with the same velocity. Due to the spin-transfer torque effect caused by the $s-d$ exchange interaction of conduction electrons and localized electrons, the motion of $\mathbf{m}(\mathbf{r}, t)$ will cause the helix $\mathbf{M}(\mathbf{r}, t)$ to move with the same velocity $\mathbf{w}$. The spin wave spectrum for such a moving helix, which we denote as $\omega_w(\mathbf{Q})$, can be written as

$$\omega_w(\mathbf{Q}) = \omega(\mathbf{Q}) + \mathbf{Q} \cdot \mathbf{w} \,. \tag{22}$$

For the Goldstone mode $\omega(\mathbf{Q}) = \omega_0(\mathbf{Q})$ with wave vector $\mathbf{Q} = \mathbf{q}_0$, the frequency $\omega_w(\mathbf{Q})$ is written as

$$\omega_w(\mathbf{q}_0) = \mathbf{q}_0 \cdot \mathbf{w} \,. \tag{23}$$

In contrast to the Cherenkov mechanism of excitation of helimagnons, where generation has a threshold character and is realized at finite values of velocity $w \geqslant w_0$, the excitation of the Goldstone mode of spin waves in chiral helimagnets due to the spin-transfer torque effect is, according to (23), a thresholdless process.

4. Basic equations for describing charge and spin transport of conduction electrons in inhomogeneous conducting magnets

In this section, we formulate general basic equations for describing electron spin transport in inhomogeneous conducting magnets. We assume the existence of two magnetic subsystems in a magnetic conductor: a subsystem of noninteracting conduction electrons with magnetization $\mathbf{m}$ and a subsystem of 'localized' electrons (inner-shell electrons of atoms located at crystal lattice sites) with magnetization $\mathbf{M}$. We believe that exchange interactions in the system of localized electrons can lead to the emergence of inhomogeneous magnetic ordering in the crystal, characterized by a spatially inhomogeneous magnetization distribution. We will consider the exchange interaction of conduction electrons and localized electrons in the simplest mean-field approximation.

To describe electron spin transport under the action of arbitrary electric $\mathbf{E}(\mathbf{r}, t)$ and magnetic $\mathbf{B}(\mathbf{r}, t)$ fields created by external sources, as well as a nonuniform internal exchange field $\mathbf{B}_\Lambda(\mathbf{r}, t) = \Lambda\mathbf{M}(\mathbf{r}, t)$, on conduction electrons, the quantum kinetic equation for the single-electron quantum distribution function $\hat{f}(\mathbf{r}, \mathbf{p}, t)$ can be used [97, 98, 270]:

$$\frac{\partial \hat{f}}{\partial t} + \mathbf{v} \cdot \frac{\partial \hat{f}}{\partial \mathbf{r}} + \frac{1}{2}\left\{\hat{\mathbf{F}}, \frac{\partial \hat{f}}{\partial \mathbf{p}}\right\} + \mu \frac{i}{\hbar}(\mathbf{B} + \mathbf{B}_\Lambda) \cdot \left[\hat{\boldsymbol{\sigma}}, \hat{f}\right] + \hat{\mathcal{R}} = 0 \,. \tag{24}$$

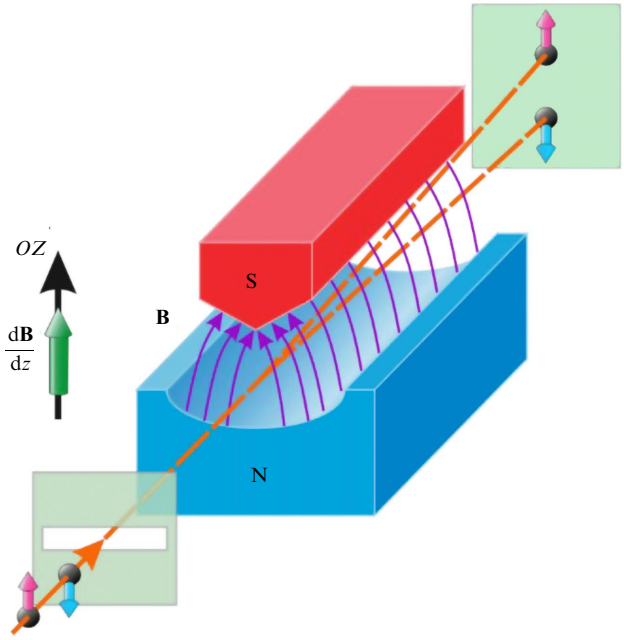

Figure 9. Schematic diagram of Stern and Gerlach experiment. Blue and pink arrows indicate directions of magnetic moment $\boldsymbol{\mu}$ of silver atoms. Stern and Gerlach experimentally demonstrated that particles with different magnetic moments $\boldsymbol{\mu}$, and therefore different spins, in nonuniform external magnetic field $\mathbf{B}(\mathbf{r})$ deviate from their original trajectory in different directions due to action of a force equal to $\nabla(\boldsymbol{\mu} \cdot \mathbf{B})$.

A quantum kinetic equation in a form similar to Eqn (24) was formulated and successfully used to describe spin-transport phenomena in paramagnetic metals by Silin [271] and by Azbel', Gerasimenko, and Lifshitz [272, 273].

In equation (24), the operator

$$\hat{\mathbf{F}} = e\mathbf{E} + \frac{e}{c}[\mathbf{v} \times \mathbf{B}] - \mu \frac{\partial}{\partial \mathbf{r}}(\mathbf{B} + \mathbf{B}_\Lambda) \cdot \hat{\boldsymbol{\sigma}} \tag{25}$$

describes the nondissipative mechanisms of changing $\hat{f}(\mathbf{r}, \mathbf{p}, t)$ under the action of the fields $\mathbf{E}$, $\mathbf{B}$, and $\mathbf{B}_\Lambda$, and the collision integral $\hat{\mathcal{R}}$ describes the relaxation of $\hat{f}$ to its instantaneous local equilibrium value. In equations (24) and (25), $\mathbf{v}$ is the electron velocity, $e = -|e|$ is the electron charge, $\mu = g\mu_B/2$ is the electron magnetic moment, $\hat{\boldsymbol{\sigma}}$ are the Pauli spin matrices, $[\hat{a}, \hat{b}] = \hat{a}\hat{b} - \hat{b}\hat{a}$ denotes the commutator, and $\{\hat{a}, \hat{b}\} = \hat{a}\hat{b} + \hat{b}\hat{a}$ denotes the anticommutator of the operators $\hat{a}$ and $\hat{b}$.

The quantities $\hat{f}(\mathbf{r}, \mathbf{p}, t)$ and $\hat{\mathbf{F}}(\mathbf{r}, \mathbf{p}, t)$ are operators in spin space whose matrix elements are considered to be functions of classical variables — the coordinate $\mathbf{r}$, the quasi-momentum $\mathbf{p}$, and the time t. The quantum distribution function $\hat{f}$ carries information about both the distribution of particles and the distribution of the spin of these particles. The first two terms in expression (25) for the operator $\hat{\mathbf{F}}$ are the well-known Lorentz force acting on conduction electrons from the fields $\mathbf{E}$ and $\mathbf{B}$. The third term, $-\mu(\partial/\partial\mathbf{r})(\mathbf{B} + \mathbf{B}_\Lambda) \cdot \hat{\boldsymbol{\sigma}}$, can be interpreted as a quantum correction to the classical Lorentz force arising in the inhomogeneous effective magnetic field $\mathbf{B}_\mathbf{m}^{(\mathrm{eff})} = \mathbf{B} + \Lambda\mathbf{M}$ acting on conduction electrons due to the presence of electron spin. It was precisely the action of such a quantum force on spin-bearing particles in a nonuniform external magnetic field that was discovered in the Stern–Gerlach experiments [274] (Fig. 9). The spin carriers in the Stern–Gerlach experiments were silver atoms freely moving in a vacuum.

Further in this review, we will consider electron transport under conditions where the mean free path of conduction electrons is the smallest parameter of the length dimension. In this case, we can move from describing the system in terms of the quantum distribution function $\hat{f}(\mathbf{r}, \mathbf{p}, t)$ to describing it in terms of 'average' quantities: the density of conduction electrons $n(\mathbf{r}, t) = \sum_{\mathbf{p}} \mathrm{Tr}\, \hat{f}(\mathbf{r}, \mathbf{p}, t)$, the spin density $\mathbf{s}(\mathbf{r}, t) = \sum_{\mathbf{p}} \mathrm{Tr}\, \hat{\boldsymbol{\sigma}} \hat{f}(\mathbf{r}, \mathbf{p}, t)$, the electron flux density $\mathbf{I}(\mathbf{r}, t) = \sum_{\mathbf{p}} \mathbf{v}\, \mathrm{Tr}\, \hat{f}(\mathbf{r}, \mathbf{p}, t)$, and the spin current density $\boldsymbol{J}(\mathbf{r}, t) = \sum_{\mathbf{p}} \mathbf{v} \otimes \mathrm{Tr}\, \hat{\boldsymbol{\sigma}} \hat{f}(\mathbf{r}, \mathbf{p}, t)$ In the above definitions, $\mathrm{Tr}\, \hat{A}$ denotes the operation of taking a trace of the matrix $\hat{A}$ with respect to the spin variables, the symbol $\boldsymbol{J}$, typed in bold italics, denotes a second-rank tensor, and the sign $\otimes$ denotes the tensor product of the corresponding quantities. Proceeding from the equation for $\hat{f}(\mathbf{r}, \mathbf{p}, t)$ to the equations for $n(\mathbf{r}, t)$, $\mathbf{s}(\mathbf{r}, t)$, $\mathbf{I}(\mathbf{r}, t)$, and $\boldsymbol{J}(\mathbf{r}, t)$ is described in detail in [97, 98, 270]. Here and below, we restrict ourselves to the case when $|\mathbf{B}_{\mathbf{m}}^{(\mathrm{eff})}| = B_{\mathbf{m}}^{(\mathrm{eff})} = \mathrm{const}$, and when the spin splitting energy $\mu B_{\mathbf{m}}^{(\mathrm{eff})}$ and the change in the chemical potential under the action of the fields $\mathbf{E}$, $\mathbf{B}$, and $\mathbf{B}_{\mathcal{A}}$ are small compared to the value of the equilibrium chemical potential. The system of coupled equations for n, $\mathbf{s}$, $\mathbf{I}$, and $\boldsymbol{J}$ obtained from equation (24) in [97] can be written in the following form:

$$\frac{\partial}{\partial t} n + \frac{\partial}{\partial \mathbf{r}} \cdot \mathbf{I} = 0\,, \tag{26}$$

$$\frac{\partial}{\partial t} \mathbf{s} + \frac{\partial}{\partial \mathbf{r}} \cdot \boldsymbol{J} + \left[\mathbf{s} \times (\boldsymbol{\Omega}_{\mathrm{L}} + \boldsymbol{\Omega}_{\mathcal{A}})\right] + \frac{1}{\tau_{\mathrm{S}}} \delta\mathbf{s} = 0\,, \tag{27}$$

$$\frac{\partial}{\partial t} \mathbf{I} + \frac{v_{\mathrm{F}}^2}{3} \frac{\partial}{\partial \mathbf{r}} \delta n - \frac{e}{m_{\mathrm{e}}} \mathbf{E} n - [\boldsymbol{\Omega}_{\mathrm{C}} \times \mathbf{I}] + \frac{\hbar}{2m_{\mathrm{e}}} \left(\frac{\partial}{\partial \mathbf{r}} \otimes (\boldsymbol{\Omega}_{\mathrm{L}} + \boldsymbol{\Omega}_{\mathcal{A}})\right) \cdot \delta\mathbf{s} + \frac{1}{\tau_{\mathrm{O}}} \mathbf{I} + \frac{1}{\tau_{\mathrm{SO}}} [\boldsymbol{\mathcal{E}} \times \cdot \boldsymbol{J}] = 0\,, \tag{28}$$

$$\frac{\partial}{\partial t} \boldsymbol{J} + \frac{v_{\mathrm{F}}^2}{3} \frac{\partial}{\partial \mathbf{r}} \otimes \delta\mathbf{s} - \frac{e}{m_{\mathrm{e}}} \mathbf{E} \otimes \mathbf{s} - [\boldsymbol{\Omega}_{\mathrm{C}} \times \boldsymbol{J}] + \left[\boldsymbol{J} \times (\boldsymbol{\Omega}_{\mathrm{L}} + \boldsymbol{\Omega}_{\mathcal{A}})\right] + \frac{\hbar}{2m_{\mathrm{e}}} \left(\frac{\partial}{\partial \mathbf{r}} \otimes (\boldsymbol{\Omega}_{\mathrm{L}} + \boldsymbol{\Omega}_{\mathcal{A}})\right) \delta n + \frac{1}{\tau_{\mathrm{O}}} \boldsymbol{J} - \frac{1}{\tau_{\mathrm{SO}}} [\boldsymbol{\mathcal{E}} \times \mathbf{I}] = 0\,. \tag{29}$$

Here, $\boldsymbol{\Omega}_{\mathrm{L}} = \gamma \mathbf{B}$, $\boldsymbol{\Omega}_{\mathcal{A}} = \gamma \mathbf{B}_{\mathcal{A}}$, $\boldsymbol{\Omega}_{\mathrm{C}} = (|e|/m_{\mathrm{e}}c)\mathbf{B}$, where $\gamma = 2\mu/\hbar$ is the gyromagnetic ratio. The quantity $\delta n = n - n_0$ in equations (27)–(29) is the deviation in the electron density n from its equilibrium value n_0, whereas $\delta\mathbf{s} = \mathbf{s} - \mathbf{s}_{\mathrm{L}}$ is the deviation in spin density $\mathbf{s}$ from its locally equilibrium value $\mathbf{s}_{\mathrm{L}} = -\chi(\mathbf{B} + \mathbf{B}_{\mathcal{A}})/\mu$, χ being the Pauli magnetic susceptibility of the electron gas. Equations (27)–(29) also involve the following quantities: m_{e} is the effective electron mass, v_{F} is the mean value of the electron velocity modulus, which in a degenerate electron gas coincides with the Fermi velocity, τ_{O} is the relaxation time for the momentum of electrons in their 'orbital' motion, τ_{S} is the spin relaxation time, and τ_{SO} is the time-dimensioned quantity characterizing skew spin scattering of electrons caused by the spin-orbital coupling. The symbols '$\otimes$,' '$\cdot$,' '$\times$,' and '$\times\cdot$' are used to denote the mathematical operations of tensor, scalar, and vector-scalar product of vectors and tensors (see [270] for details), the symbol $\boldsymbol{\mathcal{E}}$ denotes the unit tensor of second rank.

Details of deriving expressions for the times τ_{O}, τ_{S}, and τ_{SO} in terms of the matrix elements of the scattering amplitude operator, which is determined by the scattering potential and is found as a solution to the Lippmann–Schwinger equation, can be found in Refs [97, 98, 270]. Giving no specific expressions for τ_{O}, τ_{S}, and τ_{SO} here, we note only that these quantities in equations (27)–(29) can be considered phenomenological parameters to be determined by comparing the predictions of the theory based on these equations with experiment.

Equation (26) is the continuity equation for the electron flux [275]. The presence of two terms on the left-hand side of this equation reflects the fulfillment of the law of conservation of the number of particles: the rate of change of the particle density at a given point is equal to the divergence of the particle flux density vector at this point, taken with the opposite sign.

Equation (27) is the motion for the spin density. This equation can also be considered a continuity equation for the spin current; however, it allows for the possibility of spin dissipation, which is described by the last term on the left-hand side of this equation. The third term on the left-hand side of Eqn (27) describes the precessional motion of electrons with a frequency $|\boldsymbol{\Omega}_{\mathrm{L}} + \boldsymbol{\Omega}_{\mathcal{A}}|$. The second term describes the local change in spin density caused by spin transfer, which occurs when the spin current $\boldsymbol{J}$ flows from one region of space with a fixed spin density to another region with a spin density different in magnitude or direction. Due to the momentum relaxation time τ_{O} being small compared to the spin relaxation time τ_{S}, the above motion of the electron spin can be described as a diffusion process. In this case, the value of the spin diffusion coefficient is determined as $D = v_{\mathrm{F}}^2 \tau_{\mathrm{O}}/3$.

Equation (28) is for finding the electron flux density vector for given fields $\mathbf{E}$ and $\mathbf{B}$. The second term on the left-hand side of Eqn (28) describes the diffusion component of the electron flux, the magnitude of which is determined by the diffusion coefficient D. The third term describes the occurrence of conduction current due to the presence of an electric field $\mathbf{E}$, the magnitude of which is determined by the specific electrical conductivity of the conductor $\sigma_0 = n_0 e^2 \tau_{\mathrm{O}}/m_{\mathrm{e}}$. The fourth term describes the change in the electric current density due to the action of the Lorentz force, which forces electrons to move in cyclotron orbits with an angular velocity $\boldsymbol{\Omega}_{\mathrm{C}}$ and leads to the appearance of the classical Hall effect [276–278]. The fifth term is responsible for the change in the conductivity of the metal due to the coordinate dependence of the effective magnetic field $\mathbf{B} + \mathbf{B}_{\mathcal{A}}$ acting in the metal. It is this contribution that describes new galvanomagnetic effects in the conductivity of inhomogeneously magnetized conductors. The last term is responsible for the asymmetric spin scattering of electrons, the intensity of which is given by the time τ_{SO}. This term describes the specific features of the physical phenomenon known as the inverse spin Hall effect [12, 22, 23, 25, 26, 29–31].

Equation (29) is for finding the spin current tensor $\boldsymbol{J}$. The second term on the left-hand side of (29) describes the diffusion component of the spin flux, the value of which is determined by the spin diffusion coefficient D. The third term describes the effects of spin density drift under the action of an electric field. The fourth term, the vector product of the vector $\boldsymbol{\Omega}_{\mathrm{C}}$ and the spin current tensor $\boldsymbol{J}$, describes the influence of the Lorentz force, similar to the fourth term of Eqn (28). The fifth term, the vector product of the spin current tensor $\boldsymbol{J}$ and the vector $(\boldsymbol{\Omega}_{\mathrm{L}} + \boldsymbol{\Omega}_{\mathcal{A}})$, describes the spin precession of moving electrons. The sixth term describes the influence of inhomogeneities of the effective magnetic field $\mathbf{B} + \mathbf{B}_{\mathcal{A}}$ on spin transport. The last term describes the specific features of the physical phenomenon known as the 'spin Hall effect' [12, 22–26, 29, 31].

The system of coupled equations (26)–(29) can be used as a basis for describing a wide range of spin-transport phenomena in inhomogeneous conducting magnets with a given magnetization $\mathbf{M}(\mathbf{r}, t)$. It should be noted that equations (28)–(29) presented above for the charge flux and spin flux in the absence of inhomogeneous internal and external magnetic fields coincide with the phenomenological equations for the charge flux and spin flux obtained by Dyakonov and Perel [12, 22, 23].

For the following discussion, instead of equations involving the spin density **s**, it will be convenient to write equations expressed in terms of the magnetization of conduction electrons **m**. Note that the spin density of conduction electrons **s** and their magnetization **m** are related by the simple relation $\mathbf{m} = -\mu\mathbf{s}$. It is also convenient to introduce the following quantities: the electric current density vector $\mathbf{j} = e\mathbf{I}$ and the magnetization flux density tensor $\boldsymbol{J}_\mathbf{m} = -\mu\boldsymbol{J}$. For brevity, we will also call $\boldsymbol{J}_\mathbf{m}$ the spin current of conduction electrons. Then, Eqn (27) can be represented as

$$\frac{\partial}{\partial t}\,\mathbf{m} + \frac{\partial}{\partial \mathbf{r}}\cdot\boldsymbol{J}_\mathbf{m} + \gamma\,[\mathbf{m}\times\mathbf{B}] + \frac{1}{\tau_\mathrm{S}}\,\delta\mathbf{m} + \gamma\Lambda\,[\mathbf{m}\times\mathbf{M}] = 0\,, \tag{30}$$

where $\delta\mathbf{m} = \mathbf{m} - \mathbf{m}_\mathrm{L}$ represents the deviation of the magnetization of conduction electrons **m** from its local equilibrium value $\mathbf{m}_\mathrm{L} = \chi(\mathbf{B} + \Lambda\mathbf{M})$. Equation (30) is nothing more than the Bloch–Torrey equation [279] with the diffusion term $\partial/\partial\mathbf{r}\cdot\boldsymbol{J}_\mathbf{m}$, written for the case when the electron is under the action of an effective magnetic field $\mathbf{B}_\mathbf{m}^{(\mathrm{eff})} = \mathbf{B} + \Lambda\mathbf{M}$.

Further in our consideration, we will be interested in situations where the quantity δn, which characterizes the deviation of the system from the state of electroneutrality, can be considered negligibly small compared to the equilibrium value of the electron density n_0. This will allow us to formally omit all terms containing δn in equations (26)–(29). Below, to simplify the notation, we will omit the index '0' in the quantity n_0. We will also assume that the asymmetry of the spin-orbit scattering of conduction electrons is negligibly small, which allows us to omit the last terms on the left-hand sides of equations (28)–(29). The field **B** will be assumed to be uniform and constant throughout time.

The assumptions formulated above allow us to write the equations for the electric current density vector **j** and the magnetization flux density tensor $\boldsymbol{J}_\mathbf{m}$, which follow from Eqns (28)–(29), in the following form:

$$\frac{\partial}{\partial t}\,\mathbf{j} + \frac{e}{m_\mathrm{e}c}\,[\mathbf{B}\times\mathbf{j}] + \frac{1}{\tau_\mathrm{O}}\,\mathbf{j} = \frac{e^2 n}{m_\mathrm{e}}\,\mathbf{E} + \Lambda\,\frac{e}{m_\mathrm{e}}\left(\frac{\partial}{\partial\mathbf{r}}\otimes\mathbf{M}\right)\cdot\delta\mathbf{m}\,, \tag{31}$$

$$\frac{\partial}{\partial t}\,\boldsymbol{J}_\mathbf{m} + \frac{e}{m_\mathrm{e}c}\,[\mathbf{B}\times\boldsymbol{J}_\mathbf{m}] + \gamma\big[\boldsymbol{J}_\mathbf{m}\times(\mathbf{B}+\Lambda\mathbf{M})\big] + \frac{1}{\tau_\mathrm{O}}\,\boldsymbol{J}_\mathbf{m} = \frac{e}{m_\mathrm{e}}\,\mathbf{E}\otimes\mathbf{m} - \frac{v_\mathrm{F}^2}{3}\,\frac{\partial}{\partial\mathbf{r}}\otimes\delta\mathbf{m}\,. \tag{32}$$

Equation (30) for the magnetization of conduction electrons **m** together with Eqn (7) for the magnetization **M**, as well as Eqn (31) for the electric current **j**, Eqn (32) for the spin current of conduction electrons $\boldsymbol{J}_\mathbf{m}$, and Eqn (8) for the exchange spin current $\boldsymbol{J}_\mathbf{M}$ form the basic system of coupled equations for describing charge and spin transport in conducting chiral helimagnets.

5. Effect of helical magnetism on charge and spin transport

In this section, we describe the main features of charge and spin transport in conducting helimagnets, caused by the action of a constant nonuniform exchange field on conduction electrons.

5.1 Longitudinal magnetoresistance and electric current-induced electron magnetization of helimagnets

In this section, we present an overview of the results of applying the system of equations (30)–(32) to calculate the electrical resistance of helimagnets, as well as their nonequilibrium electron magnetization induced by a direct electric current flowing through the helimagnet. We will consider here only the case where the external magnetic field vector **B**, the electric field vector **E**, and the electric current density vector **j** are oriented along the axis of the magnetization helix, which coincides with the OZ axis, the direction of which will be specified by the unit vector $\mathbf{e}_z$. In this case, due to the symmetry of the problem, the magnetizations **m** and **M** depend only on the coordinate z. We assume that the magnetic helix $\mathbf{M} = \mathbf{M}(z)$ is in a state of equilibrium and its shape does not differ from that of the equilibrium helix $\mathbf{M}_0(z)$, described by equations (10). Below, the index '0' for the quantities q_0 and θ_0, which characterize the helix $\mathbf{M}_0(z)$, will be omitted to simplify the notation. For the helices $\mathbf{M}(z) = \mathbf{M}_\ell + \mathbf{M}_t(z)$ and $\mathbf{m}(z) = \mathbf{m}_\ell + \mathbf{m}_t(z)$, each of which is characterized by a wave vector **q**, the relations $\partial\mathbf{M}/\partial z = [\mathbf{q}\times\mathbf{M}]$ and $\partial\mathbf{m}/\partial z = [\mathbf{q}\times\mathbf{m}]$ are valid.

Then, the solution of equation (31) for the electric current density in the case under consideration can be written explicitly:

$$\mathbf{j} = \sigma\mathbf{E} - \Lambda\,\frac{e\tau_\mathrm{O}}{m_\mathrm{e}}\,\mathbf{e}_z\left(\mathbf{q}\cdot[\delta\mathbf{m}\times\mathbf{M}]\right), \tag{33}$$

where $\sigma = ne^2\tau_\mathrm{O}/m_\mathrm{e}$ is the specific electrical conductivity of the gas of free conduction electrons with a momentum relaxation time τ_O.

When considering equation (32) for the spin current $\boldsymbol{J}_\mathbf{m}$, we will assume that the cyclotron frequency $\Omega_\mathrm{C} = |e|B/m_\mathrm{e}c$, the Larmor frequency $\Omega_\mathrm{L} = \gamma B$, and the frequency $\Omega_\Lambda = \gamma\Lambda M$ are small compared to the momentum relaxation rate $1/\tau_\mathrm{O}$. Then, the solution of Eqn (32) can be represented as

$$\boldsymbol{J}_\mathbf{m} = \frac{e\tau_\mathrm{O}}{m_\mathrm{e}}\,\mathbf{E}\otimes\mathbf{m} - D\mathbf{e}_z\otimes[\mathbf{q}\times\delta\mathbf{m}]\,, \tag{34}$$

where $D = v_\mathrm{F}^2\tau_\mathrm{O}/3$ is the diffusion coefficient of free electron gas.

Substituting expression (34) into equation (30) for **m**, in the stationary case, we obtain the following system of equations for the longitudinal $\mathbf{m}_\ell$ and transverse $\mathbf{m}_t$ components of the electron magnetization:

$$\delta\mathbf{m}_\ell = -\tau_\mathrm{S}\gamma\Lambda\,[\delta\mathbf{m}_t\times\mathbf{M}_t]\,, \tag{35}$$

$$\left\{\nu_\mathrm{S} + \nu_\mathrm{D} + \nu_\mathrm{P}\left[\frac{(\mathbf{M}_t^2 - \mathbf{M}_t\otimes\mathbf{M}_t)}{M^2}\right]\right\}\cdot\delta\mathbf{m}_t + \gamma\big[\delta\mathbf{m}_t\times(\mathbf{B}+\Lambda\mathbf{M}_\ell)\big] + \frac{e\tau_\mathrm{O}}{m_\mathrm{e}}\,(\mathbf{E}\cdot\mathbf{e}_z)[\mathbf{q}\times\mathbf{m}_t] = 0\,. \tag{36}$$

When writing equation (36), the quantities ν_S, ν_D, and ν_P, which have the dimension of inverse time, are introduced into consideration: $\nu_\mathrm{S} = 1/\tau_\mathrm{S}$, $\nu_\mathrm{D} = q^2 D$, and $\nu_\mathrm{P} = \Omega_\Lambda^2\tau_\mathrm{S}$. Each of

these quantities characterizes the decay rate of the electron magnetization oscillations by one electron spin relaxation mechanism or another.

The quantity $\nu_S = 1/\tau_S$ represents the rate of spin-lattice relaxation, which results from the dissipation of the nonequilibrium spin of conduction electrons when they are scattered by defects in the crystal lattice. The corresponding spin relaxation mechanism is called the Elliot–Yafet mechanism.

The quantity $\nu_D = q^2 D$ characterizes the rate of change of the spin density at a given point in space due to the 'diffusion escape' of electron spins from this point. It is important to emphasize that spin diffusion in a conducting helimagnet is not a process of electrons 'flowing' from a region of space where the concentration of electrons with a given spin projection is high to a region where such electrons are fewer. In a helimagnet, the values of the nonequilibrium spin density vector at adjacent points along the helicoid axis differ only in direction, and, therefore, diffusion in this case ensures electron spin relaxation exclusively 'in direction.' This mechanism of spin relaxation of conduction electrons in helimagnets is naturally called 'diffusion.'

The quantity $\nu_P = \Omega_\Lambda^2 \tau_S$ characterizes the rate of change of the spin density of conduction electrons due to the specific features of the precessional motion of the spins of moving electrons in the effective exchange field of the helimagnet. The physical reason for the appearance of such a contribution is the Larmor precession of the electron spin under conditions where the axis of precessional motion changes its direction as the electron moves along the helicoid axis. This mechanism of spin relaxation of conduction electrons in helimagnets is naturally called 'precessional.'

Equation (36) for $\delta\mathbf{m}_t$ is essentially nonlinear. Considering the electric current density $\mathbf{j}$ to be a given quantity, from Eqns (33) and (36), one can find the relationship between the absolute values of the electric field E and the current density j of the form $E = \rho j$, where the quantity ρ, which we will henceforth call the electrical resistance for brevity, is, generally speaking, a nonlinear function of j.

For convenience, we introduce the electron drift velocity vector $\mathbf{w} = \mathbf{j}/en$. To characterize the direction of the drift velocity vector $\mathbf{w}$, we introduce the unit vector $\mathbf{i} = \mathbf{w}/w$, where $w = |\mathbf{w}|$. In Ref. [98], the authors of this review showed that, from the system of equations (33), (36), the following expression for the electrical resistance ρ of a helimagnet follows:

$$\rho = \rho_F + \rho_H R_B (1 + \varepsilon A_B)\,, \tag{37}$$

where

$$\rho_F = \frac{m_e}{ne^2\tau_O}\,, \tag{38}$$

$$\rho_H = \frac{\chi}{\nu_H}\left(\frac{q\Lambda M}{en}\right)^2, \tag{39}$$

$$R_B = \frac{\left(\nu_B^2 + \Omega_B^2 + (qw)^2\right)v^2\cos^2\theta}{\left(\nu_B^2 + \Omega_B^2 + (qw)^2\right)^2 - (2qw\Omega_B)^2}\,, \tag{40}$$

$$A_B = \frac{2qw\Omega_B}{\nu_B^2 + \Omega_B^2 + (qw)^2}\,, \tag{41}$$

$$\varepsilon = (\mathbf{k}\cdot\mathbf{e}_z)(\mathbf{b}\cdot\mathbf{e}_z)(\mathbf{i}\cdot\mathbf{e}_z) \equiv K(\mathbf{b}\cdot\mathbf{i})\,. \tag{42}$$

In definitions (37)–(41), the newly introduced quantities ρ_F, ρ_H, R_B, and A_B have the following physical meaning. The quantity ρ_F characterizes the electrical resistance of a helimagnet in the field of transition to the induced 'ferromagnetic' state (when the magnetic field B reaches the value $B_F = M(\mathcal{B} + \mathcal{D}^2/\mathcal{A})/(1 + \chi\Lambda)$ (see Section 2); ρ_H is the absolute value of the total magnetoresistance of the helimagnet (the difference between the values of electrical resistance at $B = 0$ and $B = B_F$) in the limit of small measuring currents; R_B is the relative magnetoresistance in the field B; and A_B is the magnetochiral anisotropy coefficient.

Expressions (39)–(41) for ρ_H, R_B, and A_B involve the effective precession frequency Ω_B, defined by the equation

$$\Omega_B = \Omega_L + \Omega_\Lambda \sin\theta\,, \tag{43}$$

as well as spin relaxation rates ν_H, ν, and ν_B, defined by the following relations:

$$\nu_H = \nu_S + \nu_D + \nu_P\,, \tag{44}$$

$$\nu^2 = (\nu_S + \nu_D)(\nu_S + \nu_D + \nu_P)\,, \tag{45}$$

$$\nu_B^2 = (\nu_S + \nu_D)(\nu_S + \nu_D + \nu_P\cos^2\theta)\,. \tag{46}$$

The quantity ν_H has the meaning of the effective spin relaxation frequency of conduction electrons in a helimagnet and is defined according to (44) as the sum of the spin relaxation rates ν_S, ν_D, and ν_P, characterizing three different spin relaxation mechanisms.

Considering ρ for fixed values of the external magnetic field $B = |\mathbf{B}|$ and the density of the current flowing through the helimagnet $j = |\mathbf{j}|$ to be a function of three vectors $\mathbf{k}$, $\mathbf{b}$, and $\mathbf{i}$, we obtain from equations (37)–(42) the following symmetry properties of the electrical resistance ρ:

$$\rho(\mathbf{k}, -\mathbf{b}, -\mathbf{i}) = \rho(-\mathbf{k}, \mathbf{b}, -\mathbf{i}) = \rho(-\mathbf{k}, -\mathbf{b}, \mathbf{i}) = \rho(\mathbf{k}, \mathbf{b}, \mathbf{i})\,. \tag{47}$$

The property of changing the sign of the quantity $\varepsilon = (\mathbf{k}\cdot\mathbf{e}_z)(\mathbf{b}\cdot\mathbf{e}_z)(\mathbf{i}\cdot\mathbf{e}_z)$ when changing the direction of one of the vectors $\mathbf{b}$, $\mathbf{i}$, or $\mathbf{k}$ has the following consequences:

(1) nonreciprocity effects, manifested in a change in the electrical resistance of a helimagnet with a given chirality when changing the direction of the electric current relative to the direction of the external magnetic field and when changing the direction of the magnetic field relative to the direction of the current:

$$\rho(\mathbf{k}, \mathbf{b}, -\mathbf{i}) \neq \rho(\mathbf{k}, \mathbf{b}, \mathbf{i})\,, \qquad \rho(\mathbf{k}, -\mathbf{b}, \mathbf{i}) \neq \rho(\mathbf{k}, \mathbf{b}, \mathbf{i})\,, \tag{48}$$

(2) the effect of magnetochiral anisotropy, manifested in the fact that the electrical resistance of a helimagnet has a different value for two samples of a helimagnet with different magnetic chirality, all other conditions being similar:

$$\rho(-\mathbf{k}, \mathbf{b}, \mathbf{i}) \neq \rho(\mathbf{k}, \mathbf{b}, \mathbf{i})\,. \tag{49}$$

According to equations (33)–(36), an electric current flowing along the axis of the helimagnet's helix induces nonequilibrium magnetization of conduction electrons $\delta\mathbf{m}$, which has a component $\delta\mathbf{m}_\ell$, directed along the axis of the magnetic helicoid. In Ref. [98], the authors of this review showed that

$$\delta\mathbf{m}_\ell = -\chi\,\frac{qw\nu_P}{\gamma\nu_H}\,R_B(K\mathbf{i} + \mathbf{b}A_B)\,. \tag{50}$$

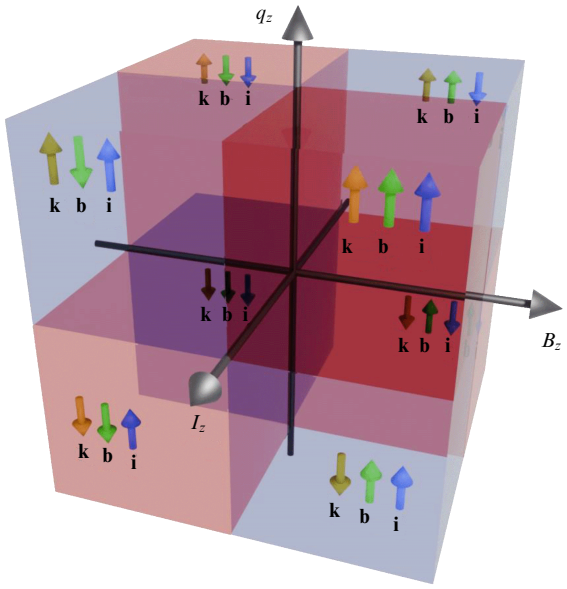

Figure 10. Diagram of chiral current states of helimagnet in magnetic field in variables q_z, I_z, B_z. Colored arrows indicate directions of unit vectors **k**, **b**, and **i**.

The total magnetization of a helical magnet is the sum of the magnetization of localized electrons **M** and the magnetization of conduction electrons **m**. For the longitudinal component $\mathbb{M}$ of the total magnetization, taking into account Eqn (50), we obtain [98]

$$\mathbb{M} = M_{\mathrm{B}}\mathbf{b} - \chi\,\frac{qwv_{\mathrm{P}}}{\gamma v_{\mathrm{H}}}\,R_{\mathrm{B}}K\mathbf{i}\,, \tag{51}$$

where $M_{\mathrm{B}} = (1+\chi\Lambda)M\sin\theta + \chi(B - qwv_{\mathrm{P}}R_{\mathrm{B}}A_{\mathrm{B}}/\gamma v_{\mathrm{H}})$.

Expression (51) describes the nonreciprocity effect, which manifests itself in the fact that the longitudinal magnetization of a helimagnet changes when the direction of current passing through the sample changes, $\mathbb{M}(\mathbf{k},\mathbf{b},-\mathbf{i}) \neq \mathbb{M}(\mathbf{k},\mathbf{b},\mathbf{i})$, as well as the magnetochiral anisotropy effect, which manifests itself in the fact that the longitudinal magnetizations of two helimagnets with different magnetic chirality have different values, all other conditions being the same: $\mathbb{M}(-\mathbf{k},\mathbf{b},\mathbf{i}) \neq \mathbb{M}(\mathbf{k},\mathbf{b},\mathbf{i})$.

To systematize the discovered effects, we constructed a diagram of the chiral current states of the helimagnet (Fig. 10). The variables in this diagram are $q_z \equiv \mathbf{q}\cdot\mathbf{e}_z$, $B_z \equiv \mathbf{B}\cdot\mathbf{e}_z$, and $I_z \equiv \mathbf{I}\cdot\mathbf{e}_z$. Colored arrows indicate the directions of the unit vectors **k**, **b**, and **i** corresponding to a given region. States for which $\varepsilon = +1$ are realized in regions marked in red; regions of states with $\varepsilon = -1$ are shown in blue. When moving from a region of one color to a region of another color, nonreciprocity effects (if the regions share a common vertical face) or magnetochiral anisotropy (if the regions share a common horizontal face) will manifest themselves.

Recall that the physical cause of the electrical magnetochiral and kinetic magnetoelectric effects in our consideration is the action of a spatially inhomogeneous exchange magnetic field on conduction electrons with spin. The influence of an external inhomogeneous magnetic field on moving particles with spin was first experimentally observed in the famous experiments of Stern and Gerlach [274]. To emphasize the physical nature of the mechanism of the electrical magnetochiral and kinetic magnetoelectric effects in helimagnets, we proposed to introduce special terms for their designation: 'Stern–Gerlach electrical magnetochiral effect' and 'Stern–Gerlach kinetic magnetoelectric effect,' respectively [98]. The introduction of such terms may also be motivated by the fact that there is a need to distinguish the above-mentioned effects from similar ones that arise due to the presence of a helical ordering of atoms in a crystal–crystalline chirality. The occurrence of the electrical magnetochiral effect due to the presence of crystalline chirality was discussed in [85, 280–283], and the kinetic magnetoelectric effect (there are papers in which this effect is called 'chirality-induced spin selectivity'), in [215, 284–293].

5.2 Determining magnetic chirality of helimagnets using electrical magnetochiral or kinetic magnetoelectric effects

In this section, we will demonstrate how the magnetic chirality of a helical magnet can be determined using the Stern–Gerlach electrical magnetochiral effect or the Stern–Gerlach kinetic magnetoelectric effect.

From expression (37), it follows that the electrical magnetochiral effect causes the electrical resistance of helical magnets to depend on their magnetic chirality, as well as on the relative orientation of the electric current and the external magnetic field along the helicoid axis. This property of the electrical resistance of a helical magnet can be used to determine the magnetic chirality of the magnetization helix. To do this, it is necessary to do the following:

(1) measure the electrical resistance of the helimagnet along the axis of the magnetization helix with the electric current and external magnetic field vectors configured in opposite directions: $\rho_{\mathbf{j}\downarrow\mathbf{B}} = \rho_{\mathrm{F}} + \rho_{\mathrm{H}}R_{\mathrm{B}}(1 + KA_{\mathrm{B}})$;

(2) measure the electrical resistance of the helimagnet along the axis of the magnetization helix with the electric current and external magnetic field vectors configured in the same direction: $\rho_{\mathbf{j}\uparrow\mathbf{B}} = \rho_{\mathrm{F}} + \rho_{\mathrm{H}}R_{\mathrm{B}}(1 - KA_{\mathrm{B}})$;

(3) find the difference between the obtained electrical resistances $\Delta\rho = \rho_{\mathbf{j}\downarrow\mathbf{B}} - \rho_{\mathbf{j}\uparrow\mathbf{B}}$:

$$\Delta\rho = 2\rho_{\mathrm{H}}R_{\mathrm{B}}A_{\mathrm{B}}K\,. \tag{52}$$

The sign of the difference between the obtained electrical resistances is equal to the sign of the magnetic chirality of the helimagnet: if $\Delta\rho > 0$, then $K = +1$ and this helimagnet has a right-handed magnetization helix; if $\Delta\rho < 0$, then $K = -1$ and this helimagnet has a left-handed magnetization helix.

From expression (51), it follows that the kinetic magnetoelectric effect causes the magnetization of the helimagnet along the helix axis to depend on its magnetic chirality and on the direction of current flow through the sample. This property of the magnetization of the helimagnet can also be used to determine the magnetic chirality of the magnetization helix.

In the absence of an external magnetic field, for the magnetization of helimagnets along the helical axis, from (51) we obtain

$$\mathbb{M}_0 = K\,\frac{\rho_{\mathrm{H}}}{\rho_{\mathrm{F}}}\,\frac{\tau_{\mathrm{S}}}{\tau_{\mathrm{O}}}\,\frac{m_{\mathrm{e}}\gamma}{q|e|}\,\mathbf{j}\,. \tag{53}$$

If the experimentally determined direction of helimagnet magnetization along the helical axis $\mathbb{M}_0$ coincides with the direction of electric current **j**, then the helimagnet has a magnetic chirality $K = +1$, corresponding to a right-handed

magnetization helix. If the direction of $\mathbb{M}_0$ is opposite to the direction of electric current $\mathbf{j}$, then the helimagnet has a magnetic chirality $K = -1$, corresponding to a left-handed magnetization helix.

The following protocol can be used for experiments with external magnetic fields:

(1) all measurements are performed with a fixed direction of electric current along the helix axis; only the direction of the external magnetic field can be changed;

(2) measure the total magnetization of the helimagnet along the helix axis with oppositely directed electric current and external magnetic field vectors: $\mathbb{M}_{\mathbf{j}\downarrow\uparrow\mathbf{B}}$;

(3) measure the total magnetization of the helimagnet along the helix axis with identically directed electric current and external magnetic field vectors: $\mathbb{M}_{\mathbf{j}\uparrow\uparrow\mathbf{B}}$;

(4) find the vector sum of the resulting magnetizations: $\Delta\mathbb{M} = \mathbb{M}_{\mathbf{j}\downarrow\uparrow\mathbf{B}} + \mathbb{M}_{\mathbf{j}\uparrow\uparrow\mathbf{B}}$:

$$\Delta\mathbb{M} = K\,\frac{\rho_{\mathrm{H}}}{\rho_{\mathrm{F}}}\,\frac{\tau_{\mathrm{S}}}{\tau_{\mathrm{O}}}\,\frac{2m_{\mathrm{e}}\gamma}{q|e|}\,R_{\mathrm{B}}\mathbf{j}\,. \tag{54}$$

The direction of the vector $\Delta\mathbb{M}$ turns out to be independent of the direction of the external magnetic field in which $\mathbb{M}_{\mathbf{j}\downarrow\uparrow\mathbf{B}}$ and $\mathbb{M}_{\mathbf{j}\uparrow\uparrow\mathbf{B}}$ are measured. If the experimentally determined direction of the total magnetization $\Delta\mathbb{M}$ turns out to coincide with the direction of the electric current $\mathbf{j}$, then the helimagnet under study has magnetic chirality $K = +1$, corresponding to a right-handed magnetization helix. If the direction of the total magnetization $\Delta\mathbb{M}$ turns out to be opposite to the direction of the flow of electric current $\mathbf{j}$, then the studied helimagnet has a magnetic chirality $K = -1$, corresponding to a left-handed helix of magnetization.

In the above consideration, we focused on the study of helimagnets in which a conical helix magnetic structure is formed under the action of an external magnetic field. However, it is worth noting that there are helimagnets in which the conical helix magnetic ordering is observed even in the absence of an external magnetic field. Examples of such 'conical' helimagnets include holmium and erbium. In such helimagnets, the direction of the vector $\mathbf{b}$ should be understood as the direction of the longitudinal magnetization. Thus, determining the magnetic chirality in such helimagnets does not require the use of an external magnetic field. However, determining the magnetic chirality in such helimagnets in the absence of an external magnetic field is possible only using the Stern–Gerlach electrical magnetochiral effect.

5.3 Numerical estimates of effect of helical magnetic order on electrical resistance and magnetization

In this section, we present the results of a numerical estimate of the theoretical parameters that determine the magnitude of the Stern–Gerlach electrical magnetochiral and Stern–Gerlach kinetic magnetoelectric effects. This estimate is based on the values of the characteristics of specific metallic helimagnets Dy, MnSi, $CrNb_3S_6$, and FeGe, calculated by the authors of this review in Ref. [99]. Columns 2–5 of Table 1 present the results of a numerical estimate of spin-lattice relaxation rate $\nu_{\mathrm{S}} = 1/\tau_{\mathrm{S}}$, diffusion rate $\nu_{\mathrm{D}} = q^2 D$, precession frequency $\nu_{\mathrm{P}} = \Omega_{\mathit{\Lambda}}^2\tau_{\mathrm{S}}$, and frequency $\Omega_{\mathrm{B_F}} = \Omega_{\mathrm{F}} + \Omega_{\mathit{\Lambda}}$ for each of these helimagnets.

Let us first estimate the value of $\rho_{\mathrm{H}}/\rho_{\mathrm{F}}$, which characterizes the relative magnetoresistance of a helimagnet — the difference between the electrical resistance values $\rho(B)$ at $B = 0$ and $B = B_{\mathrm{F}}$ divided by the value of $\rho_{\mathrm{F}} \equiv \rho(B_{\mathrm{F}})$. From Eqns (38), (39), when $\nu_{\mathrm{S}}, \nu_{\mathrm{D}} \ll \nu_{\mathrm{P}}$, we obtain

$$\frac{\rho_{\mathrm{H}}}{\rho_{\mathrm{F}}} = \frac{3}{4}\,\frac{\tau_{\mathrm{O}}}{\tau_{\mathrm{S}}}\left(\frac{q}{k_{\mathrm{F}}}\right)^2, \tag{55}$$

where $k_{\mathrm{F}} = (3\pi^2 n)^{1/3}$ is the Fermi wavenumber. The values of $\rho_{\mathrm{H}}/\rho_{\mathrm{F}}$ calculated using Eqn (55) are presented in the sixth column of Table 1. Since the momentum relaxation time τ_{O} is always shorter than the spin relaxation time τ_{S}, and the wavenumber of the magnetic helix q is always smaller than the Fermi wavenumber of electrons, the ratio $\rho_{\mathrm{H}}/\rho_{\mathrm{F}}$ for the metallic helimagnets under consideration turns out to be small. Therefore, experimental detection of the 'helimagnetic' contribution to the electrical resistance may be difficult. In this regard, a possible solution to the problem may be to use the sinusoidal current measurement technique tested in [192, 193, 195, 213].

Another quantity to be estimated is the magnetochiral anisotropy coefficient A_{B}, which directly determines the magnitude of the electrical magnetochiral effect. According to Eqn (41), the magnetochiral anisotropy coefficient A_{B} is a nonlinear function of the variable w: $A_{\mathrm{B}} = A_{\mathrm{B}}(w)$. For definiteness, we will estimate the coefficient A_{B} at the phase transition point in the field $B = B_{\mathrm{F}}$.

If the frequencies ν_{S}, ν_{D}, and ν_{P} significantly exceed the values $\Omega_{\mathrm{B_F}} = \Omega_{\mathrm{F}} + \Omega_{\mathit{\Lambda}}$ and qw, then $A_{\mathrm{B_F}}(w) \simeq 2qw\Omega_{\mathrm{B_F}}/\nu_{\mathrm{B_F}}^2 \ll 1$ and the value of $A_{\mathrm{B_F}}(w)$ turns out to be small compared to unity. If the spin relaxation rates ν_{S} and ν_{D} are significantly smaller than $\Omega_{\mathrm{B_F}}$, then the magnetochiral anisotropy coefficient $A_{\mathrm{B_F}}(w) \simeq 2qw\Omega_{\mathrm{B_F}}/[\Omega_{\mathrm{B_F}}^2 + (qw)^2]$. Obviously, when the condition $qw = \Omega_{\mathrm{B_F}}$ is satisfied, this magnetochiral anisotropy coefficient $A_{\mathrm{B_F}}(w)$ asymptotically approaches unity. Thus, if the relaxation frequencies ν_{S} and ν_{D} are significantly smaller than $\Omega_{\mathrm{B_F}}$, then, in the vicinity of the phase transition point $B = B_{\mathrm{F}}$, the magnetochiral anisotropy coefficient A_{B} can reach its maximum value of unity. In other words, the theory predicts the possibility of the existence of a giant electrical magnetochiral effect.

From equation (37) it follows that, to observe the giant electrical magnetochiral effect as $B \to B_{\mathrm{F}}$, in addition to the conditions described earlier, the condition $\varepsilon = +1$ must be satisfied, which happens when one of the vectors $\mathbf{k}$, $\mathbf{b}$, or $\mathbf{i}$ is co-directed with the vector $\mathbf{e}_z$, and the other two are co-

Table 1. Values of theoretical parameters for helimagnets Dy, MnSi, $CrNb_3S_6$, and FeGe (according to data from Ref. [99]).

Helimagnet	ν_{S}, s^{-1}	ν_{D}, s^{-1}	ν_{P}, s^{-1}	$\Omega_{\mathrm{B_F}}$, s^{-1}	$\rho_{\mathrm{H}}/\rho_{\mathrm{F}}$, %	$qw_{\max}$, s^{-1}	$A_{\max}$	$\mathbb{M}_{\max}$, G
1	2	3	4	5	6	7	8	9
Dy	5×10^{14}	3×10^{15}	2×10^{16}	3×10^{15}	2	2×10^{11}	6×10^{-5}	1×10^{-2}
MnSi	3×10^{13}	2×10^{15}	3×10^{15}	3×10^{14}	6×10^{-2}	3×10^{10}	4×10^{-6}	2×10^{-3}
$CrNb_3S_6$	1×10^{13}	4×10^{13}	4×10^{14}	8×10^{13}	1×10^{-1}	9×10^{11}	1×10^{-2}	1×10^{-2}
FeGe	9×10^{13}	3×10^{13}	1×10^{15}	3×10^{14}	8×10^{-3}	2×10^{10}	1×10^{-4}	9×10^{-4}

directed with each other. In particular, $\varepsilon = +1$ if all four vectors **k**, **b**, **i**, and $\mathbf{e}_z$ are co-directed. In Figure 10, the regions in which the existence of a giant electrical magnetochiral effect is possible are marked in red.

The effect of increasing the electrical resistance of the helix with increasing current density when the condition $qw = \Omega_B$ is reached has a transparent physical meaning. To clearly illustrate this effect, consider the situation where the vectors **k**, **b**, **i**, and $\mathbf{e}_z$ are aligned. In such a configuration, the magnetic moments of electrons moving along the helicoid axis with a drift velocity w will precess clockwise in the effective magnetic field directed along the helicoid axis with a precession frequency Ω_B. In a coordinate system moving with the electrons at a velocity w, the transverse component of the internal exchange field vector induced by the magnetization helix of localized electrons with a wave vector q will rotate clockwise with an angular velocity $\omega_w = qw$. When the frequencies Ω_B and ω_w coincide, the precession of the magnetic moments of the conduction electrons will occur synchronously with the change in the direction of the internal exchange field, which will lead to an increase in the electrical resistance of the helix.

Here, a direct analogy with the phenomenon of conduction electron spin resonance [14–21] suggests itself, in which a resonant enhancement of the absorption of the energy of an alternating external magnetic field by conduction electrons is observed when the frequency of the Larmor precession of electrons coincides with the frequency of the alternating field ω. In a helimagnet in which a stream of electrons with a velocity q flows along the axis of a helix with a wave vector w, the role of the frequency ω is played by the frequency $\omega_w = qw$. This analogy allows us to call the effect of nonmonotonic change in the chiral magnetoresistance of a helimagnet with increasing density of the measuring current 'magnetochiral kinetic resonance' [98].

In real helimagnets, the spin relaxation frequencies ν_S, ν_D, and ν_P can differ significantly from each other, as well as from the precession frequencies Ω_F and Ω_Λ. Consequently, the behavior of the electrical resistance of helimagnets is not limited to the two cases described above. We present here the results of estimates for $A_{B_F}(w)$, restricting ourselves to considering currents with a density $j \leqslant j_{max}$, where $j_{max} = 10^8$ A cm^{-2}. The drift velocity $w_{max} = j_{max}/|e|n$ corresponds to the current density j_{max}. The values of the parameter qw_{max} for the helimagnets under consideration are given in column 7 of Table 1.

It should be noted that achieving a high electric current density of the order of 10^8 A cm^{-2} in conducting helimagnets is a completely realistic task. Thus, in experiments [220, 294–298], currents with a density of $10^7 - 10^8$ A cm^{-2} were practically used to observe the motion of domain walls in metals, and in the review [299], the use of electric currents of the same magnitude for manipulating skyrmions was reported.

The values of $A_{max} \equiv A_{B_F}(w_{max})$ calculated according to Eqn (41) are given in column 8 of Table 1. For all the helimagnets considered, an estimate of the magnetochiral anisotropy coefficient gives $A_{max} \ll 1$. From Table 1, it is also evident that, in all the cases under consideration, the relations ν_S, ν_D, $\nu_P \gg qw_{max}$ are satisfied. Thus, in metallic helimagnets such as Dy, MnSi, $CrNb_3S_6$, and FeGe, one should not expect to detect a giant electric magnetochiral effect.

Let us finally estimate the magnitude of the magnetization $\mathcal{M}_{max} \equiv |\mathbb{M}_0(j_{max})|$, arising due to the kinetic magnetoelectric effect in the absence of an external magnetic field at a current $j = j_{max}$. When ν_S, $\nu_D \ll \nu_P$, we obtain

$$\mathcal{M}_{max} \simeq \frac{3}{4}\,\frac{q}{ck_F^2}\,j_{max}\,. \tag{56}$$

From (56), it is clear that, the smaller the helimagnet helix period, the greater magnetization $\mathcal{M}_{max}$ for a given current j_{max}. Numerical estimates of $\mathcal{M}_{max}$ in specific helimagnets, performed using Eqn (56), are presented in Table 1. In no case does $\mathcal{M}_{max}$ exceed an extremely small value of the order of 10^{-2} G.

However, it should be noted that Ref. [219] reported indirect evidence of the possibility of detecting a change in magnetization under the action of a flowing electric current using SQUID magnetometry methods. In addition, in some cases, the possibility of studying the change in magnetization under conditions of the kinetic magnetoelectric effect using nuclear magnetic resonance can be considered, as was done in Refs [285, 287].

6. Effect of charge and spin transport on helical magnetism

In this section, we describe the main features of magnetic dynamics and charge and spin transport in conducting helimagnets, arising from the transfer of spin moment when a direct electric current flows through them. Unlike Section 5, we will consider a situation in which the magnetizations of localized electrons **M** and conduction electrons **m** can both change over time under the influence of a current flowing through the helimagnet.

It should be noted that, in general, when describing the dynamics of current-induced magnetization, it is necessary to consider not only the influence of the spin-transfer torque effect on the magnetization, but also the 'Cherenkov' emission of spin waves. However, in this paper, we consider a time-constant macroscopic current whose magnitude is independent of the coordinate along the helimagnet's helical axis. Under such conditions, the electric current itself does not induce alternating electric and magnetic fields, which leads to the absence of amplification of spin waves under the influence of Cherenkov radiation.

Nevertheless, the electric current under consideration, via the $s-d$ exchange interaction and the spin-transfer torque effect, causes rotation of the magnetization helix, which leads to the generation of alternating electric and magnetic fields. These fields, in turn, can induce transverse alternating macroscopic currents and, on the other hand, can influence the dynamics of the helix rotation. As will be shown below, their influence leads to an effective increase in the Gilbert damping parameter in the equations of motion for the magnetization of the helimagnet.

6.1 Basic equations of magnetic dynamics of conducting helimagnets

The discussion is based on Eqn (7) for **M** and Eqn (30) for **m**, presented above in Sections 2 and 4. They form a system of interconnected equations that can be written as follows:

$$\frac{\partial \mathbf{M}}{\partial t} + \gamma\left[\mathbf{M} \times (\mathbf{B} + \mathbf{B}_a)\right] + \nabla \cdot \boldsymbol{J}_{\mathbf{M}} + \frac{\alpha}{M}\left[\frac{\partial \mathbf{M}}{\partial t} \times \mathbf{M}\right] + \mathbf{T}_{\mathbf{M}} = 0\,, \tag{57}$$

$$\frac{\partial}{\partial t}\,\mathbf{m} + \gamma\left[\mathbf{m} \times \mathbf{B}\right] + \nabla \cdot \boldsymbol{J}_{\mathbf{m}} + \frac{1}{\tau_S}\,\delta\mathbf{m} + \mathbf{T}_{\mathbf{m}} = 0\,. \tag{58}$$

Equations (57) and (58) involve the tensors of the exchange spin current $\boldsymbol{J}_{\mathbf{M}}$ and the spin current of conduction electrons $\boldsymbol{J}_{\mathbf{m}}$, which are defined by the following relations:

$$\boldsymbol{J}_{\mathbf{M}} = -\gamma\mathcal{A}\left[(\nabla\otimes\mathbf{M})\times\mathbf{M}\right] + 2\gamma\mathcal{D}\mathbf{M}\otimes\mathbf{M}\,, \tag{59}$$

$$\boldsymbol{J}_{\mathbf{m}} = \frac{e\tau_{\mathrm{O}}}{m_{\mathrm{e}}}\,\mathbf{E}\otimes\mathbf{m} - D\nabla\otimes\delta\mathbf{m}\,. \tag{60}$$

The last term $\mathbf{T}_{\mathbf{M}}$ on the left-hand side of equation (57) is determined by the equation

$$\mathbf{T}_{\mathbf{M}} = \gamma\Lambda\,[\mathbf{M}\times\mathbf{m}] \tag{61}$$

and describes the effect of spin transfer from the system of itinerant electrons to the system of localized electrons. The vector $\mathbf{T}_{\mathbf{M}}$ has the meaning of the torque acting on the magnetization $\mathbf{M}$ of localized electrons from conduction electrons with magnetization $\mathbf{m}$, generating a nonuniform exchange field $\Lambda\mathbf{m}$. Similarly, the term $\mathbf{T}_{\mathbf{m}}$ in (58), defined by the equation

$$\mathbf{T}_{\mathbf{m}} = \gamma\Lambda\,[\mathbf{m}\times\mathbf{M}]\,, \tag{62}$$

is nothing but the vector of the torque acting on the magnetization of conduction electrons from localized electrons via the exchange field $\Lambda\mathbf{M}$. From definitions (61) and (62), it is obvious that $\mathbf{T}_{\mathbf{m}} = -\mathbf{T}_{\mathbf{M}}$.

The density of the electric current $\mathbf{j}$ flowing in a helimagnet is related to the electric field $\mathbf{E}$ acting in the metal and the magnetizations $\mathbf{M}$ and $\mathbf{m}$ by a constitutive equation of the form

$$\mathbf{j} = \sigma\mathbf{E} + \Lambda\,\frac{e\tau_{\mathrm{O}}}{m_{\mathrm{e}}}\,(\nabla\otimes\mathbf{M})\cdot\delta\mathbf{m}\,. \tag{63}$$

Since the change in time and space of the total magnetization of the system $\mathbf{M}+\mathbf{m}$ generates a nonuniform alternating electromagnetic field, the above system of coupled equations (57)–(63) should generally be solved jointly with Maxwell's equations for the magnetic $\mathbf{B}$ and electric $\mathbf{E}$ fields:

$$\begin{aligned}
&[\nabla\times\mathbf{B}] = \frac{4\pi}{c}\mathbf{j} + 4\pi\big[\nabla\times(\mathbf{M}+\mathbf{m})\big] + \frac{1}{c}\,\frac{\partial\mathbf{E}}{\partial t}\,,\\
&[\nabla\times\mathbf{E}] = -\frac{1}{c}\,\frac{\partial\mathbf{B}}{\partial t}\,, \qquad \nabla\cdot\mathbf{B} = 0\,, \qquad \nabla\cdot\mathbf{E} = 4\pi e\delta n\,.
\end{aligned} \tag{64}$$

6.2 Spin-transfer torque and rotation of magnetization helix in helimagnet under electric current

In Ref. [99], the authors of this review showed that, for a helimagnet in which an electric current of a given density $\mathbf{j}$ and a magnetic field $\mathbf{B}$ are directed along the axis of the magnetic helix OZ, the system of Eqns (57), (58) can have a solution in the form of two coupled coaxial magnetic helices $\mathbf{M}(z,t)$ and $\mathbf{m}(z,t)$, the axis of which is determined by the unit vector $\mathbf{e}_z$. This solution corresponds to excitation of the Goldstone mode of a spin wave with the wave vector $\mathbf{Q} = \pm\mathbf{q}$, in which both helices rotate around their axis as a single whole. In this case, the helices are characterized by the same wave vector $\mathbf{q}$ and can rotate harmonically synchronously around a common axis with an angular frequency ω. For such a solution, the relations $\partial\mathbf{M}/\partial t = \omega[\mathbf{M}\times\mathbf{e}_z]$ and $\partial\mathbf{M}/\partial z = [\mathbf{q}\times\mathbf{M}]$ (and similar ones for $\mathbf{m}$) are valid, the substitution of which into Eqns (57), (58) makes it possible to write a dispersion equation determining the rotation frequency of the helices as a function of the wave vector $\mathbf{q}$ for a given current density $\mathbf{j}$.

In Ref. [99], it was shown that a constant electric current of density $\mathbf{j}$ flowing through a helimagnet leads to the rotation of the helimagnet's magnetization helix around its axis with a frequency ω, which depends on the magnitude of $\mathbf{j}$ and the magnetic field $\mathbf{B}$. In addition, the flowing electric current, simultaneously with the rotation of the magnetic helix, transforms the 'simple helix' magnetic structure into a 'conical helix' type structure. The cone angle θ, by which the magnetization $\mathbf{M}$ deviates from the plane perpendicular to the helix axis during rotation, is related to the rotation frequency ω of the helix by a simple formula:

$$\theta = \arcsin\frac{\omega + \Omega_{\mathrm{L}}(\mathbf{b}\cdot\mathbf{e}_z)}{\Omega}\,, \tag{65}$$

where $\Omega_{\mathrm{L}} = \gamma B$ is the Larmor precession frequency in the field B, $\Omega = \Omega_{\mathrm{F}} + \Omega_{\mathrm{M}}$, $\Omega_{\mathrm{F}} = \gamma B_{\mathrm{F}}$, $\Omega_{\mathrm{M}} = 4\pi\gamma M$.

In addition to the rotation of the helix $\mathbf{M}$ and the change in the cone angle θ, the current flowing through the helimagnet also changes the period of the helix. If the conditions $\chi\Lambda \ll 1$, $w/qD \ll 1$, and $\omega/\Omega_\sigma \ll 1$ are satisfied, where $\Omega_\sigma = q^2c^2/4\pi\sigma$, in conducting helimagnets, where exchange stiffness $\mathcal{A}$ is sufficiently large and the condition $\mathcal{A}q_0^2 \gg 1$ is satisfied, the deviation of the wave number q from the equilibrium value q_0 is small and can be ignored, setting $q = q_0$. In such helimagnets, the relationship between the rotation frequency of the magnetization helix ω and the drift velocity of conduction electrons $\mathbf{w}$ can be written as

$$\omega = \frac{\mathcal{T}_{\mathrm{eff}}}{\alpha_{\mathrm{eff}} + \mathcal{T}_{\mathrm{eff}}}\,(\mathbf{q}\cdot\mathbf{w})\,, \tag{66}$$

where $\mathcal{T}_{\mathrm{eff}} = \chi\Lambda\Omega_\Lambda/v_{\mathrm{eff}}$ is a dimensionless quantity characterizing the efficiency of the spin-transfer torque process in the helimagnet,

$$v_{\mathrm{eff}} = v_{\mathrm{S}} + v_{\mathrm{D}} + \frac{\Omega_\Lambda^2}{v_{\mathrm{S}}}\cos^2\theta + \frac{(\Omega+\Omega_\Lambda)^2}{v_{\mathrm{S}}+v_{\mathrm{D}}}\sin^2\theta\,, \tag{67}$$

and $\alpha_{\mathrm{eff}} = \alpha + \beta$ is the effective Gilbert damping constant, where $\beta = \Omega_{\mathrm{M}}/\Omega_\sigma$ is the parameter of magnetic oscillation damping because of losses caused by excitation of the electromagnetic field. Formally, relation (66) is a nonlinear equation for determining ω, since expression (67) for v_{eff} contains a dependence on the angle θ, which in turn is determined from equation (65), which contains the frequency ω.

It should be noted that, when deriving expressions (66) and (67), we disregarded the possibility of nonreciprocity effects that could cause the rotation frequency to depend on the direction of the current along the helix axis. This approximation is possible because in metallic helimagnets the condition $w/qD \ll 1$ is satisfied, under which the effects of nonreciprocity of the helix rotation are insignificant.

Equation (66) clearly describes the transformation of the linear motion of conduction electrons moving in space with a drift velocity $\mathbf{w}$ into rotational motion of the magnetic helix of a helimagnet with a frequency ω. Recalling the mechanical analogy of a helimagnet with Heron's windmill, described in the introduction, a spin device that implements this effect can be called a 'chiral spin-current turbine.'

It should be especially noted that Eqn (66) also describes the inverse effect: the rotation of the magnetic helix of a helimagnet, created by an external electromagnetic field with

a frequency ω, can be transformed into a direct electric current, the carriers of which are conduction electrons with a drift velocity $\mathbf{w}$. This inverse effect can be described by the equation that follows from (66),

$$\mathbf{w} = \left(1 + \frac{\alpha_{\text{eff}}}{\mathcal{T}_{\text{eff}}}\right)\frac{\omega}{q}\,\mathbf{k}\,. \tag{68}$$

A spin device that implements this effect can be called a 'spin-current Archimedes screw.'

From equation (66), it clearly follows that the sign of the rotation frequency of the helicoid, arising under the action of electron motion with a transport velocity $\mathbf{w}$, is determined by the sign of the scalar product $(\mathbf{k}\cdot\mathbf{i})$, in which $\mathbf{k}$ is the unit chirality vector, and $\mathbf{i} = \mathbf{w}/w$ is the unit vector in the direction of motion of the conduction electron flow.

In Ref. [99], the authors showed that considering the generation of an electromagnetic field when calculating the rotation frequency of a magnetic helix amounts to an effective increase in the Gilbert damping parameter: the quantity α is replaced by $\alpha_{\text{eff}} \equiv \alpha + \beta > \alpha$. It was shown that the absolute value of the Umov–Poynting vector, which specifies the direction of propagation of the electromagnetic field energy generated in a chiral helimagnet by a flowing electric current, in the approximations under consideration can be represented in the form

$$U \simeq 4\pi\,\frac{w^3 M^2}{c^2}\left(\frac{\mathcal{T}_{\text{eff}}}{\alpha_{\text{eff}} + \mathcal{T}_{\text{eff}}}\right)^3 \cos^2\theta\,. \tag{69}$$

It was also established that the direction of radiation propagation, coinciding with the direction of the Umov–Poynting vector, always coincides with the direction of the electron flux vector $\mathbf{i}$, regardless of the helimagnet chirality.

From the form of Eqn (65), it clearly follows that the condition for the validity of result (66) is the inequality $|\omega + \Omega_{\text{L}}(\mathbf{b}\cdot\mathbf{e}_z)| \leqslant \Omega$. The fulfillment of this condition depends on the direction of the magnetic field $\mathbf{b}$ and its magnitude B, which specifies the value of the Larmor frequency Ω_{L}. For definiteness, let the vectors $\mathbf{b}$ and $\mathbf{e}_z$ be antiparallel and $\Omega_{\text{L}} \leqslant \Omega$. Then, the condition for applicability of the obtained equations can be written as $-\Omega + \Omega_{\text{L}} \leqslant \omega \leqslant \Omega + \Omega_{\text{L}}$. If the vectors $\mathbf{b}$ and $\mathbf{e}_z$ are parallel, this condition is written as $-\Omega - \Omega_{\text{L}} \leqslant \omega \leqslant \Omega - \Omega_{\text{L}}$. Thus, a constant electric current flowing in a helimagnet can excite rotation of the helimagnet's magnetic helix, the frequency of which can reach a maximum value $\omega_{\max} = \Omega + \Omega_{\text{L}}$. From the form of Eqns (65) and (66), it also follows that harmonic rotational motion of the helimagnet's magnetic helix under the action of the flowing electric current is possible only under the condition that the current density not exceed a certain critical value. We will illustrate all of the above conditions in the next section using a simple example in the absence of an external magnetic field.

6.3 Magnetic helix dynamics in the absence of external magnetic field

In this section, we illustrate the behavior of the rotation frequency ω with a change in the current density j for the case in which there is no external magnetic field. In the absence of an external magnetic field, equations (65) and (66) are valid in the frequency range $|\omega| \leqslant \Omega$. The maximum possible value of the helicoid rotation frequency is determined by the value $\Omega \equiv \Omega_{\text{F}} + \Omega_{\text{M}}$. From Eqns (65) and (66), it follows that the flow of electric current along the axis of the magnetic helix leads not only to its rotation, but also to a change in the shape of the helix. The cone angle of the helix set in rotation with a frequency ω, according to (65), is determined by the equation

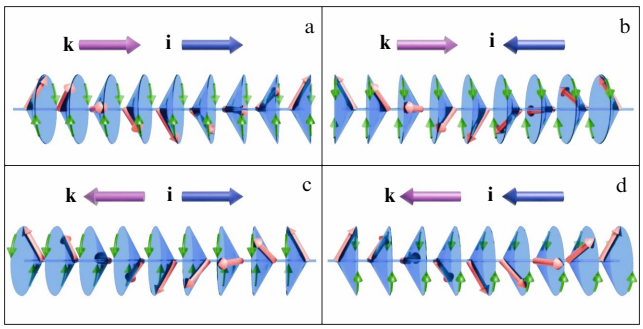

Figure 11. Schematic diagram of configurations of conical magnetic helix of helimagnet with chirality $\mathbf{k}$, rotating under the action of electron flow, direction of which is determined by unit vector $\mathbf{i}$, in the absence of magnetic field: (a) right-handed, $\mathbf{i} \uparrow\uparrow \mathbf{k}$; (b) right-handed, $\mathbf{i} \uparrow\downarrow \mathbf{k}$; (c) left-handed, $\mathbf{i} \uparrow\downarrow \mathbf{k}$; (d) left-handed, $\mathbf{i} \uparrow\uparrow \mathbf{k}$. Directions of red arrows correspond to directions of magnetic moments of localized electrons. Green arrows indicate direction of rotation of magnetic helix.

$$\theta = \arcsin\frac{\omega}{\Omega}\,. \tag{70}$$

From equation (66), it clearly follows that the sign of the helical rotation frequency ω is determined by the sign of the scalar product $(\mathbf{k}\cdot\mathbf{i})$, in which $\mathbf{k}$ is the chirality vector and $\mathbf{i}$ is the unit vector in the direction of the electron flow.

The dependence of the direction of rotation of the magnetization helix of a helimagnet and its conical configuration on the relative orientation of the chirality vectors $\mathbf{k}$ and the flux vector $\mathbf{i}$ in the absence of an external magnetic field is schematically shown in Fig. 11.

Let us introduce the dimensionless variables $\overline{\omega} \equiv \omega/\Omega$ and $\bar{j} \equiv (\mathbf{q}\cdot\mathbf{w})/\Omega$. Then, according to (70), $\theta = \arcsin\overline{\omega}$, and equation (66), which is the condition for the existence of time-periodic solutions to the system of equations (57), (58) describing the in-phase rotation of the magnetic helices $\mathbf{M}(z,t)$ and $\mathbf{m}(z,t)$ with frequency ω, can be written in the following form:

$$\left\{1 + a\left[\overline{v}_0 + (\overline{v}_1 - \overline{v}_0)\overline{\omega}^2\right]\right\}\overline{\omega} = \bar{j}\,, \tag{71}$$

where $a = \alpha_{\text{eff}}/\chi\Lambda$, $\overline{v}_0 = \overline{v}_{\text{S}} + \overline{v}_{\text{D}} + 1/\overline{v}_{\text{S}}$, $\overline{v}_1 = \overline{v}_{\text{S}} + \overline{v}_{\text{D}} + (1 + \Omega/\Omega_\Lambda)^2/(\overline{v}_{\text{S}} + \overline{v}_{\text{D}})$, $\overline{v}_{\text{S}} = v_{\text{S}}/\Omega_\Lambda$, $\overline{v}_{\text{D}} = v_{\text{D}}/\Omega_\Lambda$.

In the case where $\bar{j} \ll 1$ (i.e., when a low-density electric current with $j \ll j_0$, where $j_0 = \Omega|e|n/q$, flows in the helimagnet), we find from Eqn (71) that the relationship between the rotation frequency of the magnetization helix ω and the drift velocity of conduction electrons $\mathbf{w}$ is linear and can be written as

$$\omega = \frac{\mathcal{T}}{\alpha_{\text{eff}} + \mathcal{T}}\,(\mathbf{q}\cdot\mathbf{w})\,, \tag{72}$$

where $\mathcal{T} = \chi\Lambda\Omega_\Lambda/v_{\text{H}}$ is a dimensionless quantity characterizing the efficiency of spin-transfer torque in the helimagnet.

At high values of electric current density ($j > j_0$), depending on the ratio of parameters characterizing the helimagnet, such as the helix period, the spin relaxation time, and the Gilbert damping constant, the change in rotation frequency

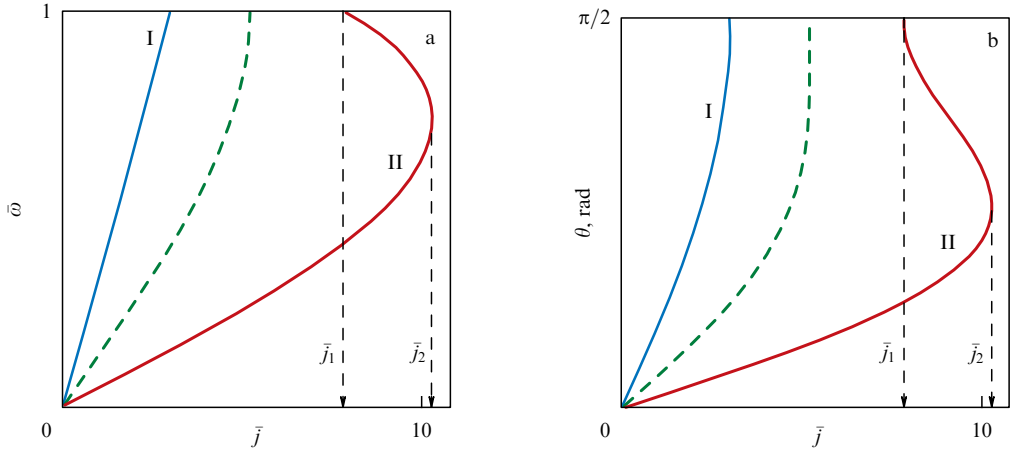

Figure 12. Illustration of two scenarios for behavior of rotation frequency (a) and cone angle (b) of magnetization helix with change in current density $\bar{j}$. Curves I correspond to scenario I; curves II represent scenario II; dashed curves correspond to boundary between regions of existence of scenarios I and II.

with increasing electric current density is not linear and can occur according to two different scenarios.

The first is realized when the inequality $a(2\bar{v}_0 - 3\bar{v}_1) < 1$ is satisfied. Under these conditions, a monotonic increase in the rotation frequency of the magnetization helix of the helimagnet ω and the cone angle of the helix θ is realized with an increase in the electric current density j.

The second scenario is realized when $a(2\bar{v}_0 - 3\bar{v}_1) > 1$. When it is realized in helimagnets, there is a region of electric current densities $\bar{j}_1 \leqslant \bar{j} \leqslant \bar{j}_2$, where $\bar{j}_1 = (1 + a\bar{v}_1)$, $\bar{j}_2 = 2(1 + a\bar{v}_0)^{3/2}/3\sqrt{3a(\bar{v}_0 - \bar{v}_1)}$, in which a phenomenon occurs that we have given the name 'spin rotational bistability of helimagnets.' This is a phenomenon in which the magnetic helix of a helimagnet can simultaneously be in two states with different rotation frequencies at the same value of current density.

Figure 12 shows the dependences of the magnetization helix rotation frequency $\overline{\omega}$ and the cone angle θ on the current density $\bar{j}$ with $a = 1$ and $\bar{v}_D = 0.1$ (these values of the parameters a and $\bar{v}_D$ are relevant for helimagnets with properties similar to $CrNb_3S_6$). Curves I correspond to scenario I with $\bar{v}_S = 1$. Scenario II is realized at $\bar{v}_S < 0.09$. Curves II correspond to scenario II with $\bar{v}_S = 0.05$. The dashed lines show the boundary between the regions of the existence of scenarios I and II when $\bar{v}_S = 0.09$.

Figure 12 shows that, in the region $\bar{j}_1 \leqslant \bar{j} \leqslant \bar{j}_2$, the spin-rotational bistability regime of helimagnets is realized. The developed theory does not answer the question of which of these two excited states of a rotating magnetic helix will be realized in the experiment at $\bar{j}_1 \leqslant \bar{j} \leqslant \bar{j}_2$. It can be assumed that current density fluctuations, spatial inhomogeneities in the momentum and electron spin relaxation parameters, and other random factors existing in a real helimagnet will cause time-chaotic transitions between states with different rotation frequencies. At $\bar{j} > \bar{j}_2$, equation (71) has no solutions describing harmonic rotation of the helimagnet's magnetization helix.

6.4 Electrical resistance of chiral helimagnet under spin-transfer torque conditions

By substituting the relationship between the magnetization of localized electrons **M** and the magnetization of conduction electrons **m**, found by joint solution of equations (57), (58), into expression (63), which relates the electric current density **j** and the electric field **E**, we can find the electrical resistance ρ of the helimagnet, with the effect of spin-transfer torque taken into account. In the absence of an external magnetic field, where the vectors **E** and **j** are oriented along the axis of the magnetization helix, assuming the frequencies Ω_C, Ω_L, and Ω_A to be small compared to the momentum relaxation rate $1/\tau_O$, we obtain [100]

$$\rho = \rho_F + \rho_S\,, \tag{73}$$

where ρ_F is the electrical resistance of the helimagnet in the field of transition to the induced 'ferromagnetic' state, and ρ_S is the spin contribution to the electrical resistance caused by the nonuniform exchange field of the magnetic helix and the STT effect, which is a function of the cone angle θ and is defined as

$$\rho_S(\theta) = \frac{Mq^2}{\gamma e^2 n^2}\,\frac{\alpha_{\rm eff}\cos^2\theta}{1 + \alpha_{\rm eff}(\bar{v}_0\cos^2\theta + \bar{v}_1\sin^2\theta)/\chi\Lambda}\,. \tag{74}$$

From the form of Eqn (74), it follows that the spin contribution ρ_S depends on the magnitude of the electric current j flowing through the helimagnet only due to the dependence of the cone angle j on θ.

For small values of current density ($j \ll j_0$), we obtain from (74)

$$\rho_S = \frac{Mq^2}{\gamma e^2 n^2}\,\frac{\alpha_{\rm eff}}{1 + \alpha_{\rm eff}/\mathcal{T}}\,. \tag{75}$$

From (75), it is clear that, if the effective Gilbert damping constant $\alpha_{\rm eff}$ has a significant value, such that the inequality $\alpha_{\rm eff} \gg \mathcal{T}$ is satisfied, then the rotation of the magnetization helix under the action of the flowing electric current is hindered. In this case, the contribution to the electrical resistance arising from the presence of the helix is directly determined by the magnitude of the effective spin relaxation frequency in the helimagnet ν_H:

$$\rho_S = \frac{\chi\Lambda^2 M^2 q^2}{e^2 n^2 \nu_H}\,. \tag{76}$$

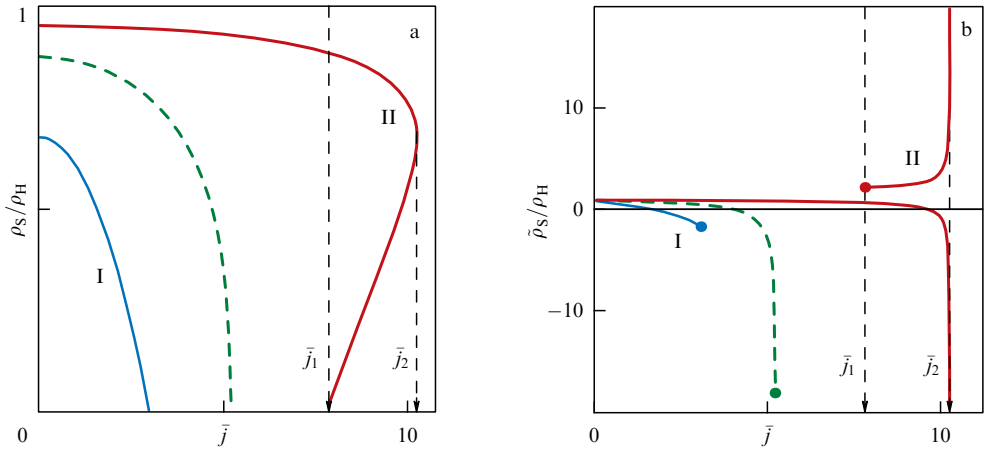

Figure 13. Behavior of relative electrical resistance ρ_S/ρ_H (a) and relative differential electrical resistance $\tilde{\rho}_S/\rho_H$ (b) with change in current density $\bar{j}$. Curves I represent scenario ($\bar{v}_S = 1$); curves II correspond to scenario II ($\bar{v}_S = 0.05$); dashed curves in green correspond to boundary between regions of existence of scenarios I and II ($\bar{v}_S = 0.15$).

In the opposite limiting case, when $\alpha_{eff} \ll \mathcal{T}$, the weak damping of the oscillations of the magnetic helix of the helimagnet leads to the fact that it easily 'adapts' to the motion of the magnetization of conduction electrons and therefore, the smaller the value of the effective Gilbert damping parameter α_{eff}, the smaller the contribution to the electrical resistance. In this case, the contribution to the electrical resistance arising from the presence of a magnetization helix rotating under the action of the STT effect can be written as

$$\rho_S = \frac{\alpha_{eff} M q^2}{\gamma e^2 n^2} . \qquad (77)$$

At high values of electric current density, Eqn (74) predicts the existence of nonlinear effects in the electrical resistance of the helix. In paper [100] by the authors of this review, it was shown that, depending on the ratio of the parameters characterizing the helimagnet, such as the period of the helix, the spin relaxation time, and the value of the Gilbert damping constant, the change in the contribution to the electrical resistance ρ_S, described by Eqn (74), can occur according to two different scenarios.

The first one (implemented when the condition $a(2\bar{v}_0 - 3\bar{v}_1) < 1$) is met) is a monotonic decrease in the spin contribution to the resistance of the helix magnet with increasing electric current density (see curve I in Fig. 13a).

When the second scenario is implemented (when $a(2\bar{v}_0 - 3\bar{v}_1) > 1$), there is a region of electric current densities $\bar{j}_1 \leqslant \bar{j} \leqslant \bar{j}_2$ in which a phenomenon arises that we have named 'spin electrical bistability of helimagnets.' This is a phenomenon in which a helimagnet can simultaneously be in two states with different values of electrical resistance at the same value of electric current density (see curve II in Fig. 13a).

The current-voltage characteristic of a helimagnet under conditions of electrical bistability is significantly nonlinear. To demonstrate the extent of this nonlinearity, in addition to the specific electrical resistance $\rho = E/j$, the specific differential electrical resistance of the helimagnet $\tilde{\rho} = \partial E/\partial j$ was found [100]. The differential electrical resistance $\tilde{\rho}_S$ can be represented as $\tilde{\rho} = \rho_F + \tilde{\rho}_S$, where $\tilde{\rho}_S$ is the contribution of the rotating spin helix. The behavior of $\tilde{\rho}_S$ is illustrated in Fig. 13b. The spin contribution $\tilde{\rho}_S$, and with it the differential electrical resistance of the helimagnet $\tilde{\rho}$, can have negative values of arbitrarily large magnitude. Thus, we have demonstrated that helimagnets may be of interest for micro- and nanoelectronics as materials that, under certain conditions, have negative differential electrical resistance [300–302].

6.5 Numerical estimates of influence of spin-transfer torque on magnetization dynamics of helimagnets

In Ref. [99], the authors of this review performed a numerical analysis of the influence of electric current on the rotation frequency and cone angle of the magnetization helix of metallic helimagnets Dy, MnSi, $CrNb_3S_6$, and FeGe. Experimental and calculated data on the characteristics of these helimagnets were used for the analysis, some of which are presented in Table 1. It should be noted that the value of the Gilbert damping constant α, of all the helimagnets considered, is known only for FeGe, for which $\alpha = 0.01$ [303]. In [304], it was shown that, in the Cu_2OSeO_3 helimagnet, the Gilbert damping parameter is of the order of 10^{-4}. Therefore, the numerical analysis was performed for two values of the Gilbert damping constant, $\alpha = 0.01$ and $\alpha \ll 0.01$.

Calculations show that for all the helimagnets under consideration, the value of β is $\sim 10^{-7} - 10^{-6}$ and, therefore, considering the losses for radiating electromagnetic waves by the helimagnet does not lead to any significant change in the pattern of the magnetic helix rotation damping. Furthermore, for all the materials under consideration, the relations $\chi \ll 1$ and $\chi\Lambda \ll 1$ are satisfied, which we used to derive analytical expressions (65) and (66).

The data in Ref. [99] allow us to estimate the critical current $j_0 = \Omega|e|n/q$ and the corresponding values of the Umov–Poynting vector U_0 for the helimagnets under consideration. The results of this estimate are presented in Table 2.

Table 2. Estimates of quantities j_0 and U_0.

Helimagnet	j_0, A cm^{-2}	U_0, W cm^{-2}
Dy	3×10^9	4×10^{-4}
MnSi	5×10^8	4×10^{-9}
$CrNb_3S_6$	5×10^7	1×10^{-6}
FeGe	9×10^8	1×10^{-6}

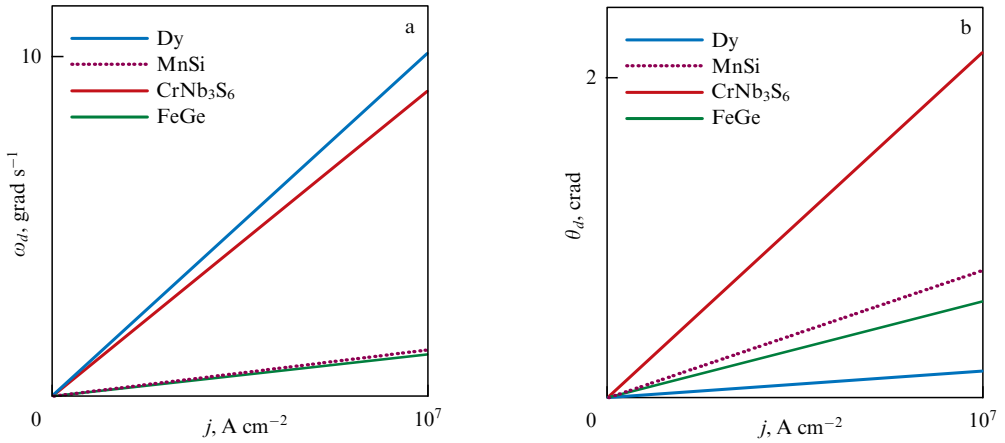

Figure 14. Highest values of spin helix rotation frequency ω_d (a) and cone angle θ_d (b) for metallic helimagnets Dy, MnSi, $CrNb_3S_6$, FeGe: $\alpha = 0.01$.

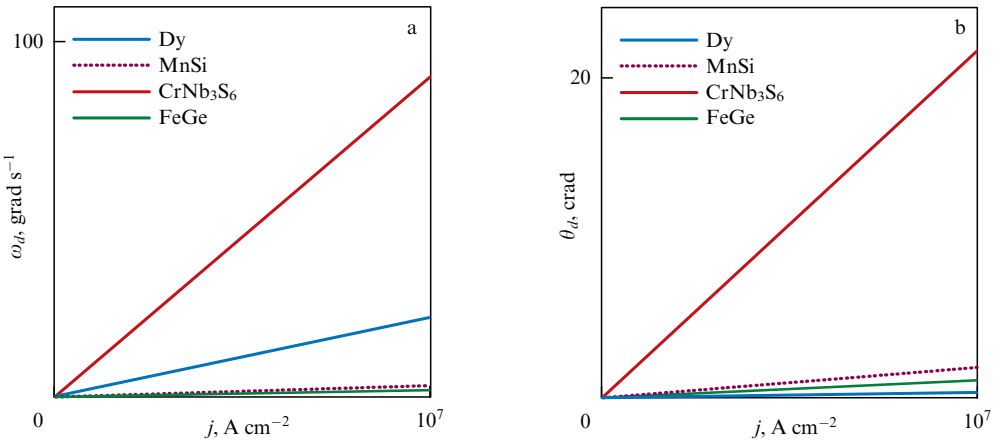

Figure 15. Highest values of spin helix rotation frequency ω_d (a) and cone angle θ_d (b) for metallic helimagnets Dy, MnSi, $CrNb_3S_6$, FeGe: $\alpha \ll \chi\Lambda$.

From the data for j_0 presented in Table 2, it is clear that scenario II, which occurs at $j_1 > j_0$, can be expected to be detected only at high current densities of $\sim 10^8$–10^9 A cm^{-2}. Here, we will consider the situation where an electric current with density $j \leqslant 10^7$ A cm^{-2} flows in a helimagnet. As can be seen from Table 2, in this case, $j \ll j_0$, and the relationship between the frequency $\overline{\omega}$ and the current density $\bar{j}$ can be described using Eqn (72), which can be represented as

$$\overline{\omega} = \frac{1}{1 + a(\overline{v}_S + \overline{v}_D + 1/\overline{v}_S)}\,\bar{j}. \tag{78}$$

The discriminant of Eqn (78) is written as

$$\overline{\omega}_d = \frac{1}{1 + a(2 + \overline{v}_D)}\,\bar{j}. \tag{79}$$

It is easy to see that discriminant (79) determines the highest possible value of function (78) for an arbitrary value of the parameter $\overline{v}_S$. In other words, the rotation frequency of the magnetization helix of a helimagnet with arbitrary values of the parameters $\overline{v}_S$, $\overline{v}_D$, and a cannot exceed the value determined by Eqn (79).

The results of calculating the frequency ω_d and the cone angle $\theta_d = \arcsin(\omega_d/\Omega)$ at $\alpha = 0.01$ and $\alpha \ll \chi\Lambda$ are shown in Figs 14 and 15, respectively.

Estimates show that, in metallic helimagnets, the spin helix rotation frequency can reach values on the order of 10 GHz at a rotation-inducing current density of $j \leqslant 10^7$ A cm^{-2}. The rotation frequency at a given current density depends significantly on the value of the parameter α: the smaller the damping parameter α, the higher the rotation frequency. For extremely small values of the parameter α, the highest rotation frequency ω_d is directly proportional to the wavenumber of the magnetic helix q_0 and inversely proportional to the concentration of conduction electrons in the helimagnet n. The highest possible cone angle θ_d of the helix under the conditions considered for these metallic helimagnets is less than 12 degrees.

Expression (69) allows us to estimate the value of the Umov–Poynting vector. It can be shown that, when the attenuation parameter α_{eff} is small compared to the product $\chi\Lambda$, the highest possible value of the Umov–Poynting vector obtained at a current of $j_0 = \Omega|e|n/q$ does not exceed $U_0 \simeq 4\pi M^2\Omega^3/c^2q^3$. The values of U_0 calculated using this formula are presented in the third column of Table 2. For dysprosium, the value of U_0 reaches 0.1 mW cm^{-2} in order of magnitude.

6.6 Spin devices utilizing magnetization helix rotation in helimagnet

Above, we demonstrated that the ability to rotate a helical magnetization helix can be used to create two new spin devices, which we will call a ‘chiral spin-current turbine’ and

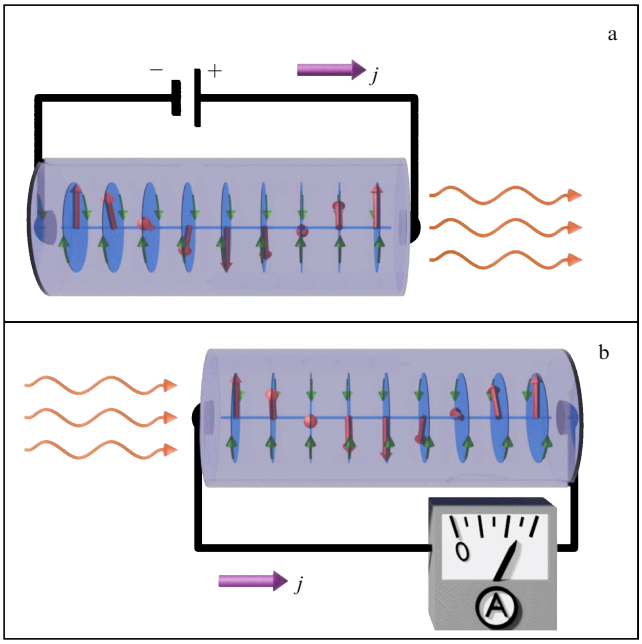

Figure 16. Illustrative diagram of operation of spin devices based on helimagnets: (a) chiral spin-current turbine; (b) spin-current Archimedes screw.

a 'spin-current Archimedes screw.' A chiral spin-current turbine is a device that converts the linear motion of conduction electrons in a helimagnet into rotational motion of its magnetic helix. A spin-current Archimedes screw is a device that realizes the opposite effect: the rotation of the magnetic helix of a helimagnet, generated by an external electromagnetic field, is converted into direct electric current.

A chiral spin-current turbine can serve as a spin-based generator, converting direct electric current into a high-frequency electromagnetic field. This field is generated by the time-varying magnetization of the helimagnet under the action of a flowing current. The power of such a spin-based generator can be estimated from calculations of the Umov–Poynting vector, the results of which are presented in Table 2. A diagram illustrating the operating principle of a chiral spin-current turbine as an electromagnetic field generator is shown in Fig. 16a. Since the possibility of rotating the magnetization helix of a helimagnet by current was experimentally established in Refs [190, 233], the practical implementation of this spin device can also be expected.

In addition to using a chiral spin-current turbine to create transmitting antennas with radiation frequencies in the subterahertz range, a potential area of application for this spin device could be microwave-assisted magnetic recording (MAMR) [305–312]. MAMR is a technology for recording data on hard magnetic disks in which switching is accomplished by exciting the precessional motion of magnetization with a radio-frequency field. The use of microwave radiation at a certain frequency helps to reduce the coercivity of the material from which the hard magnetic disk is made. This, in turn, helps to reduce the amount of energy required for data recording and allows more information to be recorded on a smaller area of the hard magnetic disk.

The spin-current Archimedes screw can be used as a spin diode, converting a high-frequency electromagnetic field into direct electric current. A theoretical justification for the possibility of using the rotation of a magnetic helix caused by an alternating magnetic field to control electron transport in a helimagnet was given in [236]. A visual diagram of the spin-current Archimedes screw is shown in Fig. 16b. It should be noted that the fact that the spin-current Archimedes screw generates a constant electric current, the magnitude of which is proportional to the frequency of the electromagnetic radiation incident on the helimagnet, can be used to detect microwave radiation and determine its characteristics. This makes the spin-current Archimedes screw a possible competitor to spin-torque microwave detectors (STMDs) [313–318], which are spin devices based on a magnetic tunnel junction. To detect an electromagnetic field using STMDs, a high-frequency electric current is passed through the magnetic tunnel junction, and the characteristics of the microwave electromagnetic field are determined by measuring the output DC voltage.

The prospects for the practical use of a chiral spin-current turbine as a spin high-frequency generator are limited by the relatively low values of the signal power generated by rotation of the spin helix in a helimagnet. Typical values of this characteristic can be estimated from the data given in Table 2. An increase in power can be achieved by creating multilayer magnetic nanostructures in which a helimagnet layer is coupled by an exchange interaction with one of the layers of a spin-valve-type nanostructure, which is a combination of two ferromagnetic layers separated by a nonmagnetic interlayer and an antiferromagnet layer. Nanostructures of this type, called 'chiral spin valves,' were successfully synthesized and studied at the M.N. Mikheev Institute of Metal Physics, Ural Branch of the Russian Academy of Sciences; the reader can find the results of these studies in Refs [123–130]. They experimentally established that, in a chiral spin valve, twist of the magnetization helix of the helimagnetic layer leads to twist of the magnetization of the exchange-coupled ferromagnetic layer.

The electrical resistance of a chiral spin valve, when a direct electric current flows along the normal to the surface of this nanostructure, depends significantly on the relative orientation of the ferromagnetic layers. This resistance will change over time if the magnetic helix of the helimagnetic layer, rotating under the action of the flowing current, rotates the magnetization of the adjacent exchange-coupled ferromagnetic layer. The time dependence of the electrical resistance will lead to the flow of direct electric current being accompanied by the generation of an alternating voltage at the external contacts of the sample. Such a spin device can be called a 'chiral spin-current nano-oscillator' (Ch-SCNO). The first discussion of a spin device that uses the rotation of a helical magnetization helix to generate high-frequency current from a direct electric current was reported in Ref. [228].

Figure 17 shows a schematic diagram of the operation of a chiral spin-current nano-oscillator.

Important advantages of Ch-SCNOs are that they can operate without the application of an external magnetic field, are easily frequency tunable by simply changing the current, and have a high-power output for generating alternating voltage.

Taking these circumstances into account, it can be expected that Ch-STNOs can be used in the future instead of 'traditional' STNOs in the construction of devices for wireless communication [319–325], ultrafast spectral analysis [326–329], AC-to-DC conversion [313, 330–336], true random number generation [337, 338], and neuromorphic computing [339–341].

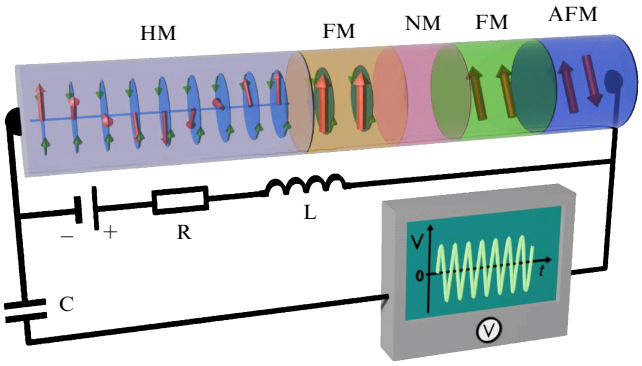

Figure 17. Illustrative diagram of operation of spin-based device called 'chiral spin-current nanooscillator.' Abbreviations HM, FM, AFM, and NM denote layers of helimagnet, ferromagnet, antiferromagnet, and nonmagnetic material, respectively. Red arrows schematically depict distribution of magnetic moments of atomic layers in corresponding magnet.

It should be noted that this review discusses the mutual influence of helical magnetism and transport in unlimited ('infinite') conducting chiral helimagnets. However, for a correct description of the operation of spin devices in which helimagnet layers are used as functional elements, their finite thickness must be taken into account. The solution to this problem represents an important next step in constructing the theoretical basis of chiral nanospintronics.

7. Conclusion

This article presents an overview of the key stages in the emergence and rapid development of chiral nanospintronics — a promising new field of quantum electronics.

It is shown that the use of the quantum kinetic equation, a quantum generalization of the well-known and widely used Boltzmann equation for charge carriers with spin angular momentum, is an effective method for describing spin and charge transport when inhomogeneities in the external magnetic field and/or internal exchange fields must be taken into account.

Application of this method demonstrated that the interaction of conduction electron spins with a spatially inhomogeneous exchange field in conducting helimagnets provides a natural explanation for two spin-transport effects: the electrical magnetochiral effect and the kinetic magnetoelectric effect. A resonant enhancement of these spin effects, termed 'magnetochiral kinetic resonance,' is predicted. It has been shown that, for a certain ratio of helimagnet parameters, a giant electrical magnetochiral effect can arise under magnetochiral kinetic resonance conditions.

An original technique is developed for determining the magnetic chirality of conducting helimagnets using galvanomagnetic experiments. For this purpose, the dependence of the helimagnets' electrical resistance on their magnetic chirality, as well as on the relative orientation of the electric current and external magnetic field along the magnetic helix axis, can be used. Alternatively, the dependence of helimagnet magnetization along the helix axis on magnetic chirality and the direction of current flow through the sample can be used. The developed technique can be used to describe the operation of spin-based devices in which conducting helimagnets serve as functional components.

A theory of the spin-transfer torque effect in conducting chiral helimagnets is developed. It is shown that the transfer of spin angular momentum in chiral helimagnets leads to rotation of the helimagnet's magnetization helix around its axis under the action of an electric current. This phenomenon can be considered a spin analog of the rotation of windmill blades under the action of wind flow. It was also shown that the rotation of the magnetization helix, induced by an external electromagnetic field, leads to the generation of an electric current. The phenomenon of converting a helimagnet's helix rotation into an electric current is a spin analog of the operation of an Archimedes screw — a mechanical pump in which the rotation of the helical surface causes the movement of a liquid. The influence of the spin-transfer torque effect on the electrical resistance of conducting chiral helimagnets is described. It was established that, when a spin helix rotates under the influence of a flowing electric current, the electrical resistance of a helimagnet will always be lower than the resistance of a helimagnet in which the spin helix is stationary. The use of the rotation of the magnetization helix of helimagnets by electric current to create new spin devices is discussed: spin generators that convert direct current into a high-frequency electromagnetic field or high-frequency electric current, and spin diodes that convert a high-frequency electromagnetic field into direct current.

Funding. This work was carried out within the framework of a state assignment from the Ministry of Science and Higher Education of the Russian Federation for the Institute of Metal Physics, Ural Branch of the Russian Academy of Sciences.

References

1. Vedyaev A V *Phys. Usp.* **45** 1296 (2002); *Usp. Fiz. Nauk* **172** 1458 (2002)
2. Grünberg P A *Phys. Usp.* **51** 1349 (2008); *Usp. Fiz. Nauk* **178** 1349 (2008)
3. Fert A *Rev. Mod. Phys.* **80** 1517 (2008); *Usp. Fiz. Nauk* **178** 1336 (2008)
4. Kusrayev Yu G *Phys. Usp.* **53** 725 (2010); *Usp. Fiz. Nauk* **180** 759 (2010)
5. Maekawa S et al. *J. Appl. Phys.* **133** 020902 (2023)
6. Borisenko V E, Danilyuk A L, Migas D B *Spintronika* (Spintronics) (Moscow: Laboratoriya Znanii, 2017) Textbook
7. Wolf S A et al. *Science* **294** 1488 (2001)
8. Gulyaev Yu V et al. *Phys. Usp.* **52** 335 (2009); *Usp. Fiz. Nauk* **179** 359 (2009)
9. Volkov N V *Phys. Usp.* **55** 250 (2012); *Usp. Fiz. Nauk* **182** 263 (2012)
10. Baranov P G et al. *Phys. Usp.* **62** 795 (2019); *Usp. Fiz. Nauk* **189** 849 (2019)
11. Maekawa S et al. (Eds) *Spin Current* (Oxford: Oxford Univ. Press, 2017) DOI: 10.1093/oso/9780198787075.001.0001
12. Dyakonov M I (Ed.) *Spin Physics in Semiconductors* (Springer Ser. in Solid-State Sciences, Vol. 157) (Cham: Springer, 2017) DOI: 10.1007/978-3-319-65436-2
13. Ustinov V V, Mushnikov N V, Irkhin V Yu (Eds) *Fizika Magnitnykh Materialov i Nanostruktur* (Physics of Magnetic Materials and Nanostructures) (Ekaterinburg: Inst. Fiziki Metallov Imeni M.N. Mikheeva UrO RAN, 2020)
14. Feher G, Kip A F *Phys. Rev.* **98** 337 (1955)
15. Dyson F J *Phys. Rev.* **98** 349 (1955)
16. Lampe M, Platzman P M *Phys. Rev.* **150** 340 (1966)
17. Walker M B *Can. J. Phys.* **48** 111 (1970)
18. Khabibullin B M, Kharakhash'yan É G *Sov. Phys. Usp.* **16** 806 (1974); *Usp. Fiz. Nauk* **111** 483 (1973)
19. Ustinov V V *Fiz. Met. Metalloved.* **45** 473 (1978)
20. Ustinov V V, in *Soviet Scientific Reviews. Sect. A Physics Reviews* Vol. 7 (Ed. I M Khalatnikov) (New York: Harwood Acad. Publ., 1986) p. 227

21. Ustinov V V, Yasyulevich I A *J. Exp. Theor. Phys.* **166** 58 (2024); *Zh. Eksp. Teor. Fiz.* **166** 63 (2024)
22. Dyakonov M I, Perel V I *JETP Lett.* **13** 467 (1971); *Pis'ma Zh. Eksp. Teor. Fiz.* **13** 657 (1971)
23. Dyakonov M I, Perel V I *Phys. Lett. A* **35** 459 (1971)
24. Chazalviel J-N *Phys. Rev. B* **11** 3918 (1975)
25. Hirsch J E *Phys. Rev. Lett.* **83** 1834 (1999)
26. Zhang S *Phys. Rev. Lett.* **85** 393 (2000)
27. Kato Y K et al. *Science* **306** 1910 (2004)
28. Wunderlich J et al. *Phys. Rev. Lett.* **94** 047204 (2005)
29. Hoffmann A *IEEE Trans. Magn.* **49** 5172 (2013)
30. Niimi Y, Otani Y *Rep. Prog. Phys.* **78** 124501 (2015)
31. Sinova J et al. *Rev. Mod. Phys.* **87** 1213 (2015)
32. Pines D, Slichter C P *Phys. Rev.* **100** 1014 (1955)
33. Griswold T W, Kip A F, Kittel C *Phys. Rev.* **88** 951 (1952)
34. Bakun A A et al. *JETP Lett.* **40** 1293 (1984); *Pis'ma Zh. Eksp. Teor. Fiz.* **40** 464 (1984)
35. Grünberg P et al. *Phys. Rev. Lett.* **57** 2442 (1986)
36. Binasch G et al. *Phys. Rev. B* **39** 4828 (1989)
37. Baibich M N et al. *Phys. Rev. Lett.* **61** 2472 (1988)
38. Agrinskaya N V, Kozub V I, Shumilin A V *JETP Lett.* **110** 495 (2019); *Pis'ma Zh. Eksp. Teor. Fiz.* **110** 482 (1971)
39. Okuno T et al. *Nat. Electron.* **2** 389 (2019)
40. Dieny B et al. *J. Appl. Phys.* **69** 4774 (1991)
41. Kang W et al. *ACM J. Emerg. Technol. Comput. Syst.* **12** 16 (2015)
42. Slonczewski J C *J. Magn. Magn. Mater.* **159** L1 (1996)
43. Berger L *Phys. Rev. B* **54** 9353 (1996)
44. Berger L *J. Appl. Phys.* **81** 4880 (1997)
45. Berger L *IEEE Trans. Magn.* **34** 3837 (1998)
46. Zvezdin A K, Zvezdin K A, Khval'kovskii A V *Phys. Usp.* **51** 412 (2008); *Usp. Fiz. Nauk* **178** 436 (2008)
47. Stiles M D, Zangwill A *J. Appl. Phys.* **91** 6812 (2002)
48. Stiles M D, Zangwill A *Phys. Rev. B* **66** 014407 (2002)
49. Tsoi M et al. *Phys. Rev. Lett.* **80** 4281 (1998)
50. Katine J A et al. *Phys. Rev. Lett.* **84** 3149 (2000)
51. Kiselev S I et al. *Nature* **425** 380 (2003)
52. Rippard W H et al. *Phys. Rev. Lett.* **92** 027201 (2004)
53. Mangin S et al. *Nature Mater.* **5** 210 (2006)
54. Moodera J S et al. *Phys. Rev. Lett.* **74** 3273 (1995)
55. Parkin S S P et al. *Nature Mater.* **3** 862 (2004)
56. Lu Y et al. *Phys. Rev. B* **54** R8357 (1996)
57. Zhang X et al. *Phys. Rev. B* **56** 5484 (1997)
58. Bratkovsky A M *JETP Lett.* **65** 452 (1997); *Pis'ma Zh. Eksp. Teor. Fiz.* **65** 430 (1997)
59. Popkov A F et al. *Inzhener. Fiz.* (9) 19 (2012)
60. Kaka S et al. *Nature* **437** 389 (2005)
61. Silva T J, Rippard W H *J. Magn. Magn. Mater.* **320** 1260 (2008)
62. Slavin A, Tiberkevich V *IEEE Trans. Magn.* **45** 1875 (2009)
63. Zvezdin K A et al. *Inzhener. Fiz.* (10) 27 (2012)
64. Zeng Z et al. *ACS Nano* **6** 6115 (2012)
65. Zeng Z, Finocchio G, Jiang H *Nanoscale* **5** 2219 (2013)
66. Zheng X, Zhou Y *Solid State Phenom.* **232** 147 (2015)
67. Chen T et al. *Proc. IEEE* **104** 1919 (2016)
68. Jiang S et al. *Appl. Phys. Review* **11** 041309 (2024)
69. Balthazar J M, Tusset Â M (Eds) *New Insights on Oscillators and Their Applications to Engineering and Science* (London: IntechOpen, 2024)
70. Mishagin K G, Shalfeev V D *Tech. Phys. Lett.* **36** 1049 (2010); *Pis'ma Zh. Eksp. Teor. Fiz.* **36** (22) 51 (2010)
71. Lebrun R et al. *Nat. Commun.* **8** 15825 (2017)
72. Aleshin K N, Matrosov V V, Mishagin K G *Tech. Phys. Lett.* **43** 281 (2017); *Pis'ma Zh. Eksp. Teor. Fiz.* **43** (6) 8 (2017)
73. Tsunegi S et al. *Sci. Rep.* **8** 13475 (2018)
74. Núñez A S et al. *Phys. Rev. B* **73** 214426 (2006)
75. MacDonald A H, Tsoi M *Philos. Trans. R. Soc. A* **369** 3098 (2011)
76. Gomonay E V, Loktev V M *Low Temp. Phys.* **40** 17 (2014); *Fiz. Nizk. Temp.* **40** 22 (2014)
77. Jungwirth T et al. *Nature Nanotechnol.* **11** 231 (2016)
78. Baltz V et al. *Rev. Mod. Phys.* **90** 015005 (2018)
79. Chen H et al. *Adv. Mater.* **36** 2310379 (2024)
80. Khalili Amiri P, Phatak C, Finocchio G *Annu. Rev. Mater. Res.* **54** 117 (2024)
81. Kim K-J et al. *Nature Mater.* **16** 1187 (2017)
82. Barker J, Atxitia U *J. Phys. Soc. Jpn.* **90** 081001 (2021)
83. Kim S K et al. *Nature Mater.* **21** 24 (2022)
84. Núñez A S, Duine R A, MacDonald A H, cond-mat/0510797
85. Rikken G L, Fölling J, Wyder P *Phys. Rev. Lett.* **87** 236602 (2001)
86. Paul A *Sci. Rep.* **6** 19315 (2016)
87. Yang S-H, in *Bulletin of the American Physical Society, March Meeting, March 4–8, 2019* (Boston, MA: APS, 2019) p. 1634
88. Yang S-H et al. *Nature Rev. Phys.* **3** 328 (2021)
89. Naaman R, Waldeck D H *Annu. Rev. Phys. Chem.* **66** 263 (2015)
90. Yang S-H *Appl. Phys. Lett.* **116** 120502 (2020)
91. Parkin S S P, Hayashi M, Thomas L *Science* **320** 190 (2008)
92. Ustinov V V, Yasyulevich I A, in *Intern. Conf. Functional Materials, ICFM-2021, Alushta, October 4–8, 2021. Book of Abstracts* (Simferopol: V.I. Vernadsky Crimean Federal Univ., 2021) p. 5
93. Vélez S, in *Proc. of the Materials for Sustainable Development Conf., MATSUS23 and Sustainable Technology Forum, STECH23, València, Spain, March 6–10, 2023*
94. Parkin S S P, in *Samarkand Intern. Symp. on Magnetism, July 2–6, 2023, Samarkand, Uzbekistan. Book of Abstracts*, p. 7
95. Ustinov V V, Yasyulevich I A, in *Samarkand Intern. Symp. on Magnetism, July 2–6, 2023, Samarkand, Uzbekistan. Book of Abstracts*, p. 237
96. Bläsing R et al. *Proc. IEEE* **108** 1303 (2020)
97. Ustinov V V, Yasyulevich I A *Phys. Met. Metallogr.* **121** 223 (2020); *Fiz. Met. Metalloved.* **121** 257 (2020)
98. Ustinov V V, Yasyulevich I A *Phys. Rev. B* **102** 134431 (2020)
99. Ustinov V V, Yasyulevich I A *Phys. Rev. B* **106** 064417 (2022)
100. Ustinov V V, Yasyulevich I A *J. Exp. Theor. Phys.* **137** 422 (2023); *Zh. Eksp. Teor. Fiz.* **164** 491 (2023)
101. Izyumov Yu A *Sov. Phys. Usp.* **27** 845 (1984); *Usp. Fiz. Nauk* **144** 439 (1984)
102. Kimura T *Annu. Rev. Condens. Matter Phys.* **3** 93 (2012)
103. Kishine J, Ovchinnikov A S *Solid State Phys.* **66** 1 (2015)
104. Togawa Y et al. *J. Phys. Soc. Jpn.* **85** 112001 (2016)
105. Altynbaev E V, Chubova N M, Grigoriev S V *Crystallogr. Rep.* **67** 118 (2022); *Kristallografiya* **67** 130 (2022)
106. Salamon M B et al. *Phys. Rev. Lett.* **56** 259 (1986)
107. Rhyne J J et al. *J. Appl. Phys.* **61** 4043 (1987)
108. Erwin R W et al. *Phys. Rev. B* **35** 6808 (1987)
109. Majkrzak C F et al. *Adv. Phys.* **40** 99 (1991)
110. Jehan D A et al. *Phys. Rev. B* **48** 5594 (1993)
111. de la Fuente C et al. *J. Phys. Condens. Matter* **11** 6529 (1999)
112. Borchers J A et al. *Phys. Rev. B* **43** 3123 (1991)
113. Kosugi T et al. *Physica B* **334** 365 (2003)
114. Grigoriev S V et al. *Phys. Rev. Lett.* **100** 197203 (2008)
115. Tarnavich V V et al. *Phys. Rev. B* **89** 054406 (2014)
116. Grigoriev S V et al. *J. Surf. Investig.* **9** 974 (2015); *Poverkhnost. Rentgen. Sinkhrotron. Neitron. Issled.* (10) 5 (2015)
117. Antropov N O et al. *JETP Lett.* **108** 341 (2018); *Pis'ma Zh. Eksp. Teor. Fiz.* **108** 361 (2018)
118. Ukleev V et al. *Phys. Rev. B* **100** 134417 (2019)
119. Huang J et al. *J. Magn. Magn. Mater.* **585** 171108 (2023)
120. Antropov N O, Kravtsov E A *J. Surf. Investig.* **17** 855 (2023); *Poverkhnost'. Rentgen, Sinkhrotron. Neitron. Issled.* (8) 11 (2023)
121. Xiao X et al. *Phys. Rev. B* **109** 224403 (2024)
122. Xiao X et al. *Phys. Rev. B* **109** 174422 (2024)
123. Naumova L I et al. *Curr. Appl. Phys.* **19** 1252 (2019)
124. Naumova L I et al. *Phys. Met. Metallogr.* **120** 429 (2019); *Fiz. Met. Metalloved.* **120** 464 (2019)
125. Zavornitsyn R S et al. *Curr. Appl. Phys.* **20** 1328 (2020)
126. Zavornitsyn R S et al. *Phys. Met. Metallogr.* **121** 624 (2020); *Fiz. Met. Metalloved.* **121** 688 (2020)
127. Naumova L I et al. *IEEE Trans. Nanotechnol.* **20** 866 (2021)
128. Ustinov V V et al. *J. Surf. Investig.* **15** 1278 (2021); *Poverkhnost. Rentgen. Sinkhrotron. Neitron. Issled.* (12) 26 (2021)
129. Naumova L I et al. *Phys. Met. Metallogr.* **122** 540 (2021); *Fiz. Met. Metalloved.* **122** 581 (2021)
130. Naumova L I et al. *Phys. Met. Metallogr.* **123** 945 (2022); *Fiz. Met. Metallogr.* **123** 1011 (2022)
131. Vonsovskii S V *Magnetism* (New York: John Wiley and Sons, 1974); Translated from Russian: *Magnetism* (Moscow: Nauka, 1971)

132. Taylor K N R, Darby M I *Physics of Rare Earth Solids* (London: Chapman and Hall, 1972); Translated into Russian: *Fizika Redkozemel'nykh Soedinenii* (Moscow: Mir, 1974)
133. Nagaev E L *Physics of Magnetic Semiconductors* (Moscow: Mir Publ., 1983); Translated from Russian: *Fizika Magnitnykh Poluprovodnikov* (Moscow: Nauka, 1979)
134. Nikitin S A *Magnitnye Svoistva Redkozemel'nykh Metallov i Ikh Splavov* (Magnetic Properties of Rare Earth Metals and Their Alloys) (Moscow: Izd. MGU, 1989)
135. Jensen J, Mackintosh A R *Rare Earth Magnetism*: *Structures and Excitations* (Oxford: Clarendon Press, 1991) DOI: 10.1093/oso/9780198520276.001.0001
136. Yoshimori A *J. Phys. Soc. Jpn.* **14** 807 (1959)
137. Bar'yakhtar V G, Stefanovskii E P *Sov. Phys. Solid State* **11** 1566 (1970); *Fiz. Tverd. Tela* **11** 1946 (1969)
138. Bak P, Jensen M H *J. Phys. C* **13** L881 (1980)
139. Dzialoshinskii I E *Sov. Phys. JETP* **5** 1259 (1957); *Zh. Eksp. Teor. Fiz.* **32** 1547 (1957)
140. Dzyaloshinskii I E *Sov. Phys. JETP* **19** 960 (1964); *Zh. Eksp. Teor. Fiz.* **46** 1420 (1964)
141. Dzyaloshinskii I E *Sov. Phys. JETP* **20** 223 (1965); *Zh. Eksp. Teor. Fiz.* **47** 336 (1964)
142. Dzyaloshinskii I E *Sov. Phys. JETP* **20** 665 (1965); *Zh. Eksp. Teor. Fiz.* **47** 992 (1964)
143. Moriya T *Phys. Rev.* **120** 91 (1960)
144. Izyumov Yu A *Sov. Phys. Usp.* **23** 356 (1980); *Usp. Fiz. Nauk* **131** 387 (1980)
145. Izyumov Yu A *Sov. Phys. Usp.* **31** 689 (1988); *Usp. Fiz. Nauk* **155** 553 (1988)
146. Lebech B, Bernhard J, Freltoft T *J. Phys. Condens. Matter* **1** 6105 (1989)
147. Mühlbauer S et al. *Science* **323** 915 (2009)
148. Münzer W et al. *Phys. Rev. B* **81** 041203 (2010)
149. Dyadkin V A et al. *J. Phys. Conf. Ser.* **211** 012012 (2010)
150. Moskvin E et al. *Phys. Rev. Lett.* **110** 077207 (2013)
151. Devyaterikov D I et al. *J. Surf. Investig.* **15** 542 (2021); *Poverkhnost. Rentgen. Sinkhrotron. Neitron. Issled.* (6) 3 (2021)
152. Bykov A A et al. *J. Solid State Chem.* **322** 123951 (2023)
153. Kitaori A et al. *Phys. Rev. B* **107** 024406 (2023)
154. Yu X Z et al. *Nature* **465** 901 (2010)
155. Seki S et al. *Science* **336** 198 (2012)
156. Togawa Y et al. *Phys. Rev. Lett.* **108** 107202 (2012)
157. Tonomura A et al. *Nano Lett.* **12** 1673 (2012)
158. Togawa Y et al. *Phys. Rev. B* **92** 220412 (2015)
159. Togawa Y et al. *Phys. Rev. Lett.* **122** 017204 (2019)
160. Back C et al. *J. Phys. D* **53** 363001 (2020)
161. Togawa Y, Ovchinnikov A S, Kishine J *J. Phys. Soc. Jpn.* **92** 081006 (2023)
162. Grigoriev S V et al. *Phys. Rev. B* **74** 214414 (2006)
163. Maleyev S V *Phys. Rev. Lett.* **75** 4682 (1995)
164. Plakhty V P et al. *Physica B* **267–268** 259 (1999)
165. Plakhty V P et al. *Physica B* **297** 60 (2001)
166. Maleev S V *Phys. Usp.* **45** 569 (2002); *Usp. Fiz. Nauk* **172** 617 (2002); *Usp. Fiz. Nauk* **172** 617 (2002)
167. Maleyev S V *Phys. Rev. B* **73** 174402 (2006)
168. Plakhty V P et al. *Physica B* **385–386** 288 (2006)
169. Grigoriev S V et al. *Phys. Rev. B* **76** 224424 (2007)
170. Grigoriev S V et al. *Phys. Rev. B* **79** 144417 (2009)
171. Pappas C et al. *Phys. Rev. Lett.* **102** 197202 (2009)
172. Grigoriev S V et al. *Phys. Rev. Lett.* **102** 037204 (2009)
173. Grigoriev S V et al. *Phys. Rev. B* **81** 012408 (2010)
174. Grigoriev S V et al. *Phys. Solid State* **52** 907 (2010); *Fiz. Tverd. Tela* **52** 852 (2010)
175. Grigoriev S V et al. *Phys. Rev. B* **83** 224411 (2011)
176. Dyadkin V A et al. *Phys. Rev. B* **84** 014435 (2011)
177. Grigoriev S V et al. *Phys. Rev. B* **90** 174414 (2014)
178. Siegfried S-A et al. *Phys. Rev. B* **91** 184406 (2015)
179. Qureshi N et al. *Phys. Rev. B* **102** 054417 (2020)
180. Dally R L et al. *Phys. Rev. B* **103** 094413 (2021)
181. Grigoriev S V et al. *Ann. Physics* **447** 169132 (2022)
182. Fabrizi F et al. *Phys. Rev. Lett.* **102** 237205 (2009)
183. Sagayama H et al. *J. Phys. Soc. Jpn.* **79** 043711 (2010)
184. Mulders A M et al. *Phys. Rev. B* **81** 092405 (2010)
185. Ohsumi H, Arima T *Adv. Phys. X* **1** 128 (2016)
186. Matsumura T et al. *J. Phys. Soc. Jpn.* **86** 124702 (2017)
187. Ovchinnikova E N et al. *Crystallogr. Rep.* **67** 820 (2022); *Kristallografiya* **67** 885 (2022)
188. Ukleev V et al. *Sci. Technol. Adv. Mater.* **23** 682 (2022)
189. Koehler W C *J. Appl. Phys.* **36** 1078 (1965)
190. Masell J et al. *Phys. Rev. B* **102** 180402 (2020)
191. Bechler N T, Masell J *Neuromorphic Comput. Eng.* **3** 034003 (2023)
192. Jiang N et al. *Nature Commun.* **11** 1601 (2020)
193. Jiang N et al. *Phys. Rev. Lett.* **126** 177205 (2021)
194. Ohe J, Onose Y *Appl. Phys. Lett.* **118** 042407 (2021)
195. Masuda H et al. *Nature Commun.* **15** 1999 (2024)
196. Borisov A B, Kiselev V V *Kvaziodnomernye Magnitnye Solitony* (Quasi-One-Dimensional Magnetic Solitons) (Moscow: Fizmatlit, 2014)
197. Borisov A B, Kiselev V V *Dvumernye i Trekhmernye Topologicheskie Defekty, Solitony i Tekstury v Magnetikakh* (Two-Dimensional and Three-Dimensional Topological Defects, Solitons and Textures in Magnets) (Moscow: Fizmatlit, 2022)
198. Borisov A B *Phys. Usp.* **63** 269 (2020); *Usp. Fiz. Nauk* **190** 291 (2020)
199. Elliott R J, Wedgwood F A *Proc. Phys. Soc.* **81** 846 (1963)
200. Boys D W, Legvold S *Phys. Rev.* **174** 377 (1968)
201. Belov K P, Levitin R Z, Nikitin S A *Sov. Phys. Usp.* **7** 179 (1964); *Usp. Fiz. Nauk* **82** 449 (1964)
202. Elliott R J (Ed.) *Magnetic Properties of Rare Earth Metals* (New York: Springer, 1972) DOI: 10.1007/978-1-4757-5691-3
203. Calvo M *Phys. Rev. B* **18** 5073 (1978)
204. Calvo M *Phys. Rev. B* **19** 5507 (1979)
205. Calvo M *Phys. Rev. A* **21** 1469 (1980)
206. Taniguchi T, Imamura H *Phys. Rev. B* **81** 012405 (2010)
207. Togawa Y et al. *Phys. Rev. Lett.* **111** 197204 (2013)
208. Watanabe H, Hoshi K, Ohe J *Phys. Rev. B* **94** 125143 (2016)
209. Okumura S et al. *J. Phys. Conf. Ser.* **2164** 012068 (2022) DOI: 10.1088/1742-6596/2164/1/012068
210. Zadorozhnyi A, Dahnovsky Yu *J. Phys. Condens. Matter* **35** 015701 (2023)
211. Zadorozhnyi A, Dahnovsky Yu *Phys. Rev. B* **107** 035202 (2023)
212. Fraerman A A, Udalov O G *Phys. Rev. B* **77** 094401 (2008)
213. Yokouchi T et al. *Nature Commun.* **8** 866 (2017)
214. Aoki R, Kousaka Y, Togawa Y *Phys. Rev. Lett.* **122** 057206 (2019)
215. Levitov L S, Nazarov Yu V, Eliashberg G M *Sov. Phys. JETP* **61** 133 (1985); *Zh. Eksp. Teor. Fiz.* **88** 229 (1985)
216. Gor'kov L P, Sokol A V *Sov. Phys. JETP* **66** 1267 (1987); *Zh. Eksp. Teor. Fiz.* **93** 2219 (1987)
217. Gor'kov L P, Sokol A V *JETP Lett.* **45** 299 (1987); *Pis'ma Zh. Eksp. Teor. Fiz.* **45** 239 (1987)
218. Bebenin N G *Phys. Met. Metallogr.* **119** 1180 (2018); *Fiz. Met. Metalloved.* **119** 1241 (2018)
219. Nabei Y et al. *Appl. Phys. Lett.* **117** 052408 (2020)
220. Yamaguchi A et al. *Phys. Rev. Lett.* **92** 077205 (2004)
221. Ono T, Nakatani Y *Appl. Phys. Express* **1** 061301 (2008)
222. Zvezdin K A, Ekomasov E G *Phys. Met. Metallogr.* **123** 201 (2022); *Fiz. Met. Metalloved.* **123** 219 (2022)
223. Jonietz F et al. *Science* **330** 1648 (2010)
224. Garcia-Sanchez F et al. *New J. Phys.* **18** 075011 (2016)
225. Feng Y et al. *J. Magn. Magn. Mater.* **491** 165610 (2019)
226. Das D, Muralidharan B, Tulapurkar A *J. Magn. Magn. Mater.* **491** 165608 (2019)
227. Liang X et al. *Appl. Phys. Lett.* **116** 122402 (2020)
228. Wessely O, Skubic B, Nordström L *Phys. Rev. Lett.* **96** 256601 (2006)
229. Goto K, Katsura H, Nagaosa N, arXiv:0807.2901
230. Kudtarkar S K *Phys. Lett. A* **374** 366 (2009)
231. Iwasaki J, Mochizuki M, Nagaosa N *Nature Commun.* **4** 1463 (2013)
232. Hals K M D, Brataas A *Phys. Rev. B* **87** 174409 (2013)
233. Takeuchi Y et al. *Nature Mater.* **20** 1364 (2021)
234. Fraerman A A *JETP Lett.* **118** 520 (2023); *Pis'ma Zh. Eksp. Teor. Fiz.* **118** 533 (2023)
235. Fraerman A A, Muhamatchin K R, Tokman I D *Phys. Rev. B* **84** 012402 (2011)
236. del Ser N, Heinen L, Rosch A *SciPost Phys.* **11** 009 (2021)
237. Kurebayashi D et al. *Phys. Rev. B* **106** 205110 (2022)

238. Freimuth F, Blügel S, Mokrousov Y *J. Phys. Condens. Matter* **26** 104202 (2014)
239. Schweflinghaus B et al. *Phys. Rev. B* **94** 024403 (2016)
240. Jia H, Zimmermann B, Blügel S *Phys. Rev. B* **98** 144427 (2018)
241. Grytsiuk S et al. *Phys. Rev. B* **100** 214406 (2019)
242. Bornemann M et al. *J. Phys. Condens. Matter* **31** 485801 (2019)
243. Soboleva T K, Stefanovskii E P, Tarasenko V V *Sov. Phys. Solid State* **22** 1370 (1980); *Fiz. Tverd. Tela* **22** 2353 (1980)
244. Izyumov Yu A *Difraktsiya Neitronov na Dlinno-Periodicheskikh Strukturakh* (Diffraction of Neutrons on Long-Period Structures) (Moscow: Energoatomizdat, 1987)
245. Kataoka M *J. Phys. Soc. Jpn.* **56** 3635 (1987)
246. Bostrem I G, Kishine J, Ovchinnikov A S *Phys. Rev. B* **78** 064425 (2008)
247. Kishine J, Ovchinnikov A S *Phys. Rev. B* **79** 220405 (2009)
248. Tankeev A P, Borich M A, Smagin V V *Phys. Met. Metallogr.* **115** 425 (2014); *Fiz. Met. Metalloved.* **115** 455 (2014)
249. Yosida K, Miwa H *J. Appl. Phys.* **32** S8 (1961)
250. Kataoka M *J. Magn. Magn. Mater.* **31–34** 341 (1983)
251. Izyumov Yu A, Laptev V M *Sov. Phys. JETP* **61** 95 (1985); *Zh. Eksp. Teor. Fiz.* **88** 165 (1985)
252. Vlasov K B, Smorodinskii Ya G *Fiz. Met. Metalloved.* **45** 903 (1978)
253. Bebenin N G, Smorodinskii Ya G *Fiz. Tverd. Tela* **28** 1115 (1986)
254. Buchel'nikov V D, Shavrov V G *Sov. Phys. Solid State* **31** 765 (1989); *Fiz. Tverd. Tela* **31** (5) 81 (1989)
255. Manzhos I V, Chupis I E *Sov. J. Low Temp. Phys.* **14** 333 (1988); *Fiz. Nizk. Temp.* **14** 606 (1988)
256. Buchel'nikov V D, Bychkov I V, Shavrov V G *J. Magn. Magn. Mater.* **118** 169 (1993)
257. Bychkov I V, Kuzmin D A, Shavrov V G *J. Magn. Magn. Mater.* **329** 142 (2013)
258. Bychkov I V et al. *Vliyanie Vzaimodeistviya Podsistem na Dinamicheskie Svoistva Magnetikov* (The Influence of Interaction of Subsystems on the Dynamic Properties of Magnetic Materials) (Moscow: Fizmatlit, 2016)
259. Bychkov I V, Kuzmin D A, Shavrov V G, in *Magnetic Materials* (Ed. K Maaz) (London: IntechOpen, 2016) p. 161, DOI: 10.5772/64014
260. Shavrov V G, Buchel'nikov V D, Bychkov I V *Svyazannye Volny v Magnetikakh* (Coupled Waves in Magnets) (Moscow: Fizmatlit, 2019)
261. Belitz D, Kirkpatrick T R, Rosch A *Phys. Rev. B* **73** 054431 (2006)
262. Belitz D, Kirkpatrick T R, Rosch A *Phys. Rev. B* **74** 024409 (2006)
263. Melcher R L *Phys. Rev. Lett.* **30** 125 (1973)
264. Sato T J et al. *Phys. Rev. B* **94** 144420 (2016)
265. Takagi R et al. *Phys. Rev. B* **95** 220406 (2017)
266. Weber T et al. *Phys. Rev. B* **97** 224403 (2018)
267. Akhiezer A I, Baryakhtar V G, Peletminskii S V *Sov. Phys. JETP* **18** 235 (1964); *Zh. Eksp. Teor. Fiz.* **45** 337 (1963)
268. Akhiezer A I, Bar'yakhtar V G, Peletminskii S V *Spin Waves* (Amsterdam: North-Holland Publ. Co., 1968); Translated from Russian: *Spinovye Volny* (Moscow: Nauka, 1967)
269. Lakhno V D *Phys. Usp.* **39** 669 (1996); *Usp. Fiz. Nauk* **166** 717 (1996)
270. Ustinov V V, Yasyulevich I A, Bebenin N G *Phys. Met. Metallogr.* **124** 1745 (2023)
271. Silin V P *Sov. Phys. JETP* **3** 305 (1956); *Zh. Eksp. Teor. Fiz.* **30** 421 (1956)
272. Lifshitz I M, Azbel' M Ya, Gerasimenko V I *J. Phys. Chem. Solids* **1** 164 (1956)
273. Azbel' M Ia, Gerasimenko V I, Lifshitz I M *Sov. Phys. JETP* **5** 986 (1957); *Zh. Eksp. Teor. Fiz.* **32** 1212 (1957)
274. Gerlach W, Stern O *Z. Phys.* **9** 349 (1922)
275. Silin V P, Rukhadze A A *Elektromagnitnye Svoistva Plazmy i Plazmopodobnykh Sred* (Electromagnetic Properties of Plasma and Plasma-Like Media) (Moscow: Gosatomizdat, 1961)
276. Hall E H *Am. J. Math.* **2** (3) 287 (1879)
277. Kaganov M I, Peschansky V G *Phys. Rep.* **372** 445 (2002)
278. Maksimov L A, Mikheyenkov A V, Khabarova T V *Phys. Usp.* **60** 623 (2017); *Usp. Fiz. Nauk* **187** 669 (2017)
279. Torrey H C *Phys. Rev.* **104** 563 (1956)
280. Krstić V et al. *J. Chem. Phys.* **117** 11315 (2002)
281. Rikken G L J A, Wyder P *Phys. Rev. Lett.* **94** 016601 (2005)
282. Rikken G L J A, Avarvari N *Phys. Rev. B* **99** 245153 (2019)
283. Okumura S, Tanaka R, Hirobe D *Phys. Rev. B* **110** L020407 (2024)
284. Shalygin V A et al. *Phys. Solid State* **54** 2362 (2012); *Fiz. Tverd. Tela* **54** 2237 (2012)
285. Furukawa T et al. *Nature Commun.* **8** 954 (2017)
286. Sahin C et al. *Phys. Rev. B* **97** 205206 (2018)
287. Furukawa T et al. *Phys. Rev. Research* **3** 023111 (2021)
288. Shiota K et al. *Phys. Rev. Lett.* **127** 126602 (2021)
289. Shishido H et al. *Appl. Phys. Lett.* **119** 182403 (2021)
290. Roy A et al. *npj Comput. Mater.* **8** 243 (2022)
291. Shishido H et al. *J. Chem. Phys.* **159** 064502 (2023)
292. Bloom B P et al. *Chem. Rev.* **124** 1950 (2024)
293. Gupta R, Droghetti A *Phys. Rev. B* **109** 155141 (2024)
294. Tsoi M, Fontana R E, Parkin S S P *Appl. Phys. Lett.* **83** 2617 (2003)
295. Kläui M et al. *Phys. Rev. Lett.* **95** 026601 (2005)
296. Togawa Y et al. *Jpn. J. Appl. Phys.* **45** L683 (2006)
297. Hayashi M et al. *Phys. Rev. Lett.* **98** 037204 (2007)
298. Hayashi M et al. *Science* **320** 209 (2008)
299. Zhang X et al. *J. Phys. Condens. Matter* **32** 143001 (2020)
300. Filinyuk N A, Lazarev A A *AEU Int. J. Electron. Commun.* **68** 172 (2014)
301. Gouadria S, Najeh I, El Mir L *J. Phys. Chem. Solids* **110** 290 (2017)
302. Gherabli R et al. *Sci. Adv.* **9** eadf5589 (2023)
303. Budhathoki S et al. *Phys. Rev. B* **101** 220405 (2020)
304. Stasinopoulos I et al. *Appl. Phys. Lett.* **111** 032408 (2017)
305. Zhu J-G, Zhu X, Tang Y *IEEE Trans. Magn.* **44** 125 (2008)
306. Nozaki Y et al. *Appl. Phys. Lett.* **95** 082505 (2009)
307. Wang Y, Tang Y, Zhu J-G *J. Appl. Phys.* **105** 07B902 (2009)
308. Igarashi M, Suzuki Y, Sato Y *IEEE Trans. Magn.* **46** 3738 (2010)
309. Igarashi M et al. *IEEE Trans. Magn.* **46** 2507 (2010)
310. Okamoto S et al. *J. Phys. D* **48** 353001 (2015)
311. Zhu J-G *IEEE Trans. Magn.* **55** 6700808 (2019)
312. Chan K S et al. *IEEE Access* **7** 140134 (2019)
313. Tulapurkar A A et al. *Nature* **438** 339 (2005)
314. Prokopenko O V et al. *IEEE Trans. Magn.* **48** 3807 (2012)
315. Prokopenko O V et al., in *Magnonics*: *From Fundamentals to Applications* (Topics in Applied Physics, Vol. 125, Eds S O Demokritov, A N Slavin) (Heidelberg: Springer, 2013) p. 143, DOI: 10.1007/978-3-642-30247-3_11
316. Li X, Zhou Y, Pong P W T *J. Nanotechnol.* **2016** 8347280 (2016)
317. Fang B et al. *Nature Commun.* **7** 11259 (2016)
318. Zhang L et al. *Jpn. J. Appl. Phys.* **62** 103003 (2023)
319. Nagasawa T et al. *J. Appl. Phys.* **109** 07C907 (2011)
320. Nagasawa T et al. *J. Appl. Phys.* **111** 07C908 (2012)
321. Choi H S et al. *Sci. Rep.* **4** 5486 (2014)
322. Quinsat M et al. *Appl. Phys. Lett.* **105** 152401 (2014)
323. Ruiz-Calaforra A et al. *Appl. Phys. Lett.* **111** 082401 (2017)
324. Zeng L et al. *Nanotechnology* **31** 375205 (2020)
325. Litvinenko A et al. *Phys. Rev. Applied* **16** 024048 (2021)
326. Louis S et al. *IEEE Trans. Magn.* **53** 1400804 (2017)
327. Louis S et al. *Appl. Phys. Lett.* **113** 112401 (2018)
328. Litvinenko A et al. *Nano Lett.* **20** 6104 (2020)
329. Litvinenko A et al. *Nano Lett.* **22** 1874 (2022)
330. Suzuki Y, Kubota H *J. Phys. Soc. Jpn.* **77** 031002 (2008)
331. Ishibashi S et al. *Appl. Phys. Express* **3** 073001 (2010)
332. Cheng X et al. *Appl. Phys. Lett.* **103** 082402 (2013)
333. Miwa S et al. *Nature Mater.* **13** 50 (2014)
334. Jenkins A S et al. *Nature Nanotechnol.* **11** 360 (2016)
335. Zhang L et al. *Appl. Phys. Lett.* **113** 102401 (2018)
336. Tarequzzaman M et al. *Appl. Phys. Lett.* **112** 252401 (2018)
337. Zhang B et al. *IEEE Trans. Nanotechnol.* **21** 648 (2022)
338. Phan N-T et al. *Phys. Rev. Applied* **21** 034063 (2024)
339. Torrejon J et al. *Nature* **547** 428 (2017)
340. Romera M et al. *Nature* **563** 230 (2018)
341. Böhnert T et al. *Commun. Eng.* **2** 65 (2023)